

EXTRACTING POLAR ANISOTROPY PARAMETERS FROM
SEISMIC DATA AND WELL LOGS

A Thesis
Presented to
the Faculty of the Department of Earth and Atmospheric Sciences
University of Houston

In Partial Fulfillment
of the Requirements for the Degree
Master of Science

By

Rongrong Lin

May, 2013

Extracting polar anisotropy parameters from seismic data
and well logs

by Rongrong Lin _____

Approved by

Dr. Robert Stewart, Committee chairman

Dr. Leon Thomsen, advisor

Dr. John Castagna, committee member

Dr. Daniel Ebrom, Committee member

Dean, College of Natural Sciences and Mathematics

ACKNOWLEDGEMENTS

First of all, I would like to thank my advisor, Dr. Leon Thomsen, for his guidance and encouragements. He inspired me with many good ideas, and also taught me how to be a good computer programmer and a good writer. Although he is not a full-time professor, he is very much responsible for my thesis research and I am always impressed by his pursuit of excellence.

Second, I especially thank my committee members Dr. Robert Stewart, Dr. John Castagna, and Dr. Daniel Ebrom for their useful comments and suggestions to my thesis research. I would also like to specially thank Dr. Brian Russell, for his advice on using Hampson-Russell software and providing me the data for my research. And I also want to acknowledge Anoop William from Allied Geophysical Laboratories and Kevin Hall from University of Calgary for their help in my first-stage data searching.

My thanks and appreciations also go to the graduate students, staff, and faculty of the Dept. of Earth and Atmospheric Sciences for their help. The financial support from University of Houston is also greatly appreciated.

Finally, I want to show my gratefulness to my family and my friends. Without their support of my academic pursuit in the United States, the completion of my study would not be possible.

EXTRACTING POLAR ANISOTROPY PARAMETERS FROM
SEISMIC DATA AND WELL LOGS

An Abstract of a Thesis
Presented to
the Faculty of the Department of Earth and Atmospheric Sciences
University of Houston

In Partial Fulfillment
of the Requirements for the Degree
Master of Science

By

Rongrong Lin

May, 2013

ABSTRACT

With V_p , V_s , and density well logs, we can do isotropic AVO forward modeling, using isotropic Zoeppritz equations or its approximations, and a wavelet extracted from the seismic data, to get synthetic seismic data. Compared with real seismic data, these synthetic data are scaled differently, and ignore many propagation effects. Conventionally, the seismic data are normalized to the isotropic synthetic data for comparison; this procedure suppresses the anisotropy information in the real data.

In this study, I tested a new method, using log data of V_p , V_s , and density, together with seismic pre-stack Common Depth Point (CDP) gathers near the well site, to deduce anisotropy parameters from them. This dataset is from Colony Sand, Alberta, Canada. I calculated the normalization function, as in the conventional procedure, but then filtered it in frequency domain using a cut-off frequency to be determined empirically. The low-frequency part of the normalization function was used to eliminate the propagation factors in the real data, but not the reflection coefficients. After scaling, the difference between the real data, thus normalized, and the isotropic synthetic data are attributed to the anisotropic part of the reflection coefficients. The resulting distributions of $\delta(z)$ and $\varepsilon(z)$ are compared to the gamma-ray log. There is a positive correlation between the anisotropy parameter and the gamma-ray log, which is an indication of the validity of the method.

TABLE OF CONTENTS

ACKNOWLEDGEMENTS.....	iii
ABSTRACT.....	v
TABLE OF CONTENTS.....	vi
TABLE OF FIGURES.....	vii
TABLE OF EQUATIONS.....	ix
1. Background.....	ix
1.1 Recent methods to get anisotropy parameters and their drawbacks	3
2. New method.....	5
2.1 Overview.....	5
2.2 Data preparation.....	6
2.2.1 Well logs loading.....	6
2.2.2 Seismic data loading	9
2.2.3 Synthetic generating.....	16
2.2.4 Synthetic and seismic correlation.....	20
2.3 Methodology development.....	24
2.3.1 Anisotropy parameters in reflection coefficient equation.....	24
2.3.2 Connection between synthetic and real seismic amplitude.....	26
2.3.3 Using normalization factor in anisotropy parameter estimation	42
2.4 Test	65
2.4.1 Anisotropy parameter with gamma ray log correlation.....	65
2.4.2 Estimating the reliability of the inferred anisotropy	67
2.5 Conclusions and discussion.....	70
REFERENCES.....	73
APPENDIX A: Comparison of synthetic produced from Hampson-Russell software with what is computed from logs.....	75
APPENDIX B: Matlab codes for making synthetic using zero-phase wavelet and well logs to extract synthetic A,B,C	83
APPENDIX C: Matlab codes for extracting anisotropy parameters delta and epsilon from synthetic and seismic A,B,C	85
APPENDIX D: Correlation of the δ parameter with gamma ray log from other literature.....	87

TABLE OF FIGURES

Figure 1.	Vp,Vs, and density logs from Colony well.....	8
Figure 2.	Near well site P-wave reflections from anisotropic medium.....	9
Figure 3.	Geometry of Colony sand seismic data.....	10
Figure 4.	CDP gathers for Colony sand seismic data.....	11
Figure 5.	CDP gathers for Colony sand seismic data with P-wave log posted.....	12
Figure 6.	Seismic wavelet, in time and frequency domains.....	13
Figure 7.	Seismic wavelet in time domain, converted to zero phase.....	14
Figure 8.	The frequency spectrum of the zero-phase wavelet.....	14
Figure 9.	Supergather at CDP 330 deconvolved to zero-phase wavelet.....	15
Figure 10.	Synthetic created from colony well logs.....	18
Figure 11.	Synthetic converted to zero phase for colony well logs.....	19
Figure 12.	Synthetic and seismic super-gather comparison at location CDP330.....	21
Figure 13.	Synthetic and seismic super-gather at location CDP330 in angle domain, with the original seismic wavelet.....	22
Figure 14a.	Synthetic and seismic super-gather at location CDP330 in angle gather display, zero-phase.....	23
Figure 14b.	Horizons picked on both seismic and synthetic in angle domain, zero phase.....	31
Figure 15a.	Seismic horizon at 418ms and its Aki-Richards approximation.....	32
Figure 15b.	Seismic horizon at 436ms and its Aki-Richards approximation.....	33
Figure 15c.	Seismic horizon at 490ms and its Aki-Richards approximation.....	33
Figure 15d.	Seismic horizon at 582ms and its Aki-Richards approximation.....	34
Figure 15e.	Seismic horizon at 636ms and its Aki-Richards approximation.....	34
Figure 15f.	Seismic horizon at 688ms and its Aki-Richards approximation.....	35
Figure 16.	Amplitude intercept A ,gradient B and curvature C for the major seismic horizons, zero phase.....	36
Figure 17a.	Synthetic horizon at 418ms and its Aki-Richards approximation.....	37
Figure 17b.	Synthetic horizon at 436ms and its Aki-Richards approximation.....	38
Figure 17c.	Synthetic horizon at 490ms and its Aki-Richards approximation.....	38
Figure 17d.	Synthetic horizon at 582ms and its Aki-Richards approximation.....	39
Figure 17e.	Synthetic horizon at 636ms and its Aki-Richards approximation.....	39
Figure 17f.	Synthetic horizon at 688ms and its Aki-Richards approximation.....	40
Figure 18.	Amplitude intercept A, gradient B and curvature C for the major synthetic horizons, zero phase.....	41
Figure 19.	Comparison of A _{syn} and A _{seis}	43
Figure 20.	Comparison of B _{syn} and B _{seis}	44
Figure 21.	Comparison of C _{syn} and C _{seis}	44
Figure 22.	Normalization factor for intercept A: NA.....	45
Figure 23.	Normalization factor for gradient B: NB.....	46

Figure 24. Normalization factor for gradient C: NC.....	46
Figure 25. High and low component of normalization factor $N(\theta, t)$	47
Figure 26. NA and its linear least-square fit.....	48
Figure 27. NB, the absolute value of NB and its linear least-square fit.....	49
Figure 28. NC, the absolute value of NC and its linear least-square fit.....	49
Figure 29. $B_{seislow}$ and B_{syn} comparison.....	51
Figure 30. $C_{seislow}$ and C_{syn} comparison.....	51
Figure 31. Plot of residual gradient $\Delta B(t)$	52
Figure 32. Plot of residual curvature $\Delta C(t)$	52
Figure 33. Seismogram of the convolution of the wavelet and seismic pickings with seismic pickings shown above.....	55
Figure 34. Seismogram of the convolution of the wavelet and synthetic pickings with seismic pickings shown above.....	56
Figure 35. Comparison of one trace seismogram of the convolution of the wavelet and $\Delta B(t)$	58
Figure 36. Comparison of one trace seismogram of the convolution of the wavelet and $\Delta C(t)$	59
Figure 37. Gamma ray log for Colony well.....	61
Figure 38. Time-Depth relationship.....	64
Figure 39. Anisotropy parameter δ variation with depth for colony well.....	65
Figure 40. Anisotropy parameter δ variation with gamma ray log display.....	66
Figure 41. Synthetic seismogram computed from anisotropic reflection coefficient.....	68
Figure 42. Comparison of the original seismic and synthetic seismogram computed from anisotropic reflection coefficient.....	69
Figure A-1. Amplitude intercept A, gradient B and curvature C for the major synthetic horizons, zero phase.....	75
Figure A-2. A_{ref} calculated from well logs.....	77
Figure A-3. B_{ref} calculated from well logs.....	77
Figure A-4. C_{ref} calculated from well logs.....	78
Figure A-5. A_{syn} calculated from correlation of seismic wavelet and A_{ref}	79
Figure A-6. B_{syn} calculated from correlation of seismic wavelet and B_{ref}	79
Figure A-7. C_{syn} calculated from correlation of seismic wavelet and C_{ref}	80
Figure A-8. A_{syn} comparison from log computation and HR software.....	81
Figure A-9. B_{syn} comparison from log computation and HR software.....	81
Figure A-10. C_{syn} comparison from log computation and HR software.....	82
Figure D-1. Anisotropy parameter δ variation with gamma ray log display.....	87
Figure D-2. Anisotropy parameter δ variation with gamma ray log display.....	88
Figure D-3. Anisotropy parameter δ (from 1250ft to 1750ft, equivalent to from 381m to 533.4m) correlation with well 10-14 gamma ray log (from 381m to 533.4m).....	90

TABLE OF EQUATIONS

(1.1)	$V_p(\theta) \approx V_{p0}[1 + \delta \sin^2 \theta \cos^2 \theta + \varepsilon \sin^4 \theta]$	2
(1.2)	$V_{s\perp}(\theta) \approx V_{s0}[1 + (\frac{V_{p0}}{V_{s0}})^2 (\varepsilon - \delta) \sin^2 \theta \cos^2 \theta]$	2
(1.3)	$V_{s\parallel}(\theta) \approx V_{s0}[1 + \gamma \sin^2 \theta]$	2
(1.4)	$\varepsilon = \frac{C_{11} - C_{33}}{2C_{33}}$	2
(1.5)	$\delta = \frac{(C_{13} + C_{44})^2 - (C_{33} - C_{44})^2}{2C_{33}(C_{33} - C_{44})}$	2
(1.6)	$\gamma = \frac{C_{66} - C_{44}}{2C_{44}}$	2
(1.7)	$t_x^2 = t_0^2 + \frac{x^2}{V_{NMO,SS}^2} - \frac{2\eta x^2}{V_{NMO,SS}^2 [t_0^2 V_{NMO,SS}^2 + (1 + 2\eta)x^2]}$	4
(1.8)	$\eta = \frac{\varepsilon - \delta}{1 + 2\delta}$	4
(1.9)	$v_{NMO}(0^\circ) \approx V_p(0^\circ)(1 + 2\delta)^{1/2}$	4
(2.1)	$Vp = 1.1 Vs + 1.36$	6
(2.2)	$Vs = 0.862 Vp - 1.1724$	6
(2.3)	$s(t) = r(t) * w(t)$	16
(2.4)	$R^{iso}(\theta) = \frac{1}{2} \left[\frac{\Delta Z}{Z} \right] + \frac{1}{2} \left[\frac{\Delta Vp}{Vp} - \left(\frac{2\bar{Vs}}{Vp} \right)^2 \left[\frac{\Delta G}{G} \right] \right] \sin^2 \theta + \frac{1}{2} \left[\frac{\Delta Vp}{Vp} \right] \tan^2 \theta \sin^2 \theta$	17
(2.5)	$R^{aniso}(\theta) = \frac{1}{2} \left[\frac{\Delta Z_0}{Z_0} \right] + \frac{1}{2} \left[\frac{\Delta Vp_0}{Vp_0} - \left(\frac{2\bar{Vs}_0}{Vp_0} \right)^2 \left[\frac{\Delta G_0}{G_0} \right] + (\delta_2 - \delta_1) \right] \sin^2 \theta + \frac{1}{2} \left[\frac{\Delta Vp_0}{Vp_0} + (\varepsilon_2 - \varepsilon_1) \right] \tan^2 \theta \sin^2 \theta$	24
(2.6)	$R^{aniso}(\theta) - R^{iso}(\theta) = \Delta R^{aniso}(\theta) = \frac{1}{2} (\delta_2 - \delta_1) \sin^2 \theta + \frac{1}{2} (\varepsilon_2 - \varepsilon_1) \tan^2 \theta \sin^2 \theta$	26
(2.7a)	$s(\theta, t) = I(t) * P_{\uparrow}(\theta, t) * r(\theta, t) * P_{\downarrow}(\theta, t) * w_0(t) S_0(\theta)$	27
(2.7b)	$s(\theta, t) = [I(t) * P_{\uparrow}(\theta, t) * P_{\downarrow}(\theta, t) * S_0] w_0(t) * r(\theta, t)$ $\equiv P(\theta, t) * w(t) * r(\theta, t)$	27
(2.8)	$S(t, \theta) \equiv R_{pp}^{iso}(t, \theta) * w(t)$	28
(2.9)	$N(\theta, t) \times s(\theta, t) = N(\theta, t) \times P(\theta, t) * w(t) * r(\theta, t) \approx w(t) * R_{pp}^{iso}(\theta, t)$	28
(2.10)	$N(\theta, t) \times P(\theta, t) = 1$	28
(2.11)	$r(\theta, t) = R_{pp}^{iso}(\theta, t)$	28

$$(2.12) R^{iso}(t_0, \theta) = A(t_0) + B(t_0) \sin^2 \theta + C(t_0) \sin^2 \theta \tan^2 \theta \dots\dots\dots 29$$

$$(2.13) S(t_0, \theta) = [A(t_0) + B(t_0) \sin^2 \theta + C(t_0) \sin^2 \theta \tan^2 \theta] * w(t_0) \dots\dots\dots 29$$

$$(2.14) s(t_0, \theta) = [A_{seis}(t_0) + B_{seis}(t_0) \sin^2 \theta + C_{seis}(t_0) \sin^2 \theta \tan^2 \theta] * w(t_0) \dots\dots\dots 29$$

$$(2.15) S(t_0, \theta) = A_{syn}(t_0) + B_{syn}(t_0) \sin^2 \theta + C_{syn}(t_0) \sin^2 \theta \tan^2 \theta \dots\dots\dots 41$$

$$|A_{syn}| \equiv \langle |A_{syn}(t_0)| \rangle;$$

$$(2.16) |A_{seis}| \equiv \langle |A_{seis}(t_0)| \rangle; \dots\dots\dots 42$$

$$N_0 \equiv \frac{|A_{syn}|}{|A_{seis}|}$$

$$A_{seis}^*(t_0) = N_0 A_{seis}(t_0);$$

$$(2.17) B_{seis}^*(t_0) = N_0 B_{seis}(t_0); \dots\dots\dots 43$$

$$C_{seis}^*(t_0) = N_0 C_{seis}(t_0)$$

$$N_A(t_0) \equiv A_{syn}(t_0) / A_{seis}^*(t_0)$$

$$(2.18) N_B(t_0) \equiv B_{syn}(t_0) / B_{seis}^*(t_0) \dots\dots\dots 45$$

$$N_C(t_0) \equiv C_{syn}(t_0) / C_{seis}^*(t_0)$$

$$A_{seislow}(t_0) = N_{Alow}(t_0) \times A_{seis}^*(t_0)$$

$$(2.19) B_{seislow}(t_0) = N_{Blow}(t_0) \times B_{seis}^*(t_0) \dots\dots\dots 50$$

$$C_{seislow}(t_0) = N_{Clow}(t_0) \times C_{seis}^*(t_0)$$

$$(2.20) \Delta B(t_0) = B_{seislow}(t_0) - B_{syn}(t_0) \dots\dots\dots 50$$

$$\Delta C(t_0) = C_{seislow}(t_0) - C_{syn}(t_0)$$

$$A_{seislow} - A_{syn} + (B_{seislow} - B_{syn}) \sin^2 \theta + (C_{seislow} - C_{syn}) \sin^2 \theta \tan^2 \theta$$

$$(2.21) = 0 + \Delta B \sin^2 \theta + \Delta C \sin^2 \theta \tan^2 \theta \dots\dots\dots 53$$

$$= \frac{1}{2} (\delta_2 - \delta_1) \sin^2 \theta * w(t) + \frac{1}{2} (\varepsilon_2 - \varepsilon_1) \sin^2 \theta \tan^2 \theta * w(t)$$

$$(2.22) \left\{ \begin{array}{l} \Delta B(t) = \frac{1}{2} \Delta \delta(t) \times w(t) \\ \Delta C(t) = \frac{1}{2} \Delta \varepsilon(t) \times w(t) \end{array} \right\} \dots\dots\dots 53$$

$$(2.23) e = \Delta B(t) * w(t) - \Delta B(t) = \Delta B(t) * w(t) - \Delta B(t) * \Delta(t) = \Delta B(t) * (w(t) - \Delta(t)) \dots\dots 58$$

$$(2.24) \left\{ \begin{array}{l} \delta_2 - \delta_1 = \Delta\delta_1 \\ \delta_3 - \delta_2 = \Delta\delta_2 \\ \delta_4 - \delta_3 = \Delta\delta_3 \\ \dots\dots\dots \\ \delta_n - \delta_{n-1} = \Delta\delta_{n-1} \end{array} \right\} \dots\dots\dots 60$$

$$(2.25) \left\{ \begin{array}{l} \varepsilon_2 - \varepsilon_1 = \Delta\varepsilon_1 \\ \varepsilon_3 - \varepsilon_2 = \Delta\varepsilon_2 \\ \varepsilon_4 - \varepsilon_3 = \Delta\varepsilon_3 \\ \dots\dots\dots \\ \varepsilon_n - \varepsilon_{n-1} = \Delta\varepsilon_{n-1} \end{array} \right\} \dots\dots\dots 60$$

$$(2.26) \left\{ \begin{array}{l} A_{new}(t) = A_{syn}(t) \\ B_{new}(t) = B_{syn}(t) + \Delta\delta(t) \\ C_{new}(t) = C_{syn}(t) + \Delta\varepsilon(t) \end{array} \right\} \dots\dots\dots 67$$

$$(A.1) \quad R^{iso}(\theta) = \frac{1}{2} \left[\frac{\Delta Z_0}{Z_0} \right] + \frac{1}{2} \left[\frac{\Delta V p_0}{V p_0} - \left(\frac{2\overline{V s_0}}{V p_0} \right)^2 \left[\frac{\Delta G_0}{G_0} \right] \right] \sin^2 \theta + \frac{1}{2} \left[\frac{\Delta V p_0}{V p_0} \right] \tan^2 \theta \sin^2 \theta \quad \dots\dots 76$$

$$= A + B \sin^2 \theta + C \tan^2 \theta \sin^2 \theta$$

$$(A.2) \left\{ \begin{array}{l} A = \frac{1}{2} \left[\frac{\Delta Z_0}{Z_0} \right] = \frac{1}{2} \left[\frac{\rho_2 V p_{02} - \rho_1 V p_{01}}{\rho_2 V p_{02} + \rho_1 V p_{01}} \right] \\ B = \frac{1}{2} \left[\frac{\Delta V p_0}{V p_0} - \left(\frac{2\overline{V s_0}}{V p_0} \right)^2 \left[\frac{\Delta G_0}{G_0} \right] \right] \\ C = \frac{1}{2} \left[\frac{\Delta V p_0}{V p_0} \right] \end{array} \right\} \dots\dots\dots 76$$

1. Background

Anisotropy is the variation of a physical property depending on the direction in which it is measured (Sheriff, 1972). This is a very common phenomenon in the science fields such as chemistry, medical science, physics, and engineering. In the geophysics field, the anisotropy mostly refers to seismic anisotropy. Seismic anisotropy is the dependence of seismic velocity upon angle (Thomsen, 2002). It can come from the anisotropic rock itself or the stress-induced anisotropy due to the difference of vertical stress and horizontal stress caused by layers. The application of seismic anisotropy has improved the exploration of hydrocarbons a lot, by modifying the velocity model from simple isotropic to more realistically anisotropic. Seismic anisotropy has played roles in applications such as the long offset seismic data with greater angles of incidence (the angle-dependence of velocity is more evident), AVO (Amplitude versus offset) quantitative analysis, and anisotropic migration. (Thomsen, 2002)

The study of seismic wave propagation leads to the study of rock elasticity tensors. For the simplest realistic case, the elasticity is of type of hexagonal symmetry, which is also called polar symmetry. In this case, the elasticity tensor has five independent elements C_{11} , C_{13} , C_{33} , C_{44} , and C_{66} . This polar anisotropy case applies to horizontal massive shales and horizontal thin-bed sequences (Thomsen, 2002). Because its symmetry axis is vertical, polar anisotropy is also referred to as vertical transverse isotropy (VTI).

To express the velocities of plane waves in polar anisotropy using elasticity tensor generates complicated equations. Thomsen used the combinations of elastic modules to make the expressions much simpler. If the material is of weak anisotropy, which is the most common case, then:

$$V_p(\theta) \approx V_{p0} [1 + \delta \sin^2 \theta \cos^2 \theta + \varepsilon \sin^4 \theta] \quad (1.1)$$

$$V_{s\perp}(\theta) \approx V_{s0} [1 + (\frac{V_{p0}}{V_{s0}})^2 (\varepsilon - \delta) \sin^2 \theta \cos^2 \theta] \quad (1.2)$$

$$V_{s\parallel}(\theta) \approx V_{s0} [1 + \gamma \sin^2 \theta] \quad (1.3)$$

There,

$$\varepsilon = \frac{C_{11} - C_{33}}{2C_{33}} \quad (1.4)$$

$$\delta = \frac{(C_{13} + C_{44})^2 - (C_{33} - C_{44})^2}{2C_{33}(C_{33} - C_{44})} \quad (1.5)$$

$$\gamma = \frac{C_{66} - C_{44}}{2C_{44}} \quad (1.6)$$

The three anisotropic parameters $\delta, \varepsilon, \gamma$ can also be understood respectively as near-vertical anisotropy, near-horizontal anisotropy, and SH anisotropy.

These three anisotropy parameters are useful because:

- They are dimensionless.
- The anisotropy parameters reduce to zero when degenerating to isotropic case.
- When the parameters are much less than 1, we can take such formations as weakly anisotropic.

(Thomsen, 2002)

Nowadays the anisotropy has been developed to include azimuth anisotropy, which is about HTI (horizontal transverse isotropy) media and TTI (tilted transverse isotropy) media since it first came out during the 1970s. The theory development of anisotropy has been making a lot of progress, while the real practice of getting anisotropy parameters is relatively underdeveloped.

My thesis will try a new method to extract anisotropy parameters. Based on only the simplest polar anisotropy case, I will extract the anisotropy parameters δ and ϵ from P-wave propagation.

1.1 Recent methods to get anisotropy parameters and their drawbacks

In oil and gas reservoirs, shale is the lithology with the most significant anisotropy. The most direct way to obtain anisotropy parameters of shale is to measure the shale sample in a lab, such as using travelttime inversion and physical modeling. But in lab conditions, the rocks are under different frequencies compared with seismic waves, and they are not likely to exhibit its original anisotropy when buried underground.

Nowadays some other ways to measure anisotropy using P-wave well logs and seismic data gathers have been developed as well. The seismic arrival-time methods (such as those which measure hyperbolic and non-hyperbolic move-out (Tsvankin and Thomsen, 1994)) produce estimates of anisotropy which have low spatial resolution, and therefore cannot be used in AVO studies, which have much higher spatial resolution (depending on the seismic wavelet).

One method uses the hyperbolic move-out is based on the equation:

$$t_x^2 = t_0^2 + \frac{x^2}{V_{NMO,SS}^2} - \frac{2\eta x^2}{V_{NMO,SS}^2 [t_0^2 V_{NMO,SS}^2 + (1 + 2\eta)x^2]} \quad (1.7)$$

(Alkhalifah and Tsvankin, 1995)

The $v_{NMO,SS}$ is the short spread normal move-out velocity using conventional velocity analysis, by short-spread, we mean mute the CDP gather at offset=depth. η is dependent on the anisotropy parameters δ and ε (Thomsen, 1986):

$$\eta = \frac{\varepsilon - \delta}{1 + 2\delta} \quad (1.8)$$

The parameter δ can be obtained from formula

$$v_{NMO}(0^\circ) \approx V_p(0^\circ)(1 + 2\delta)^{1/2} \quad (1.9)$$

We can see that normally the traveltimes must be measured over thick intervals, so that the small parameters η and δ may be estimated with confidence.

Another way to measure anisotropy is anisotropy logging, or cross-dipole logging. This kind of log uses one monopole and two wideband, low-frequency, dipole transmitters perpendicular to each other, it measures compressional (quasi-P), fast and slow shear-slowness and fast-shear azimuth. The pitfall for this method is that it is very dependent on the borehole environment, and it also has dispersion characteristics due to dipole flexural waves (Patterson and Tang, 2005).

Here my study will focus on a method to extract anisotropy parameters using both well logs and seismic data. I concentrate on amplitudes; hence the results will have the resolution of the seismic wavelet.

2. New method

2.1 Overview

The goal of this study is to use log data of V_p , V_s , and density, together with seismic pre-stack Common Depth Point (CDP) gathers near the well site, to deduce anisotropy parameters from them, with the resolution of the seismic wavelet. This study will utilize the Hampson-Russell AVO package to do the AVO modeling, and will calculate normalization factors to compare log-derived synthetic data and real seismic data. Since the synthetic is based on isotropic theory, the normalization factors are modified to permit an estimate of anisotropy. The primary goal is to extract the δ and ϵ parameters, in the logged section of the well.

The method involves the comparison of surface seismic data with synthetic data calculated from logs. Before this comparison is feasible, certain conventional data preparation steps are required. These are described next and the details of the new method follow that.

2.2 Data preparation

The Colony Sand Dataset is suitable for this experiment because it has both seismic data and most well logs needed in that seismic acquisition area. The Colony Sand Dataset is acquired from Alberta, Canada and it is the default dataset for Hampson-Russell software AVO package version 6.5 CE7/R4. In this experiment, I use this AVO package extensively.

2.2.1 Well logs loading

The first step is to load the well logs from the Colony Dataset. In the dataset, we have one well in LAS format, called Colony_well. In this well, there are logs for P-wave slowness (1/velocity), density, gamma Ray, SP and resistivity. For this project, I still need an S-wave log. Although the argument would be stronger with real data, since the real data is not available, I estimate V_S as follows. Assuming the log as a wet (brine-filled log), we can use Castagna's "mudrock" equation (Castagna, 1985) to create a V_S log based on the V_P log. Castagna's equation is:

$$V_P = 1.1 V_S + 1.3 \text{ (km/s)} \quad (2.1)$$

So

$$V_s = 0.862 V_p - 1.1724 \text{ (km/s)} \quad (2.2)$$

To this point, we have assumed that the logs are from a wet well, but according to the information about the Colony data, there is gas sand present, so we still need to conduct a fluid substitution to get the correct S-wave velocity. This procedure can be simply done by performing Fluid Replacement Modeling in the Hampson-Russell AVO package. In brief, the V_p and density logs are converted to brine-filled equivalents, using separate knowledge of which layers are gas-filled, and using standard isotropic Gassmann theory (Gassmann, 1951). Then V_s is estimated using (2.2), and all logs are converted back to original fluids.

After all this process, the final logs for density, $1/V_s$, and $1/V_p$ are shown in Figure.1:

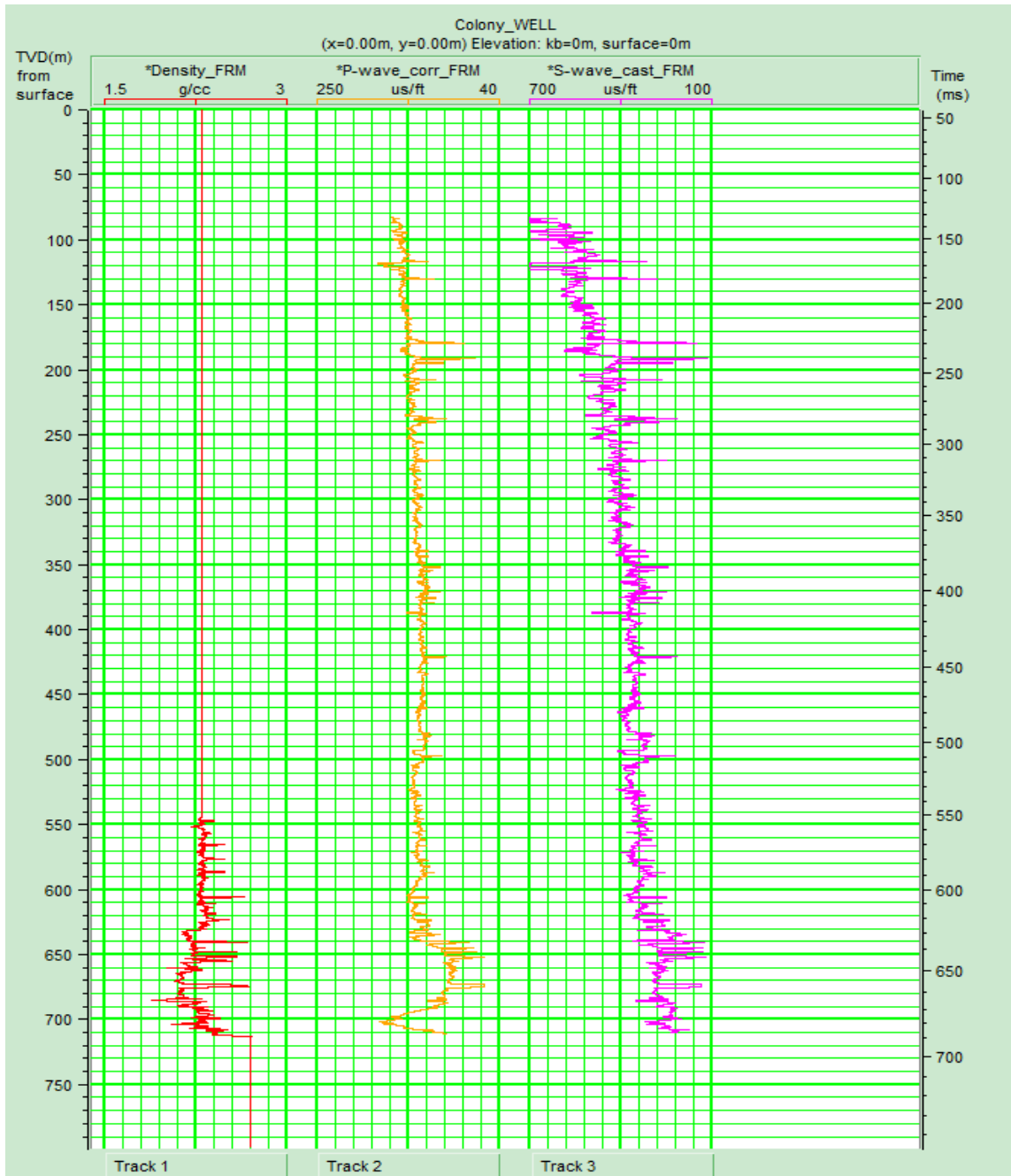


Figure 1. Vp,Vs and density logs from Colony well

The stars indicate the logs used to compute the synthetic seismograms. The density log is renamed as Density_FRM, which means density log after performing Fluid Replacement

Modeling, S-wave_{cast_FRM} means V_s log created by Castagna's mudrock line equation (2.1) and modified by Fluid Replacement Modeling. P-wave_{corr_FRM} means the P-wave log has been stretched and squeezed to correlate to the seismic event time. This is actually done after the synthetic is computed, we show the result here before the discussion about the correlation later.

2.2.2 Seismic data loading

The required geometry of a well and a corresponding CDP gather is shown in Figure 2. The synthetic seismic traces near the well site are generated from isotropic reflection coefficients (using V_p , V_s , and density logs). However, the reflections recorded in the real seismic data will contain anisotropy information, if this area has anisotropic media. For example, in the CDP gather from Figure 2, if the medium is isotropic, the velocity of the three reflection rays (S1-R1;S2-R2;S3-R3) will travel with same velocities, But if the medium is anisotropic, even though they are reflected from the same interface, their velocity is different. That is because their reflection angle is different ($\theta_1 < \theta_2 < \theta_3$).

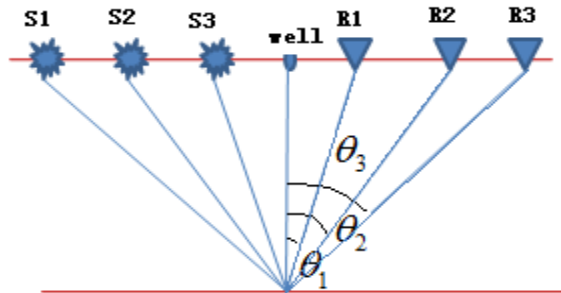


Figure 2. Near well site P-wave reflections from anisotropic medium

The seismic data in the Colony dataset is called gathers.sgy. It is a pre-stack 2D line. For the survey, there are 129 shots and the source/receiver offset interval is 40m. The CDP gathers are numbered from 260 to 390; each gather has about 10 traces. For each trace, the sample rate is 2ms and there are 250 samples in each trace. The seismic data begins from 300ms.

The geometry display is simple:



Figure 3. Geometry of Colony sand seismic data

After loading in the seismic data, it displays as:

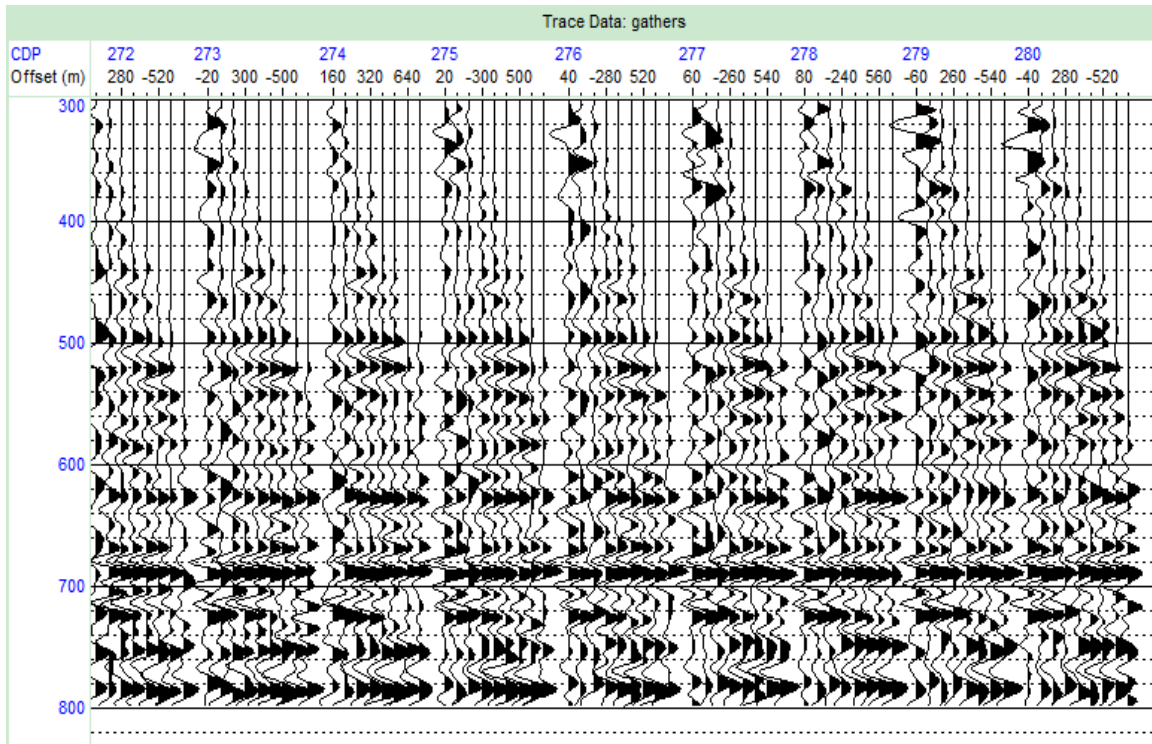


Figure 4.CDP gathers for Colony sand seismic data

As we will need to use the CDP gather near the well site, we should find the location of the CDP gather which the well site is closest to. We can find this information easily in Hampson-Russell when we load the well logs into the Geoview package. It is located at the position of CDP 330.

We project the P-wave velocity log onto that CDP gather and the display is like this:

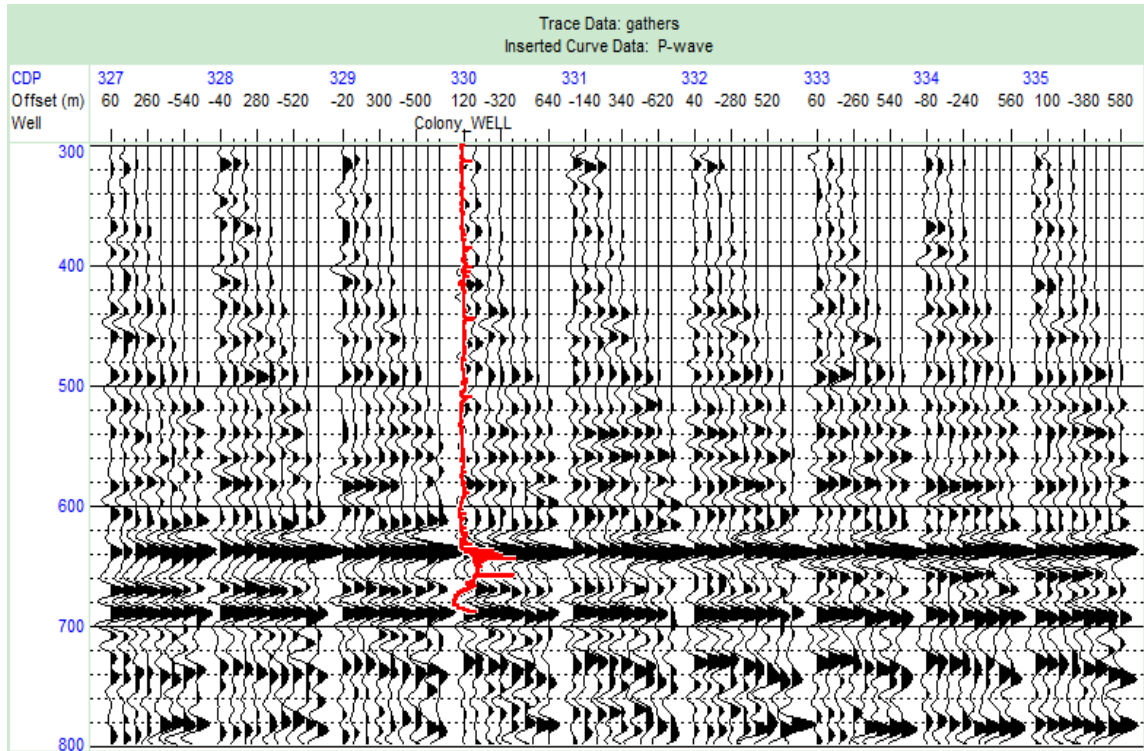


Figure 5. CDP gathers for Colony sand seismic data with P-wave log posted

In order to improve the signal/noise ratio, we use seismic CDP super-gathers in place of the original seismic CDP gathers. Super-gathers are averages of the original gathers; in this case we average over 5 CDP positions near the well.

The wavelet extracted from the seismic super-gather is shown here, along with its spectrum (amplitude and phase).

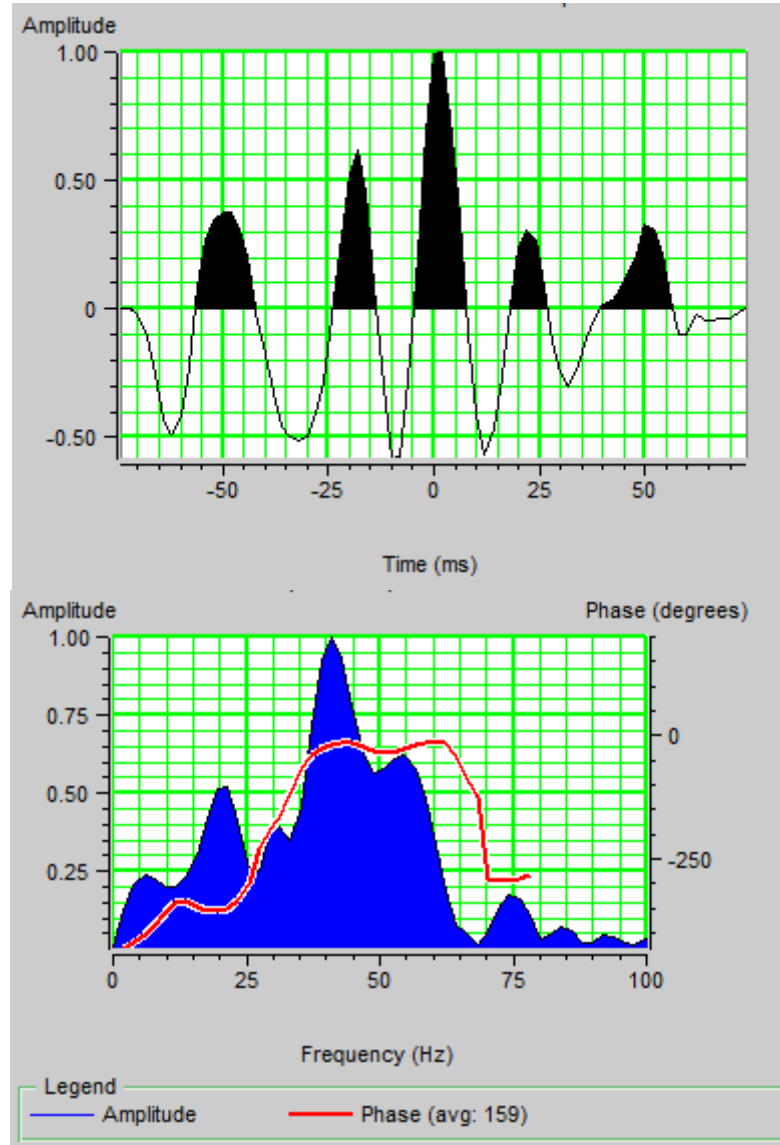


Figure 6. Seismic wavelet, in time and frequency domains

Because seismic data are usually viewed with zero-phase wavelets, Figure 7 shows the wavelet from Figure 6, shifted to zero phase. The zero-phase wavelet is extracted from the original seismic wavelet (Figure 6) using wavelet dephase deconvolution, which can shape the known input wavelet to a zero-phase wavelet with the same amplitude spectrum as the input.

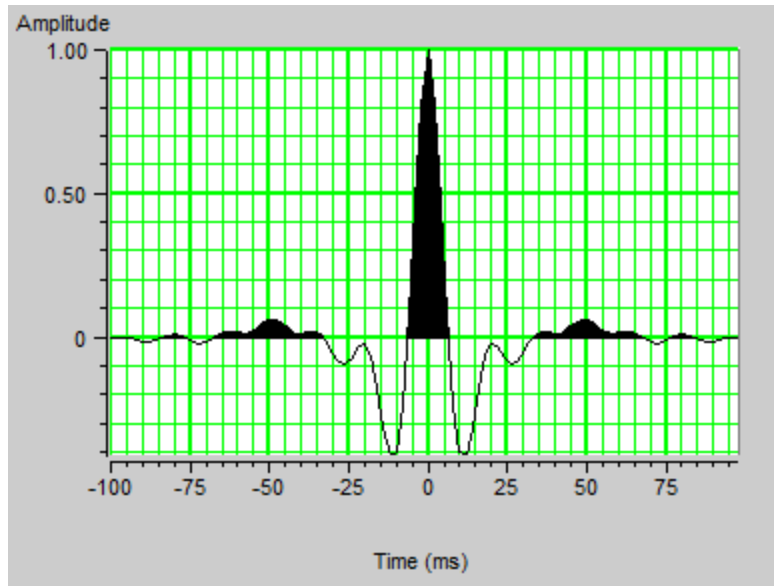


Figure 7. Seismic wavelet in time domain, converted to zero phase

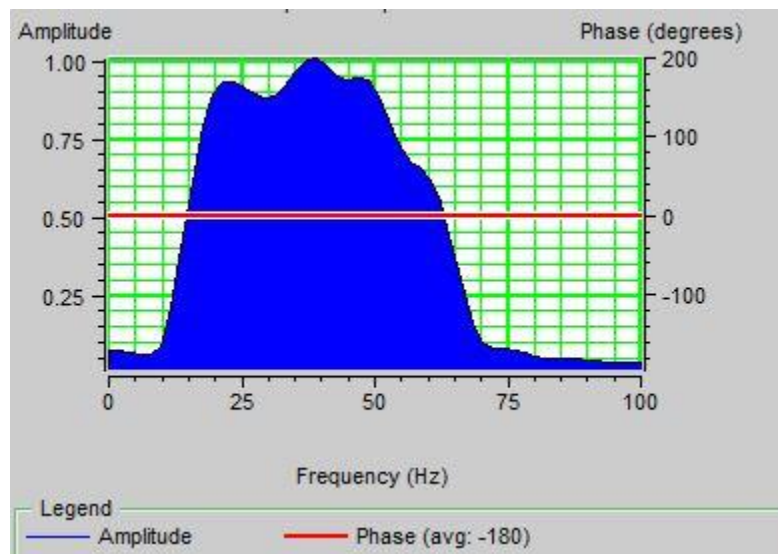


Figure 8. The frequency spectrum of the zero-phase wavelet

Also, Figure 8 shows the amplitude spectrum of this wavelet.

As we can see, it differs from the spectrum in Figure 6. Evidently the HR module which extracted this wavelet did some further wavelet-shaping; however, this is not a focus of this thesis. We show below (Figure 9) how the seismic super-gather at CDP 330 looks, deconvolved to this wavelet.

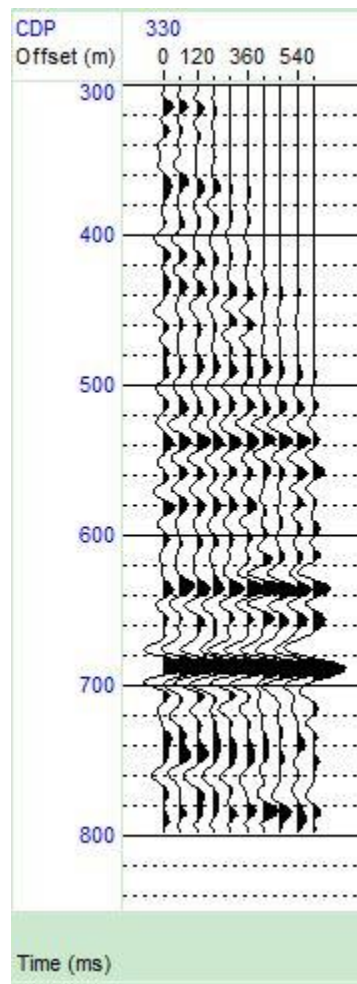


Figure 9. Super-gather at CDP 330 deconvolved to zero-phase wavelet

2.2.3 Synthetic generating

As the V_p , V_s , and density logs are ready, and the seismic wavelet is determined, we can use them to generate an isotropic synthetic containing no propagation effects. In the simplest version of the “convolutional model” of seismic wave propagation, the seismic trace $s(t)$ is given by

$$s(t) = r(t) * w(t) \quad (2.3)$$

It means one trace of the seismic reflection record is the convolution (*) of the reflection coefficients $r(t)$ (of the layers the wave traverses) with the seismic wavelet $w(t)$. The reflectivity series $r(t)$ has amplitudes r , occurring at times t , both of which are affected by anisotropy. For a synthetic trace created from well logs, this equation is true. But when it comes to real seismic traces, it neglects propagation effects and noise. We will take these factors into consideration in the anisotropy parameter calculation. Usually we can get the wavelet by extracting it from seismic data. And for the best interpretation of the seismic data, we usually convert wavelet into zero-phase.

The accurate isotropic algorithm for computing a synthetic would be the Zoeppritz equation (Zoeppritz, 1919). But as we will use the Shuey’s approximation for Aki-Richards equation (Aki and Richards, 1980, Shuey, 1985), which is an approximation for Zoeppritz equation to extract anisotropy information, here we will use Shuey’s

approximation for Aki-Richards equation(referred to as Aki-Richards equation in the following text) to create the isotropic synthetic also.

In the isotropic case, based on Aki-Richards' approximation, the P-wave reflection coefficient can be written as:

$$R^{iso}(\theta) = \frac{1}{2} \left[\frac{\Delta Z}{\bar{Z}} \right] + \frac{1}{2} \left[\frac{\Delta V_p}{\bar{V}_p} - \left(\frac{2\bar{V}_s}{\bar{V}_p} \right)^2 \left[\frac{\Delta G}{\bar{G}} \right] \right] \sin^2 \theta + \frac{1}{2} \left[\frac{\Delta V_p}{\bar{V}_p} \right] \tan^2 \theta \sin^2 \theta \quad (2.4)$$

where $Z = \rho V_p$ is the P-wave impedance, $G = \rho V_s^2$ is the shear modulus, ρ is density, and the bar denotes the average of properties (above and below the interface). V_p is the P-wave velocity and V_s is the S-wave velocity. θ is the wavefront normal angle of the incident P-wave. The synthetic gather generated (by HR) is a flattened gather, which uses a model blocking of traveltme average to convert from depth to vertical traveltme t_0 within the logged interval, and its output sample rate is 2ms. It selects a series of incident angles θ , then constructs a spike series ($\Delta t=2\text{ms}$) using equation (2.4), and convolves with a wavelet, as in equation (2.3), with $r(t) \rightarrow R^{iso}(t_0, \theta)$, constructed as just described. We found some problematic issues with the way this procedure is implemented by HR (c.f. Appendix A), and so implemented a similar procedure in Matlab.

The synthetic gather is flat in time, for easy comparison with the NMO-corrected seismic gather. The synthetic gather shown below is one with the wavelet extracted from seismic data (Figure 6):

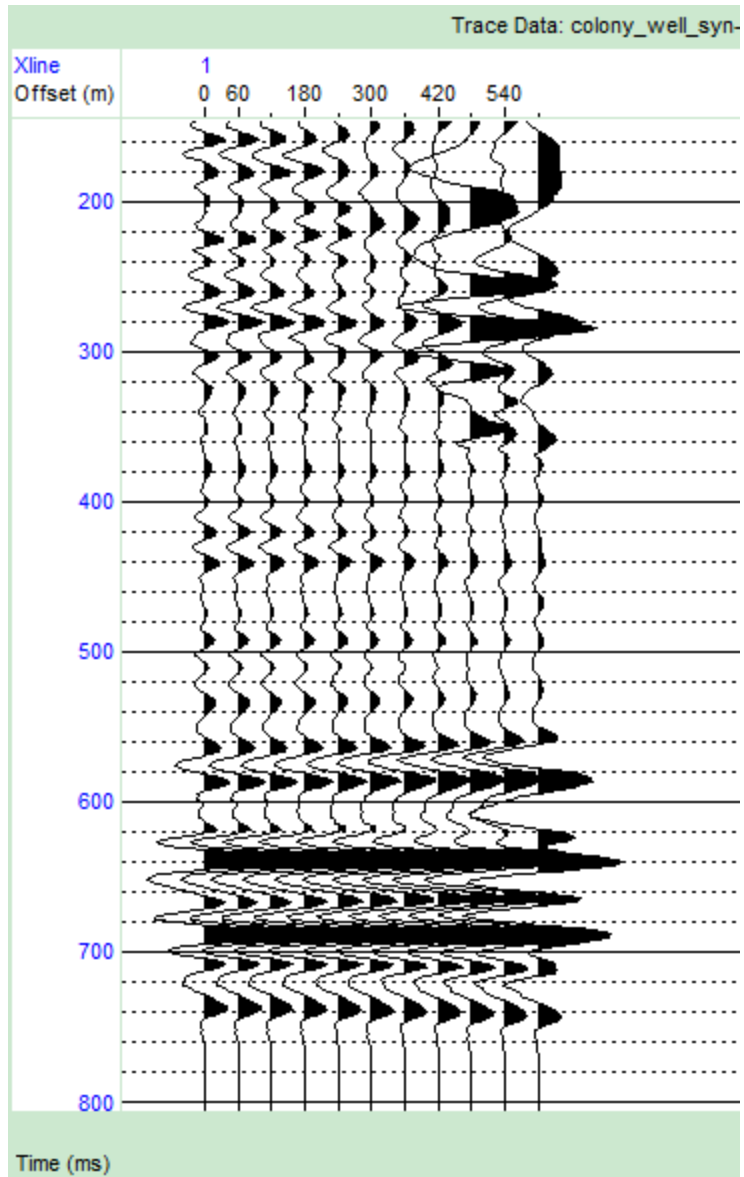


Figure 10. Synthetic created from colony well logs

The synthetic gather shown below is one with the wavelet (Figure 7) which was extracted from seismic data, and converted to zero phase:

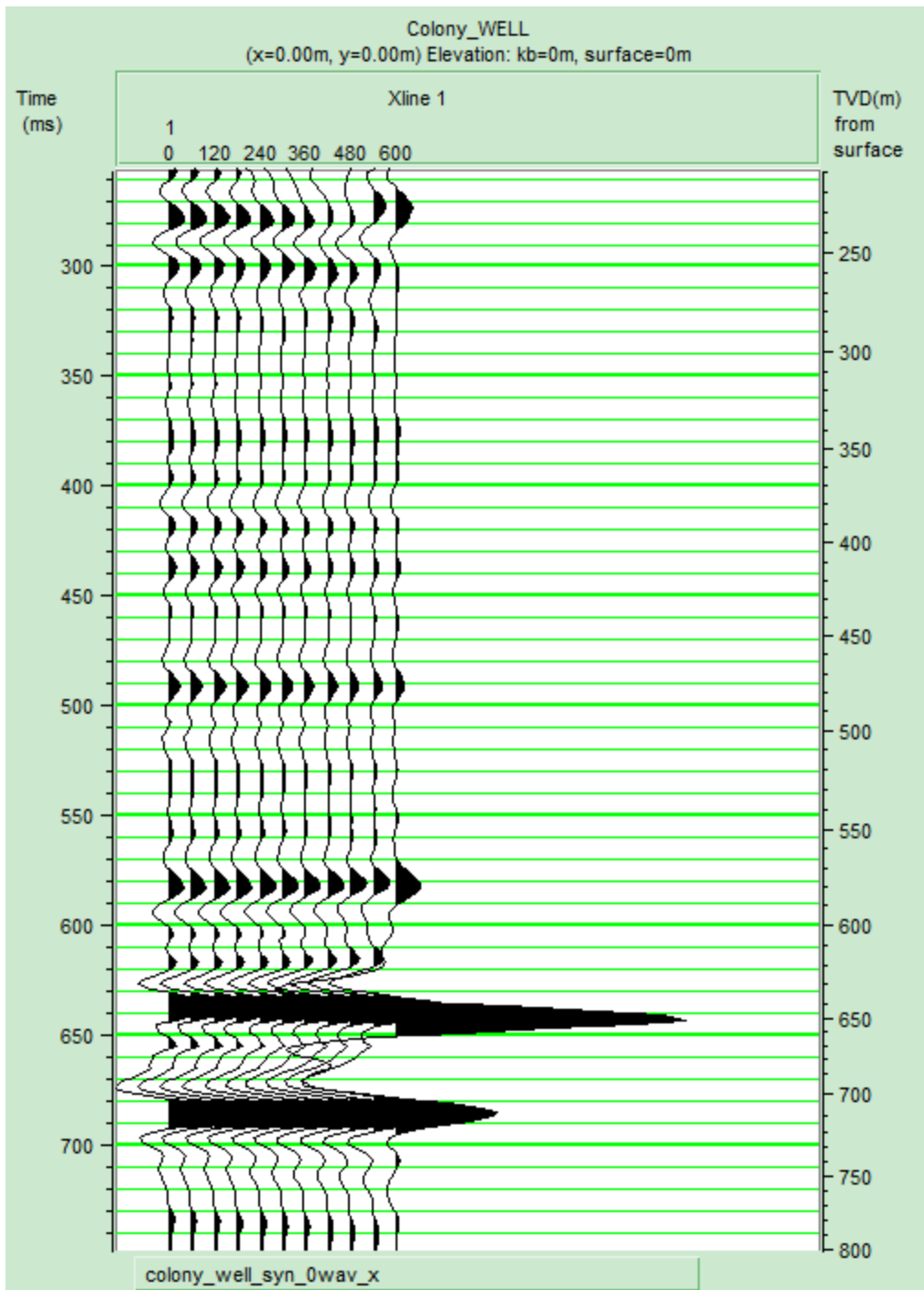


Figure 11. Synthetic converted to zero phase for colony well logs

2.2.4 Synthetic and seismic correlation

The synthetic and the real seismic differ in various ways. Some common reasons include that the check shot correction is not applied and the time-depth curve for the synthetic is not correct. And also if we use a default zero-phase wavelet to generate the synthetic, we should expect the difference because the seismic wavelet is not supposed to be zero-phase, and thus we need to extract it from the seismic.

After check shot analysis, log correlation, regenerating the synthetic with the seismic wavelet extracted from the real seismic data, and converting to angle domain, the synthetic and the seismic super-gather at location CDP330 display as in Figure 12.

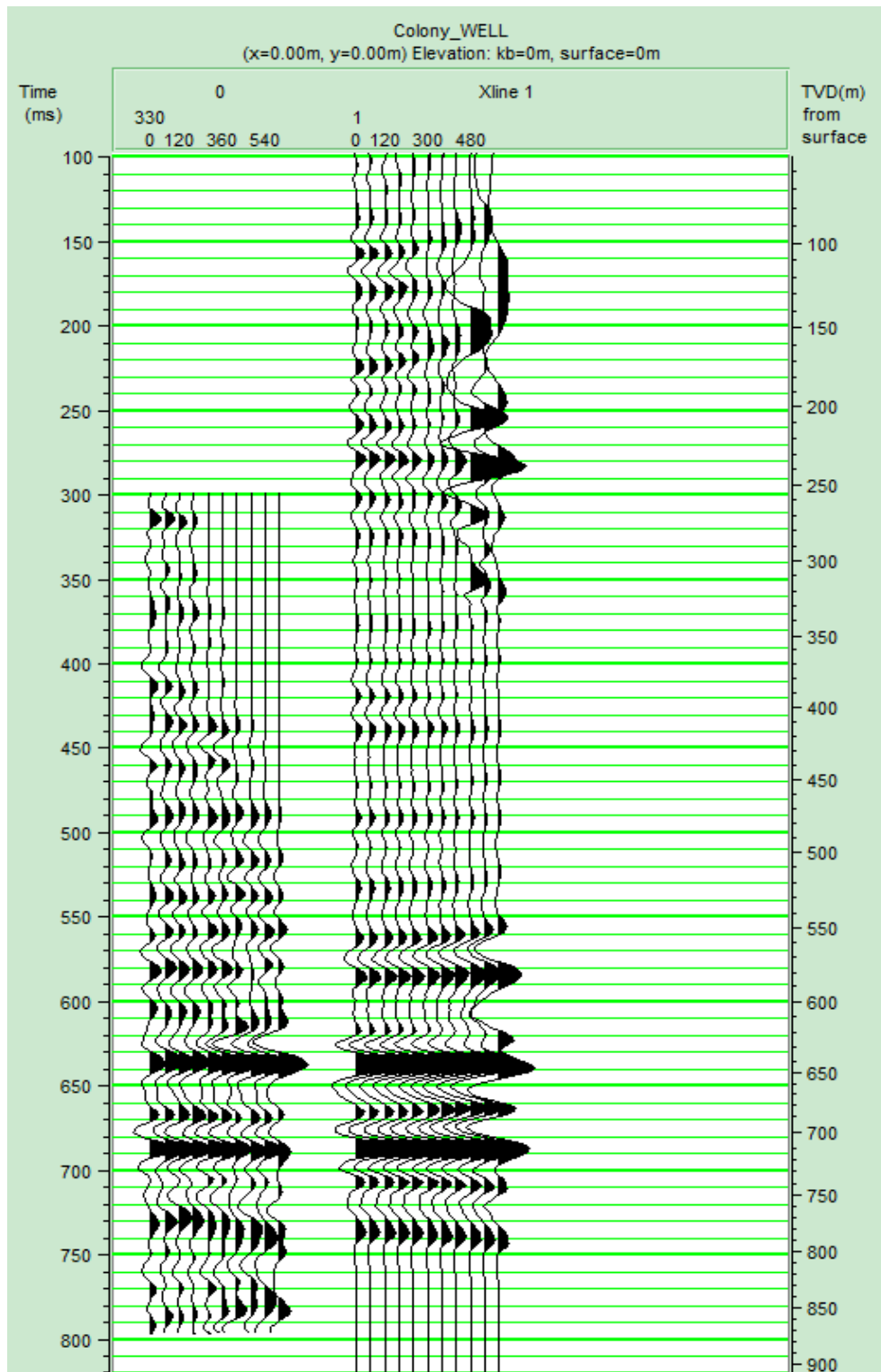


Figure 12.Synthetic (right) and seismic super-gather(left) comparison at location CDP330

And after converting the seismic and synthetic data to angle gathers, the synthetic and the seismic super-gather at location CDP330 display as in Figure 13.

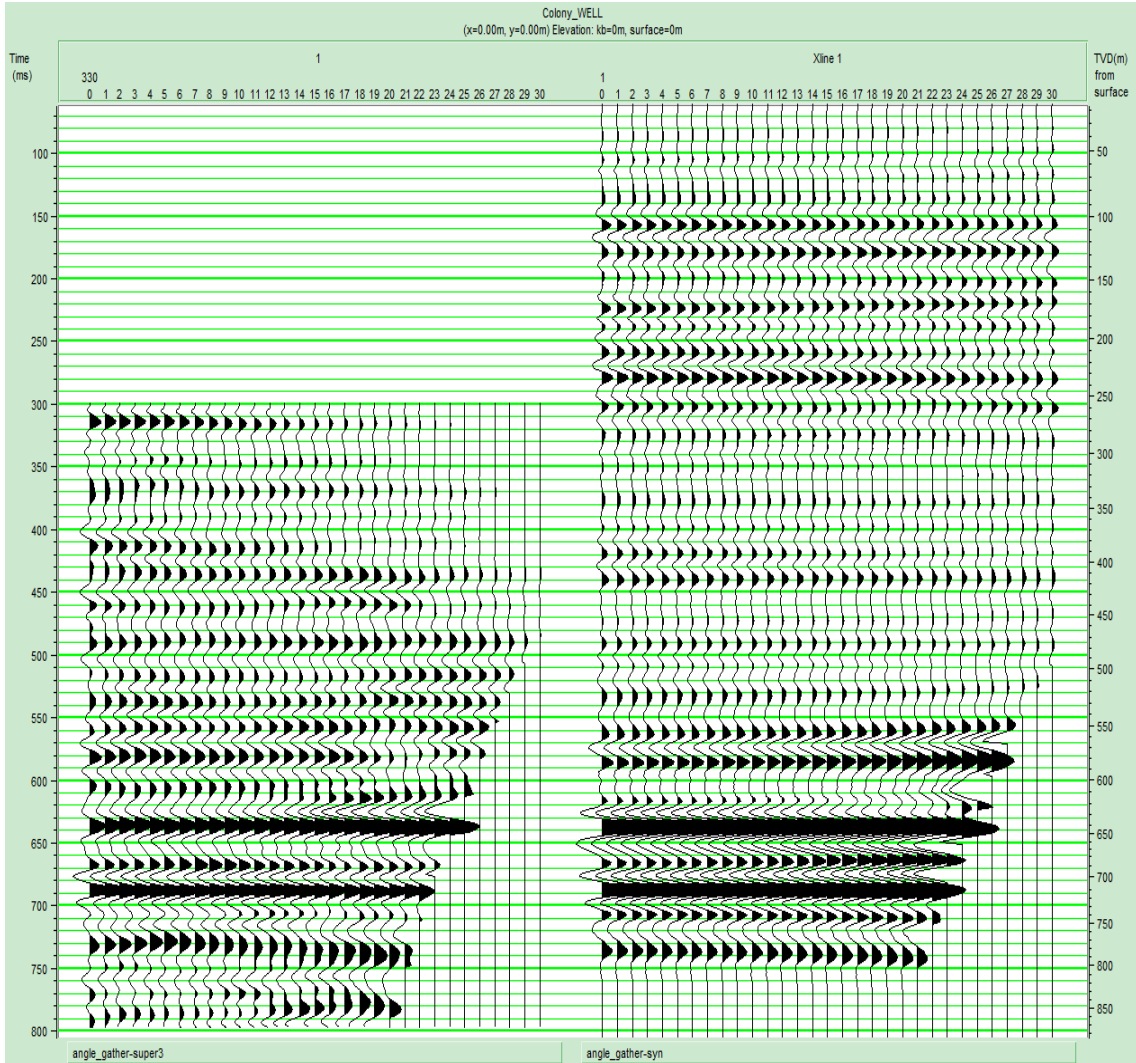


Figure 13. Synthetic and seismic super-gather at location CDP330 in angle domain, with the original seismic wavelet

Figure 14a shows the comparison between the zero-phase seismic data, and the zero-phase synthetic in the angle domain:

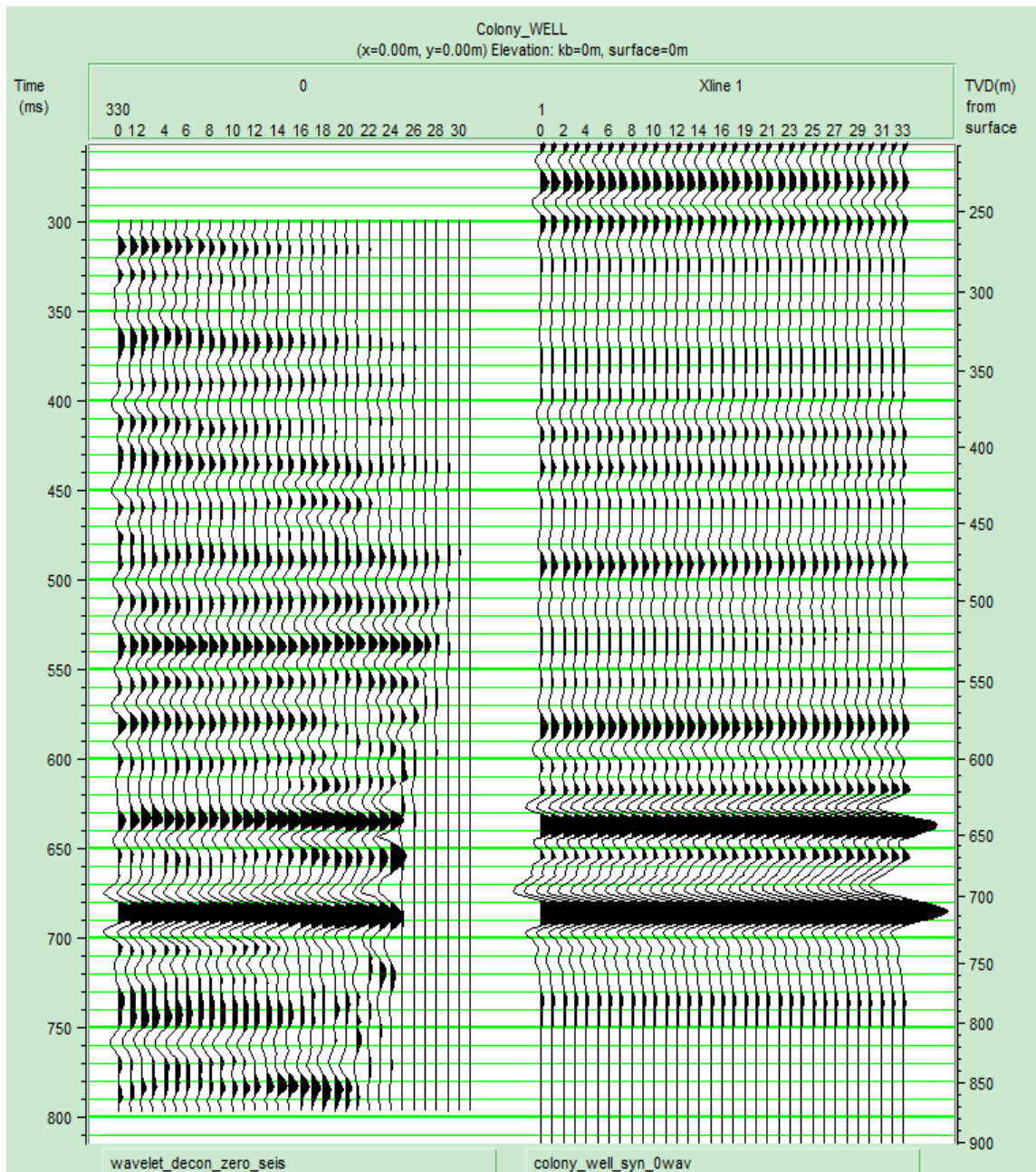


Figure 14a. Synthetic and seismic super-gather at location CDP330 in angle gather display, zero-phase

The synthetic and seismic traces thus constructed differ because the latter contain effects of propagation and anisotropy, whereas the former do not. We address these issues next.

2.3 Methodology development

With well logs of V_p , V_s , and density, we can do isotropic AVO forward modeling, using Zoeppritz equations or its approximations, to get synthetic seismic data. But we always find that the synthetic data and real seismic data differ from each other. It is partly because we do this modeling based on an isotropic assumption, whereas the seismic data contain anisotropic effects. And, it is partly because the real data contain effects of propagation, whereas the synthetic data do not. If we explore the differences between the synthetic one and the real one, we are able to extract the anisotropic information from these differences. We illustrate the theoretical development, using real examples from the Colony dataset.

2.3.1 Anisotropy parameters in reflection coefficient equation

Here we discuss the anisotropic reflection coefficient for P-waves, since these are most commonly used in exploration geophysics. Ruger (1997), based on Thomsen (1993), gave the linearized equation for plane-wave P-wave reflection at a planar interface separating two polar anisotropic media as:

$$R^{aniso}(\theta) = \frac{1}{2} \left[\frac{\Delta Z_0}{Z_0} \right] + \frac{1}{2} \left[\frac{\Delta V_{p_0}}{V_{p_0}} - \left(\frac{2\overline{V_{s_0}}}{V_{p_0}} \right)^2 \left[\frac{\Delta G_0}{G_0} \right] + (\delta_2 - \delta_1) \right] \sin^2 \theta + \frac{1}{2} \left[\frac{\Delta V_{p_0}}{V_{p_0}} + (\varepsilon_2 - \varepsilon_1) \right] \tan^2 \theta \sin^2 \theta \quad (2.5)$$

This differs from Equation (2.4) in two ways:

- Z_0, G_0, Vp_0, Vs_0 , are respectively the vertical P-impedance, shear modulus, P-velocity, and S-velocity; otherwise these terms are identical to the corresponding terms in (2.4).
- $\delta_1, \delta_2, \epsilon_1, \epsilon_2$ are the anisotropy parameters (Thomsen, 1986) for the two layers (layer 1 (above) and layer 2 (below the plane)). It is clear that the anisotropic effect on amplitudes is a simple difference in the reflectivity. It is also clear that, even though the anisotropic parameters are small compared to one, they are not necessarily small compared to the other terms in the equation, and should not be neglected.

The vertical P-wave velocity, S-wave velocity, and densities of the layers can be read from the well logs; hence we may refer to the isotropic parts of Eqn. (2.5) as the “sonic-band reflectivity”. As for θ , we use the incident phase angle (See Thomsen (1986) for discussion of the difference between wavefront-angle and ray-angle in anisotropic media). We can calculate by getting offset position from the SEG-Y file, and the depth of reflectors from the logs or VSP data, or from the moveout velocity. Alternatively, we could get velocity from Vp well logs, but they typically do not extend through the entire overburden, and they don’t contain the anisotropy in the velocities as the moveout velocities do, although the latter will be of poor vertical resolution. We can use ray tracing to get the P-wave reflection angle; the ray tracing work can be done by Hampson-Russell software, given a velocity function in the overburden. Hence, in the P-wave reflection coefficient calculation, the only unknown quantities are the anisotropic parameters.

Thus, the difference between anisotropic and isotropic reflection coefficients is, from (2.3) and (2.5):

$$R^{aniso}(\theta) - R^{iso}(\theta) = \Delta R^{aniso}(\theta) = \frac{1}{2}(\delta_2 - \delta_1)\sin^2\theta + \frac{1}{2}(\varepsilon_2 - \varepsilon_1)\tan^2\theta\sin^2\theta \quad (2.6)$$

And we can see that the anisotropy information is all contained in the difference of the synthetic and seismic, if the seismic data has been processed to only contain the primary reflections, without propagation effect and other noise.

2.3.2 Connection between synthetic and real seismic amplitude

Besides the offset-dependence of reflection coefficient of the layers, there are many other factors which affect the amplitude of the reflected wave recorded in the SEG-Y file, as functions of offset. Some factors are from the subsurface, such as attenuation/dispersion, geometrical spreading, random noise, transmission coefficients in the overburden, focusing/defocussing, non-planar reflectors, surface ghost, receiver ghost, multiple interference, etc.

Some other factors are from the recorded wavelet, such as the source radiation pattern, the geophone response, and the array response. So the real seismic data used for calculation must be processed to eliminate the factors mentioned above. But processing itself can affect the amplitude, too. For example, the processing may include various filtering and scaling operations that affect the amplitude as a function of offset.

All of these effects operate on the real wave, and they all affect the received amplitudes, variably with offset. When we normalize the real data to the synthetic data, we are implicitly correcting the real data for all of these, even without knowing any of the details, leaving the normalized amplitudes representing only the reflectivity.

With this understanding, we can refine Eqn. (2.6). We use S_0 , $P_{\downarrow}(\theta, t)$, $P_{\uparrow}(\theta, t)$ and $I(t)$ respectively to express, respectively the wavelet strength, downward wave propagation operator, upward wave propagation operator, and instrumental effects, all of these operating sequentially on the initial wavelet $w_0(t)$. Since many of these effects operate differently on different frequency components, in the time domain it appears as a series of convolutions:

$$s(\theta, t) = I(t) * P_{\uparrow}(\theta, t) * r(\theta, t) * P_{\downarrow}(\theta, t) * w_0(t) S_0(\theta) \quad (2.7a)$$

Since convolution commutes, we can re-write this as

$$\begin{aligned} s(\theta, t) &= [I(t) * P_{\uparrow}(\theta, t) * P_{\downarrow}(\theta, t) * S_0] w_0(t) * r(\theta, t) \\ &\equiv P(\theta, t) * w(t) * r(\theta, t) \end{aligned} \quad (2.7b)$$

where all of these propagation and instrumental effects are included in the propagation operator $P(\theta, t)$. Note that, as defined here, P operates on the wavelet $w(t)$, which can be determined from the seismic data using conventional techniques, rather than the initial wavelet $w_0(t)$, which is not easily determined.

To find the propagation operator $P(\theta, t)$, the conventional procedure is to:

- Use logs to compute the isotropic reflectivity $R_{pp}^{iso}(z, \theta)$, using equation (2.6).
- Convert depth to time, for example using the functionality present in H-R software, producing $R_{pp}^{iso}(t, \theta)$.
- Convolve this with the seismic wavelet $w(t)$ (determined from seismic data) to produce a synthetic seismic trace

$$S(t, \theta) \equiv R_{pp}^{iso}(t, \theta) * w(t) \quad (2.8)$$

- Define a normalization factor $N(\theta, t)$ (can be done with various methods), converting seismic amplitudes (typically lying between +/- 1000) to isotropic reflectivity (typically lying between +/- 0.1), band-limited by convolution with the seismic wavelet,
- Multiply the seismic trace (2.7b) by $N(\theta, t)$, forcing the seismic trace amplitudes to match the isotropic reflectivity.
- Set the normalized seismic data (2.9) equal to the isotropic synthetic data (2.8):

$$N(\theta, t) \times s(\theta, t) = N(\theta, t) \times P(\theta, t) * w(t) * r(\theta, t) \approx w(t) * R_{pp}^{iso}(\theta, t) \quad (2.9)$$

This procedure clearly assumes that

$$N(\theta, t) \times P(\theta, t) = 1 \quad (2.10)$$

The procedure also assumes that the reflections are isotropic:

$$r(\theta, t) = R_{pp}^{iso}(\theta, t) \quad (2.11)$$

The novelty introduced in the present proposal is two-fold:

- a) We normalize the seismic to the synthetic in an angle-dependent way, as described further below;
- b) We separate the normalization into a low-frequency part and a high-frequency part, and use only the former for normalization. As described further below, the residuals, after this partial normalization, are attributed to anisotropy.

Taking these in order:

The isotropic reflectivity equation (2.3) can be written as Aki-Richards' approximation, for an event at t_0 , as

$$R^{iso}(t_0, \theta) = A(t_0) + B(t_0)\sin^2 \theta + C(t_0)\sin^2 \theta \tan^2 \theta \quad (2.12)$$

where the coefficients A, B, C are given implicitly in equation (2.3). The Aki–Richards' equation is valid for reflection angles up to about 40°, and for isotropic layers only. As the angle range in the gathers is from 0° to 30°, we are safe to use it here.

As t_0 varies through the logged interval, this makes a spike series, with the time-resolution of the logs. After convolving with the wavelet (equation (2.8)), we have a synthetic trace with the resolution of the wavelet:

$$S(t_0, \theta) = \left[A(t_0) + B(t_0)\sin^2 \theta + C(t_0)\sin^2 \theta \tan^2 \theta \right] * w(t_0) \quad (2.13)$$

In a similar way, we can parameterize the offset-dependence of the flattened seismic gather, in the angle-domain as:

$$s(t_0, \theta) = \left[A_{seis}(t_0) + B_{seis}(t_0)\sin^2 \theta + C_{seis}(t_0)\sin^2 \theta \tan^2 \theta \right] * w(t_0) \quad (2.14)$$

If the seismic gather has zero phase, we can pick the major peaks (and troughs) of the traces $s(t_0, \theta)$, identify these with the major reflecting horizons, and find best-fit values of A_{seis} , B_{seis} , and C_{seis} for each of these major events.

We are not able to detect every impedance layer from the synthetic and seismic, we can only pick some obvious events from comparison of the seismic and synthetic. The picked events may not be representative of all the reflection interfaces, so we only try to solve the anisotropy for the picked horizons.

Here we pick the major events on synthetic and seismic zero phase. All the 6 horizons are displayed in Figure.14b. The horizons are all picked using Hampson-Russel AVO package 'Horizon selection' function.

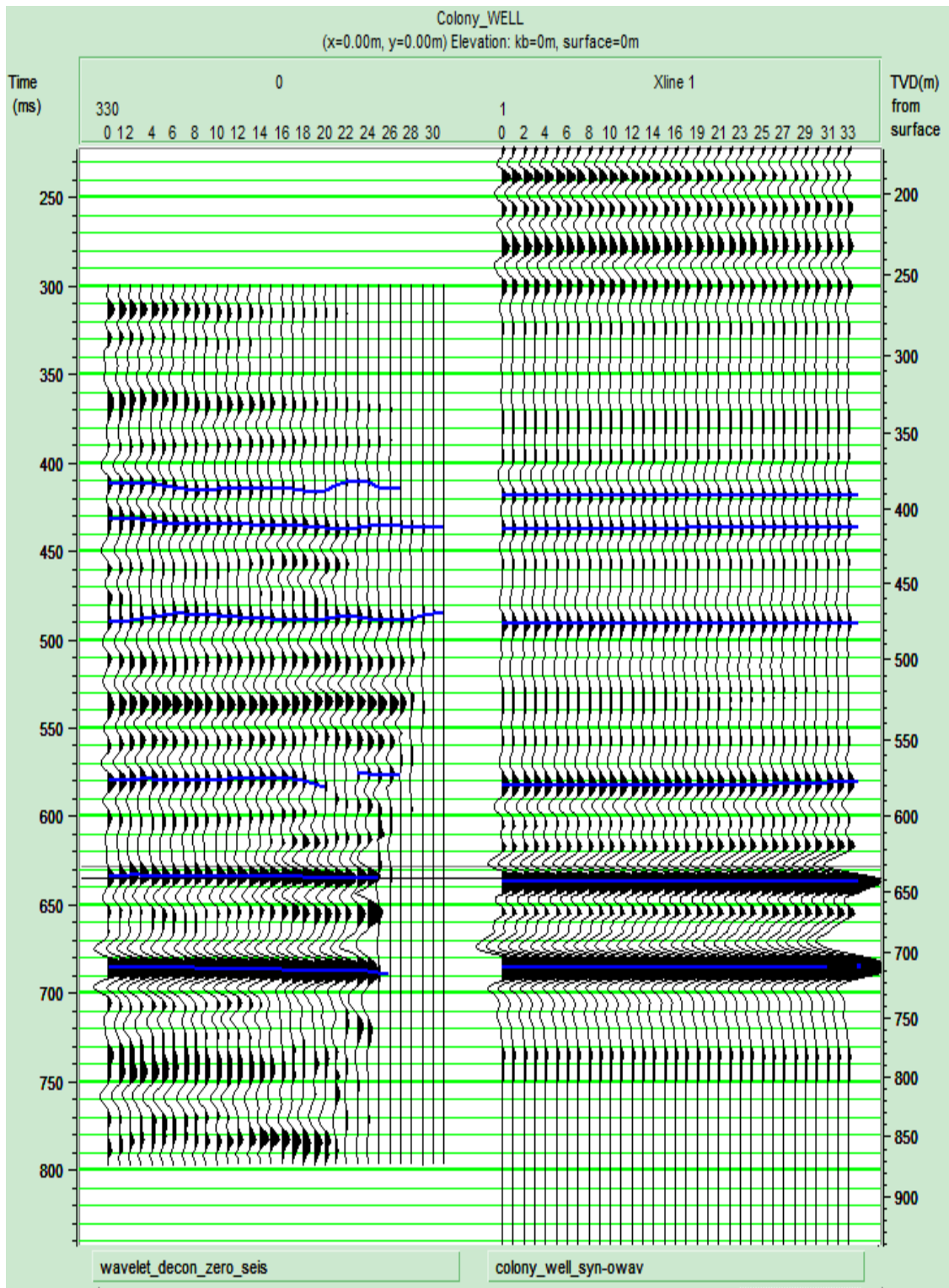


Figure 14b. Horizons picked on both seismic and synthetic in angle domain, zero phase

Figures 15a-f show the picked amplitudes, as functions of angle θ , for each of the six major seismic events. They also show, as continuous lines, the fitted curves (Eqn.2.14) for each event, constructed with the best-fit parameters using least-square method.

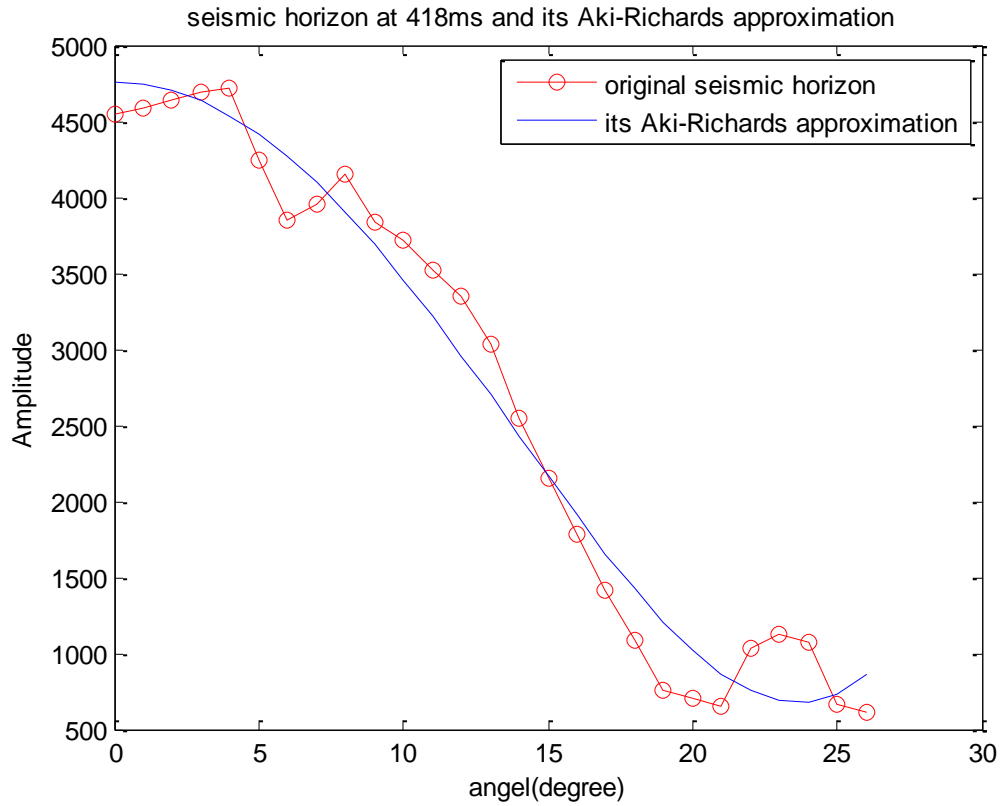


Figure 15a. Seismic horizon at 418ms and its Aki-Richards approximation

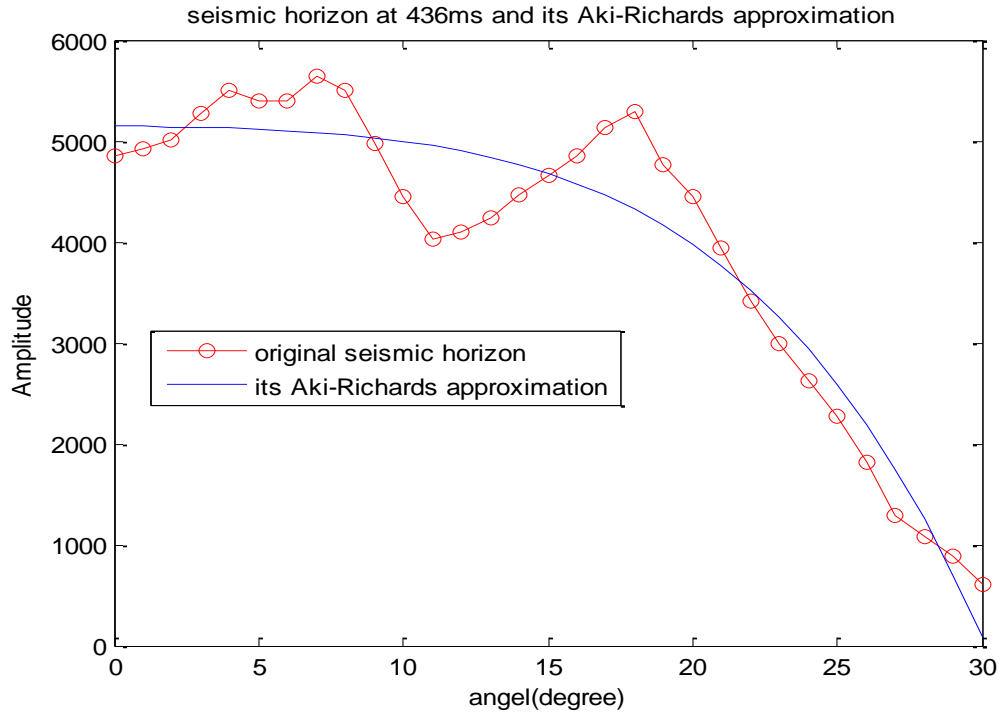


Figure 15b. Seismic horizon at 436ms and its Aki-Richards approximation

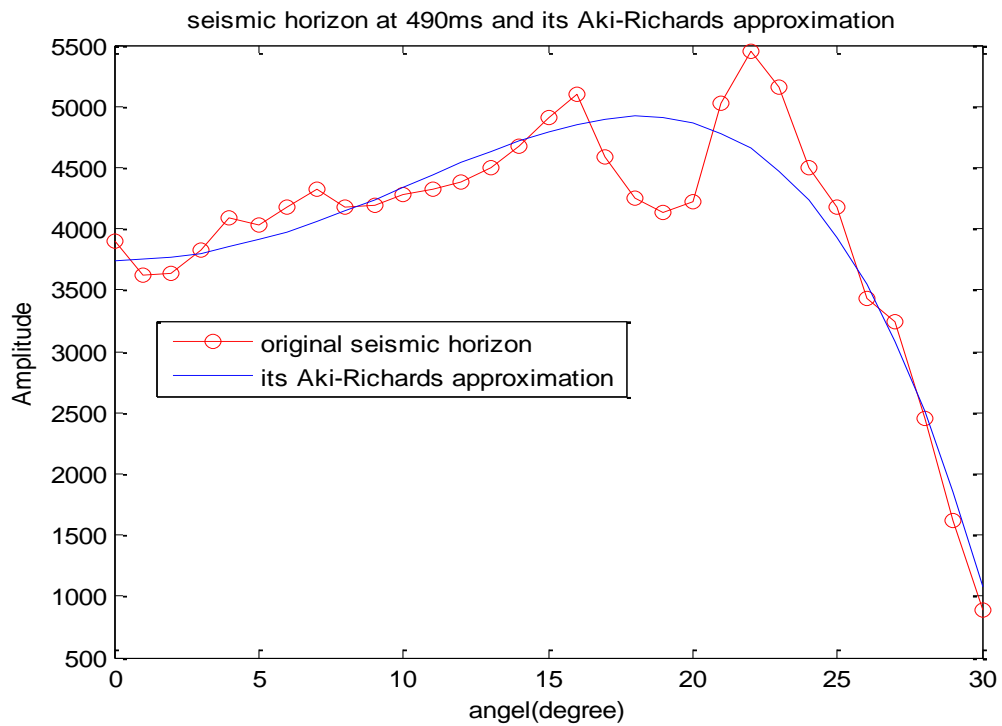


Figure 15c. Seismic horizon at 490ms and its Aki-Richards approximation

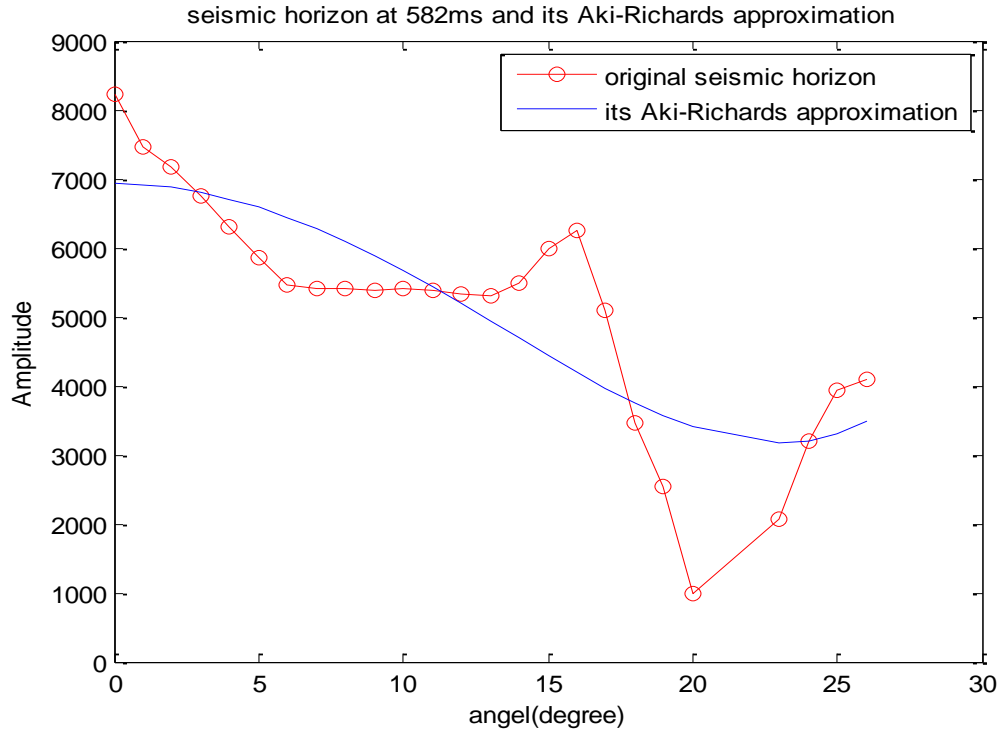


Figure 15d. Seismic horizon at 582ms and its Aki-Richards approximation

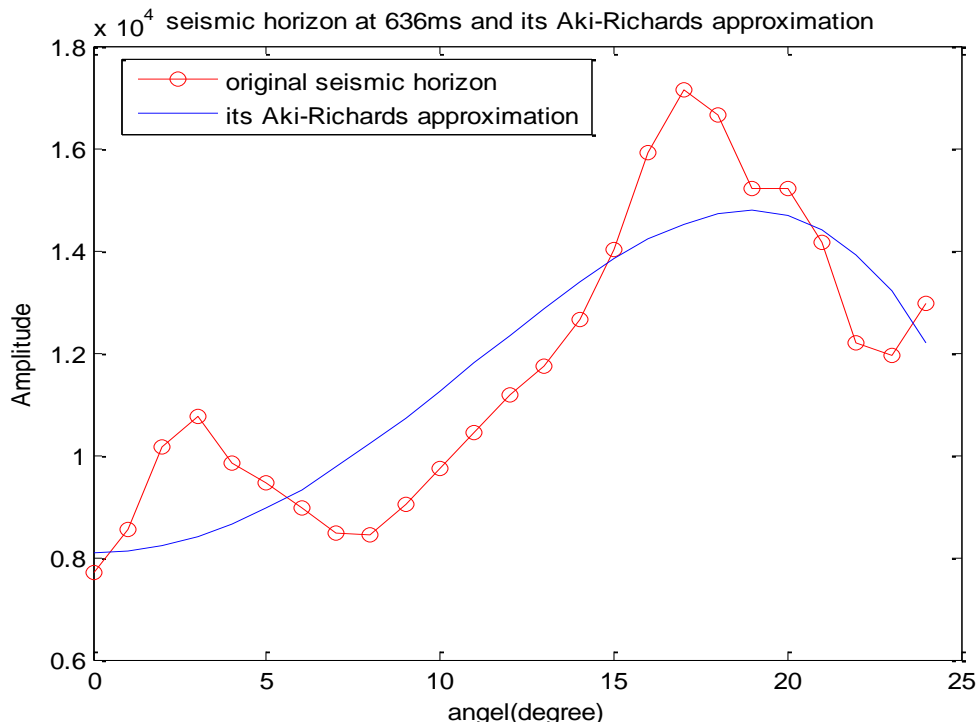


Figure 15e. Seismic horizon at 636ms and its Aki-Richards approximation

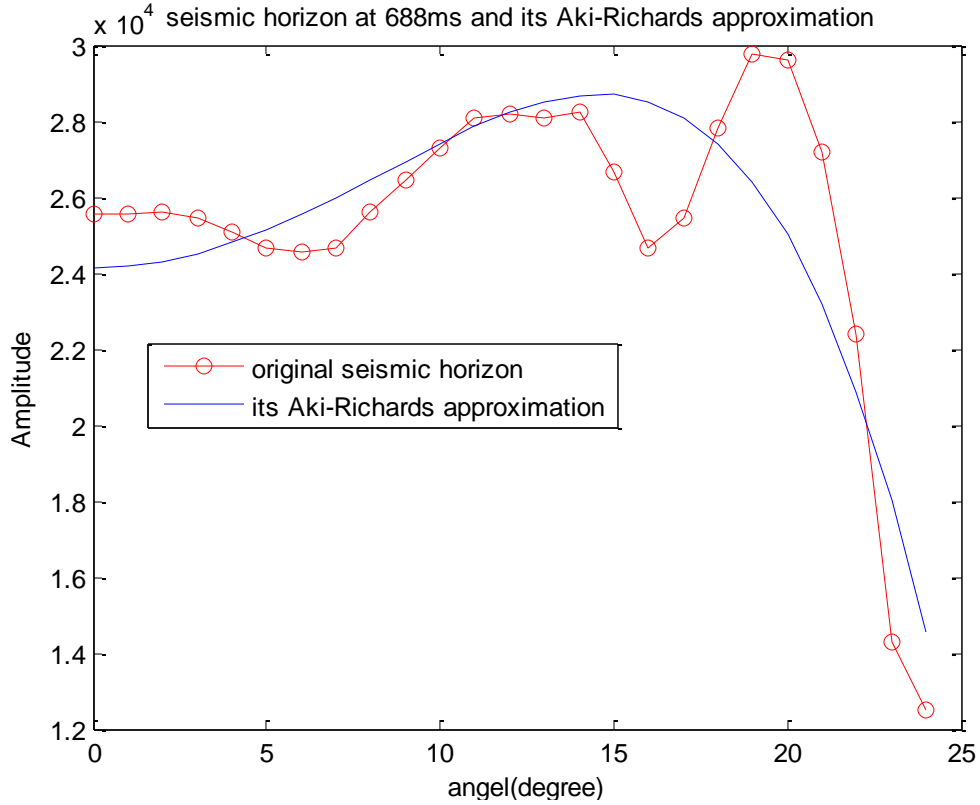


Figure 15f. Seismic horizon at 688ms and its Aki-Richards approximation

All of these figures (15a-f) show major deviations from the fitted curves, especially at large angles. This confirms the common understanding that the curvature terms of the Aki-Richards equation (2.12) are poorly determined, so that their interpretation is problematic. The deviations may be due to interference from multiples, not accounted for in prior processing. In any case, addressing this variation is outside the scope of the present work. We carry forward the analysis of the curvature in any case, anticipating that the derived values for ϵ may be spurious.

Figure 16 shows the derived parameters A_{seis} , B_{seis} , C_{seis} .

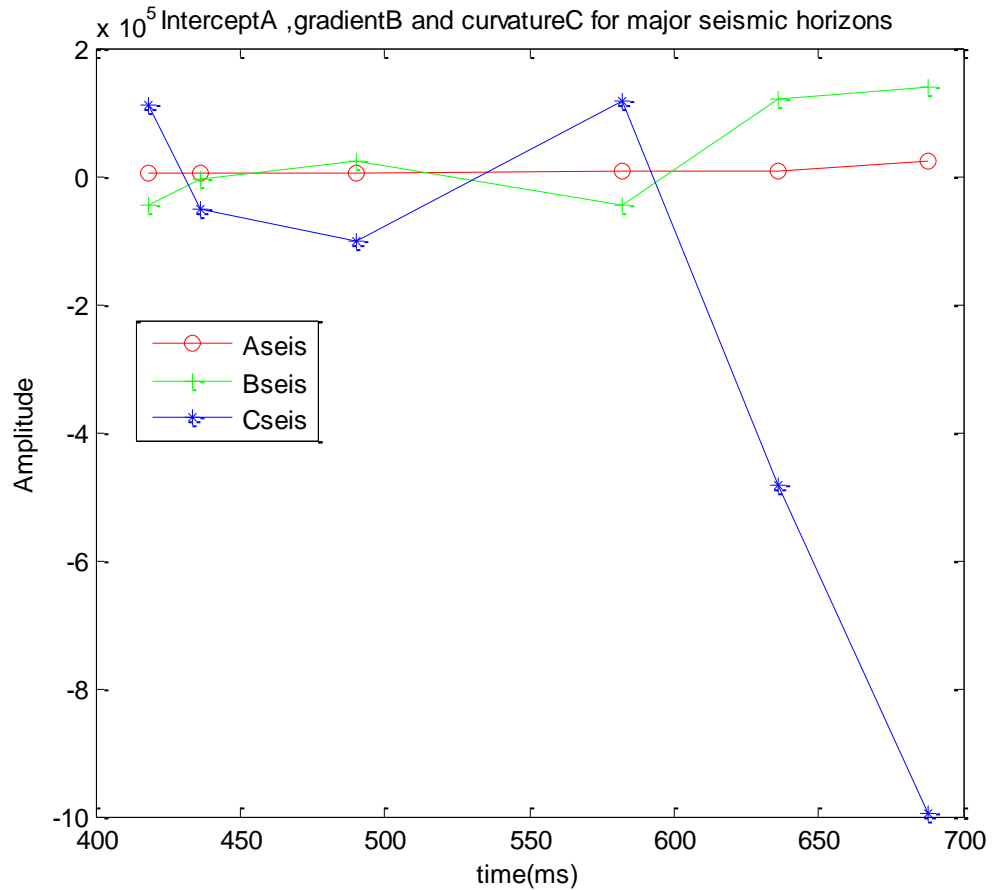


Figure 16. Amplitude intercept A ,gradient B and curvature C for the major seismic horizons, zero phase

Of course these offset parameters are not directly comparable to reflectivity parameters (2.12) because they contain the propagation effects as well as the reflection effects; we address this issue with the normalization argument in section b).

Further, we cannot directly compare *Aseis*, *Bseis*, and *Cseis*, even after normalization, with the parameters in equation (2.12) simply by reading off the values of A, B, and C from the logs. The reason is that the convolution operation “folds together” the

contribution from nearby events; we need to estimate A, B, and C in a band-limited way, on the synthetic, just as we did with the seismic. If the wavelet $w(t)$ has zero phase, we pick the same major peaks (or troughs) of these functions $A(t_0)*w(t)$ etc. (as we did on the seismic), and find best-fit parameters $A_{syn}, B_{syn}, C_{syn}$ for the major reflectors.

Figures 17a-f show the picked amplitudes, as functions of angle θ , for each of the six major synthetic event. They also show, as continuous lines, the fitted curves (2.12) for each event, constructed with the best-fit parameters.

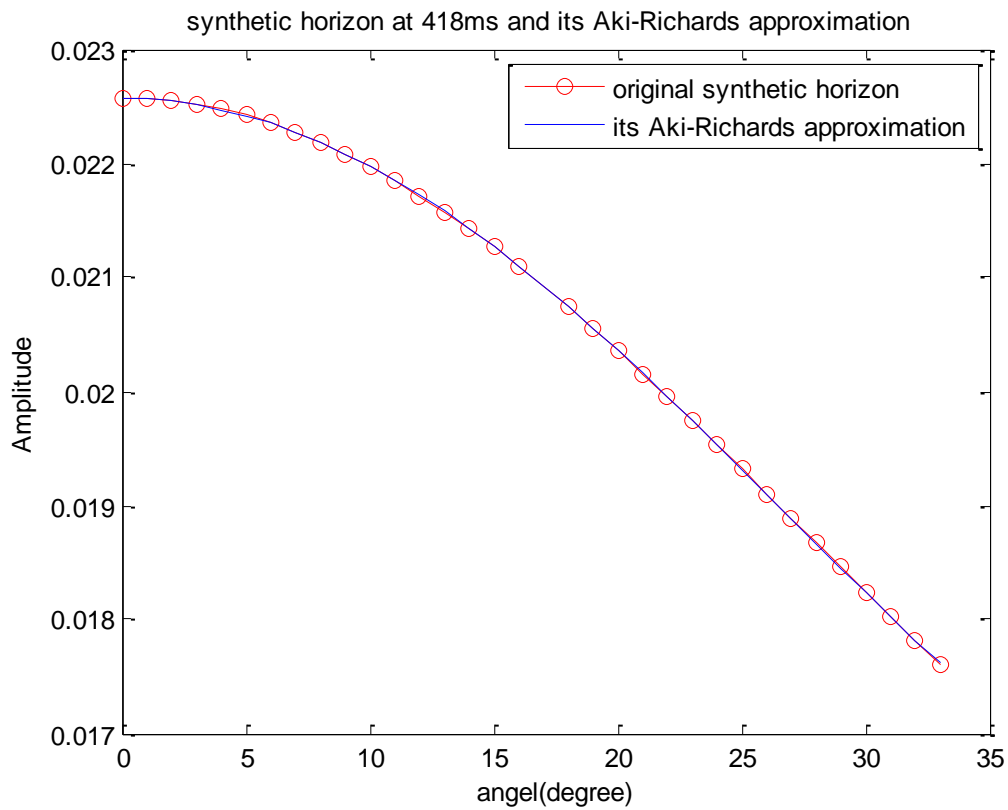


Figure 17a. Synthetic horizon at 418ms and its Aki-Richards approximation

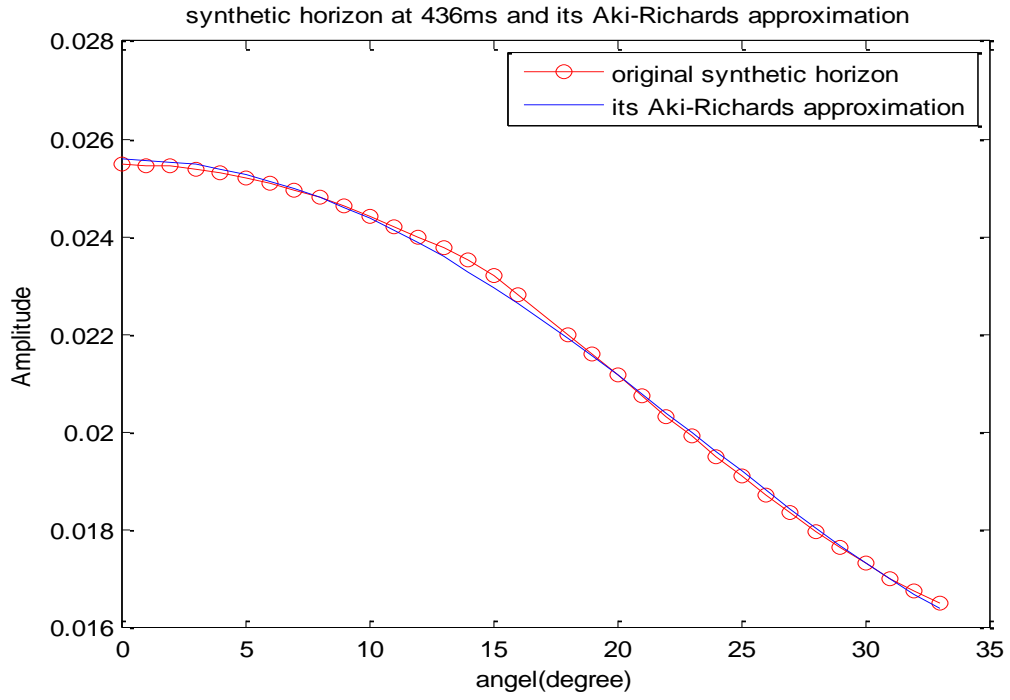


Figure 17b. Synthetic horizon at 436ms and its Aki-Richards approximation

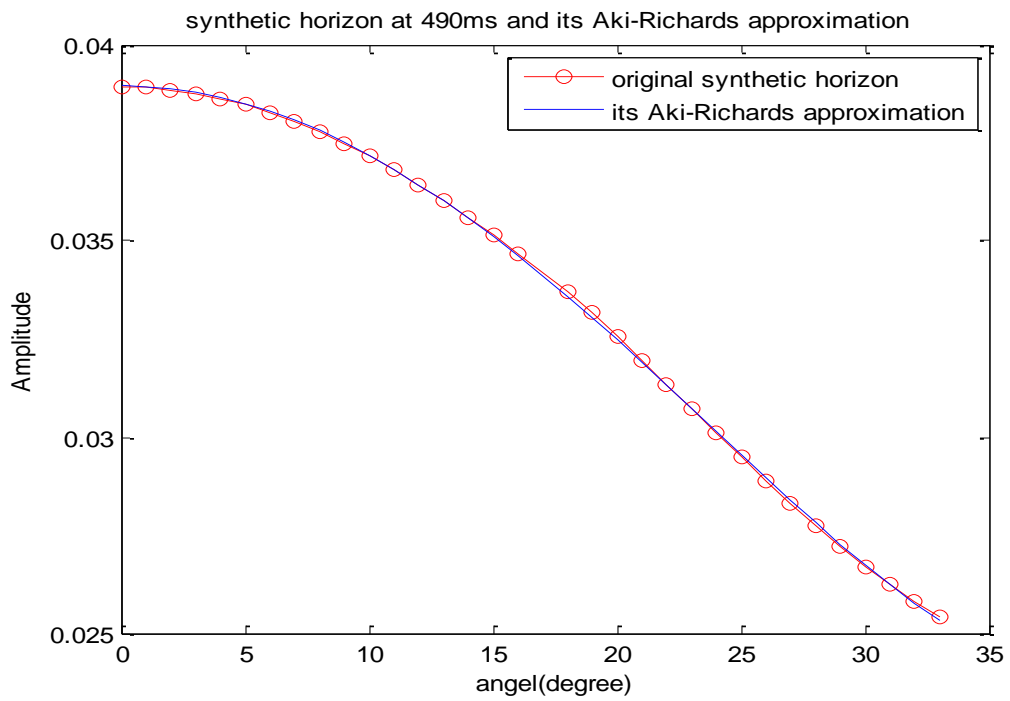


Figure 17c. Synthetic horizon at 490ms and its Aki-Richards approximation

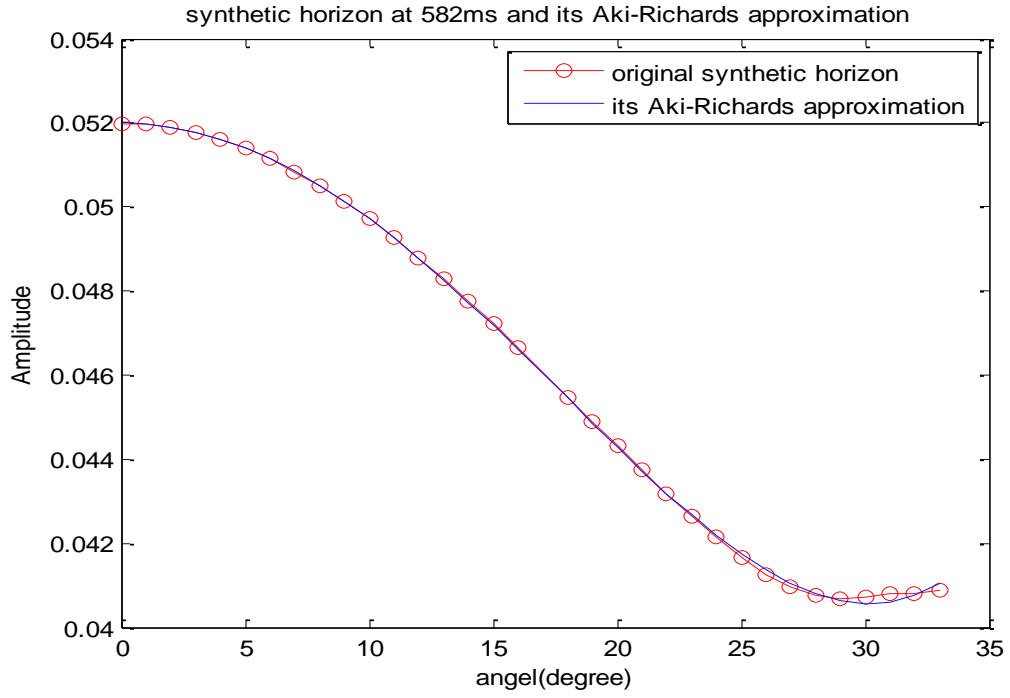


Figure 17d. Synthetic horizon at 582ms and its Aki-Richards approximation

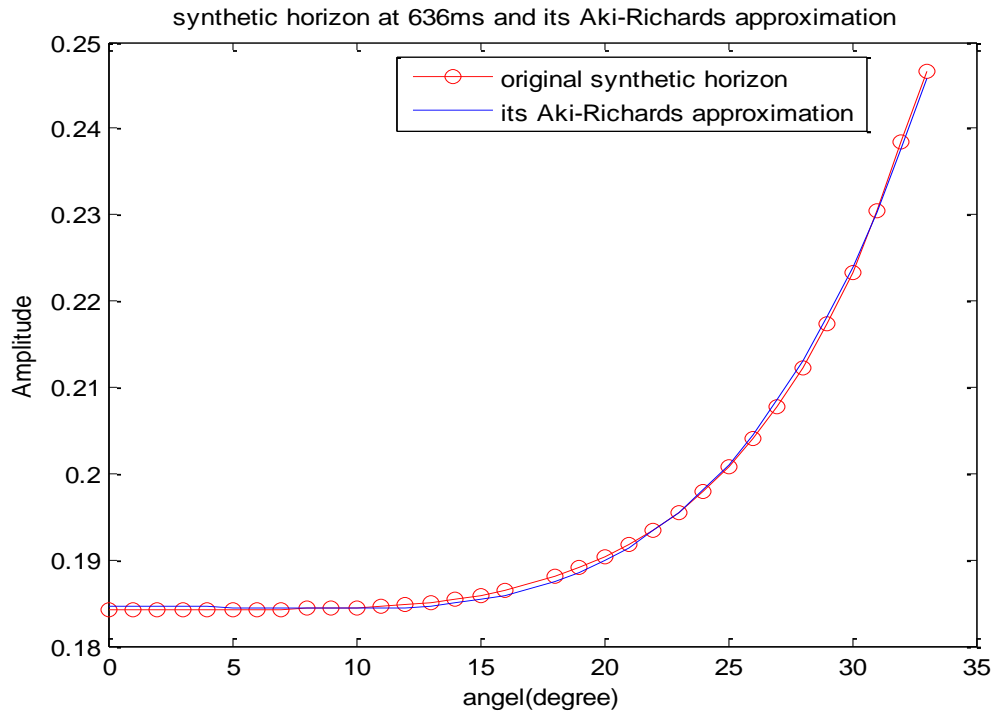


Figure 17e. Synthetic horizon at 636ms and its Aki-Richards approximation

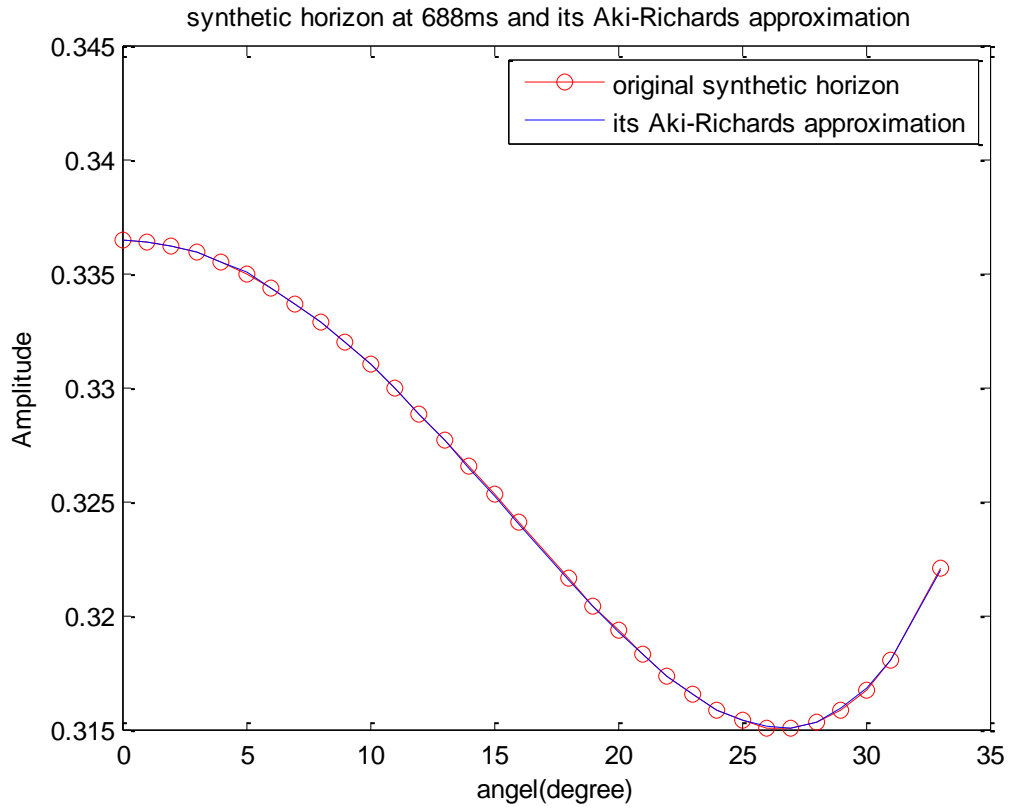


Figure 17f. Synthetic horizon at 688ms and its Aki-Richards approximation

As anticipated, the fits here are excellent (by construction), in strong contrast with figures (15a-f). Figure 18 shows the derived parameters A_{syn} , B_{syn} , C_{syn} . Note that A_{syn} and C_{syn} are positively correlated, (because of the correlation between impedance and velocity), whereas in Figure 16, A_{seis} and C_{seis} are anticorrelated.

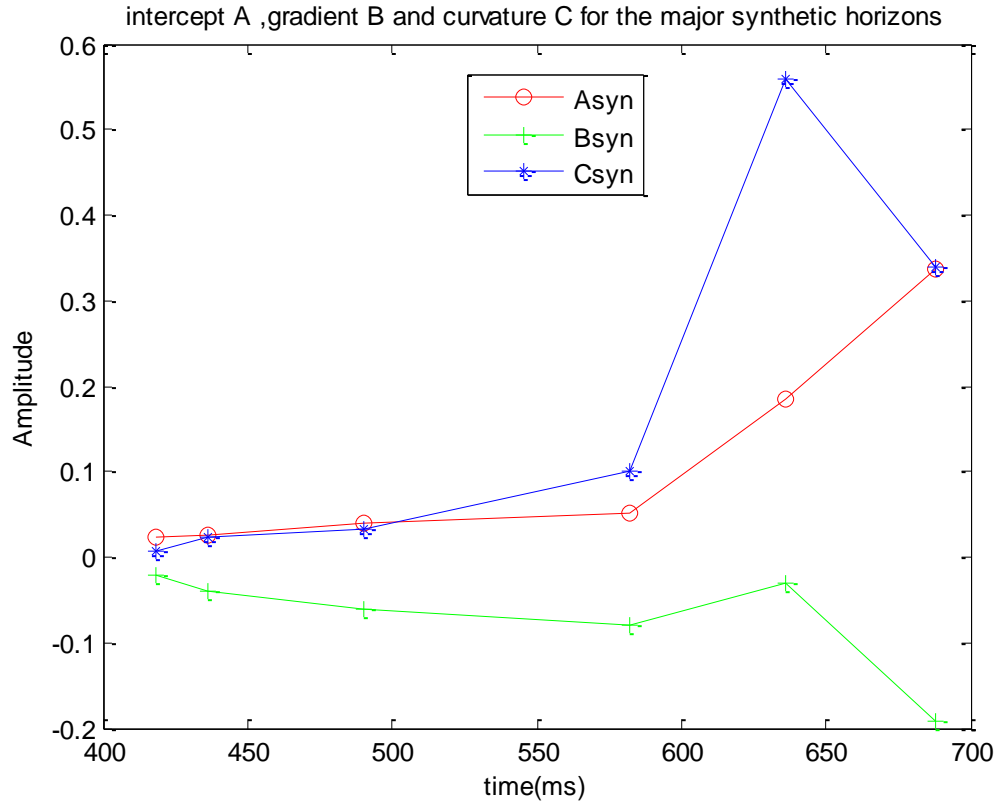


Figure 18. Amplitude intercept A, gradient B and curvature C for the major synthetic horizons, zero phase

Then convolution of these values with the wavelet produces an isotropic synthetic gather:

$$S(t_0, \theta) = A_{syn}(t_0) + B_{syn}(t_0) \sin^2 \theta + C_{syn}(t_0) \sin^2 \theta \tan^2 \theta \quad (2.15)$$

2.3.3 Using normalization factor in anisotropy parameter estimation

2.3.3.1 Getting normalization factor for intercept A, gradient B and curvature C

Now that we have characterized, the AVO behavior, separately for synthetic and seismic, we have to normalize them, in order to compare them. We can see that the seismic amplitude is of much bigger magnitude than that of synthetic. The amplitude for seismic is around +/-10000 while the synthetic amplitude is around +/-0.1.

We do this in several stages. First, we convert the seismic amplitudes in (2.14) to approximate reflectivity amplitudes by normalizing (2.14) with a constant normalization factor N_0 , based upon the average of the $A(t_0)$, function, so that they may be displayed together with the synthetic values. Specifically, we calculate

$$\begin{aligned} |A_{syn}| &\equiv \langle |A_{syn}(t_0)| \rangle; \\ |A_{seis}| &\equiv \langle |A_{seis}(t_0)| \rangle; \\ N_0 &\equiv \frac{|A_{syn}|}{|A_{seis}|} \end{aligned} \tag{2.16}$$

where the angle brackets indicate the arithmetic average, over the selected major events. We calculate with the absolute values, as shown, since we want for N_0 to be a positive number, adjusting all events (both + and -) only for this scale factor. For the Colony dataset, as prepared above, we obtain $N_0 = 1.1007e-005$.

Then we adjust each of the seismic AVO parameters by this scale factor:

$$\begin{aligned}
 A_{seis}^*(t_0) &= N_0 A_{seis}(t_0); \\
 B_{seis}^*(t_0) &= N_0 B_{seis}(t_0); \\
 C_{seis}^*(t_0) &= N_0 C_{seis}(t_0)
 \end{aligned}
 \tag{2.17}$$

Now the seismic and synthetic AVO parameters have comparable scales, so that we can plot them together, preparing for further adjustment. Figure 19 shows both $A_{syn}(t_0)$ and $A_{seis}^*(t_0)$ on the same plot for the major events of the Colony dataset; you can see that they still have significant differences. Figures 20 and 21 show the same information for the gradient parameters B and the curvature parameters C.

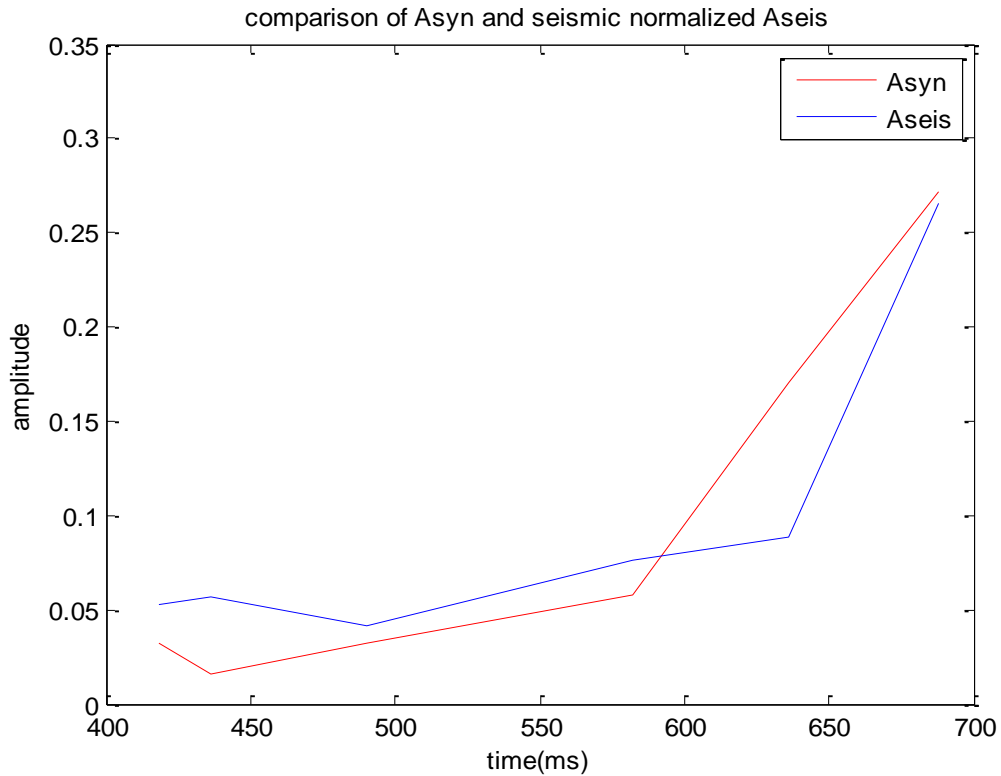


Figure 19. Comparison of Asyn and Aseis

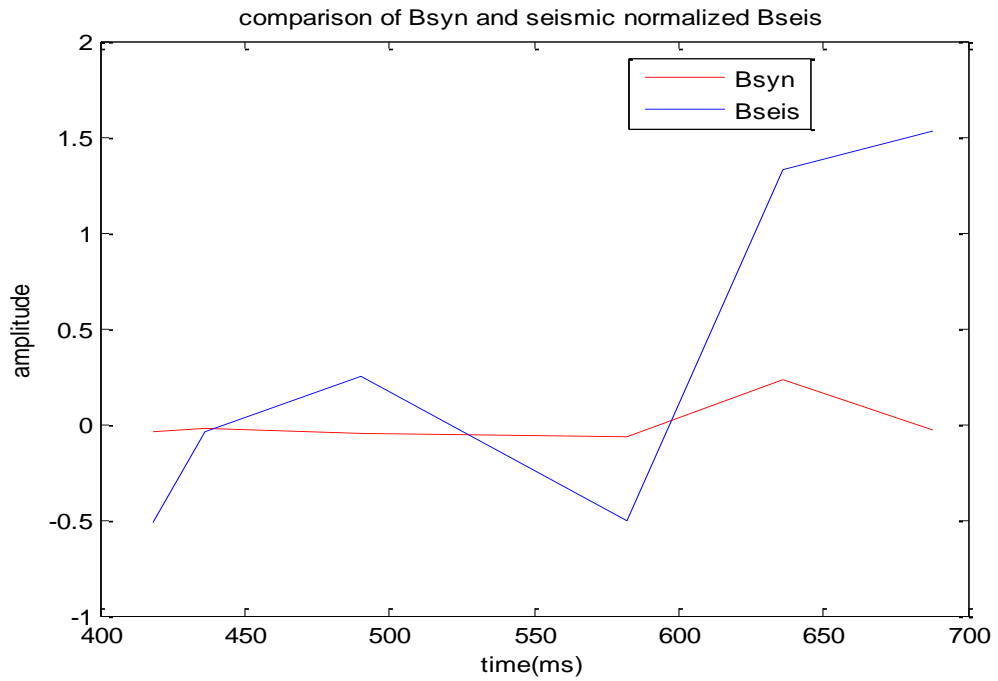


Figure 20. Comparison of Bsyn and Bseis

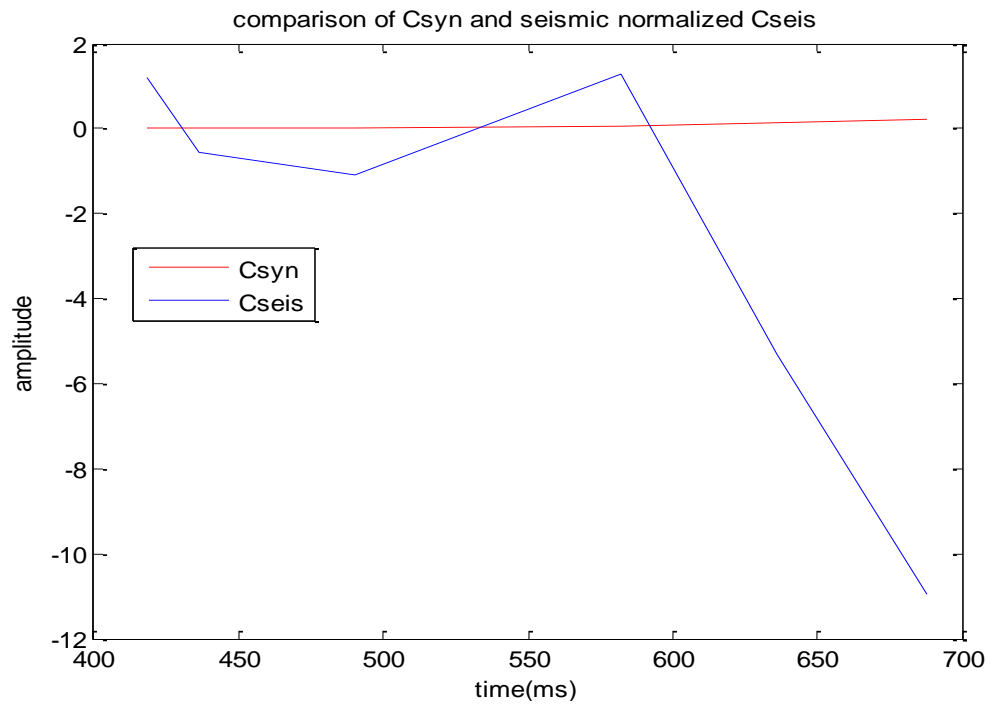


Figure 21. Comparison of Csyn and Cseis

The differences evident between seismic and synthetic parameters include both propagation effects, and anisotropy effects. If there were no anisotropy effects, we could completely account for the propagation effects by constructing normalization factors

$$\begin{aligned}
 N_A(t_0) &\equiv A_{syn}(t_0) / A_{seis}^*(t_0) \\
 N_B(t_0) &\equiv B_{syn}(t_0) / B_{seis}^*(t_0) \\
 N_C(t_0) &\equiv C_{syn}(t_0) / C_{seis}^*(t_0)
 \end{aligned}
 \tag{2.18}$$

Figures 22, 23, and 24 show these normalization functions, for the Colony dataset.

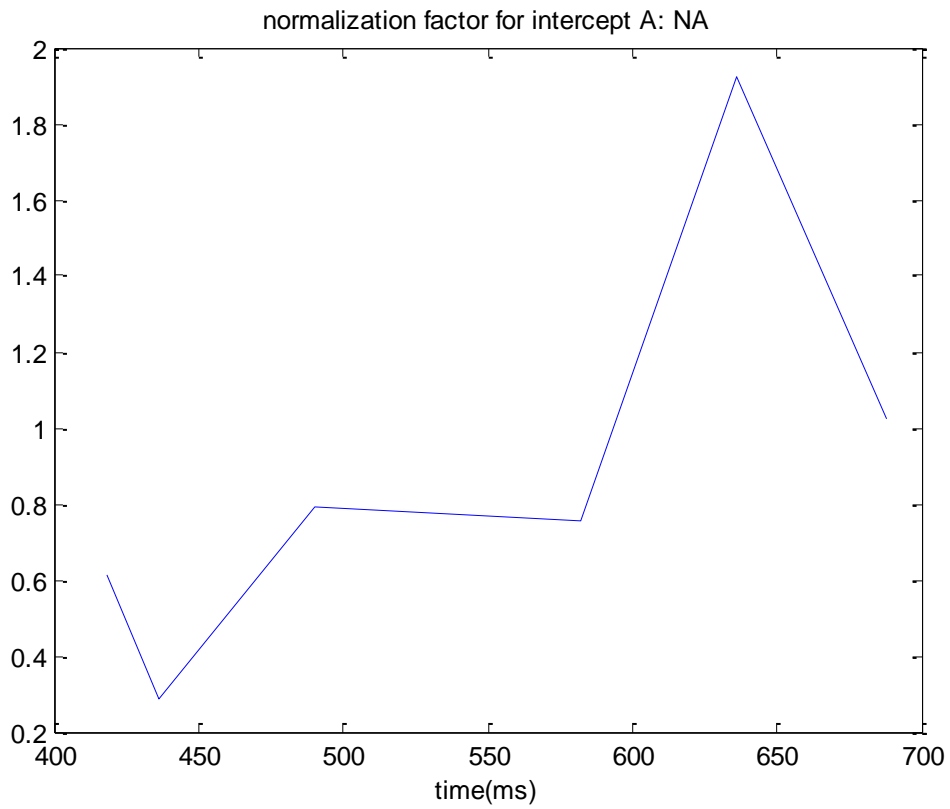


Figure 22. Normalization factor for intercept A: NA

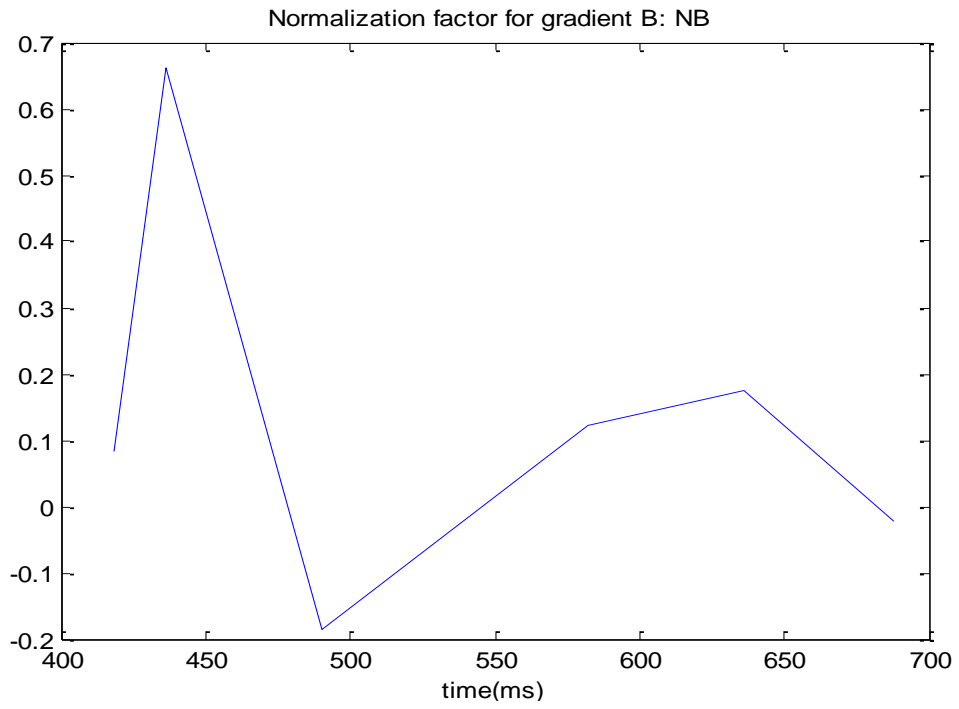


Figure 23. Normalization factor for gradient B: NB

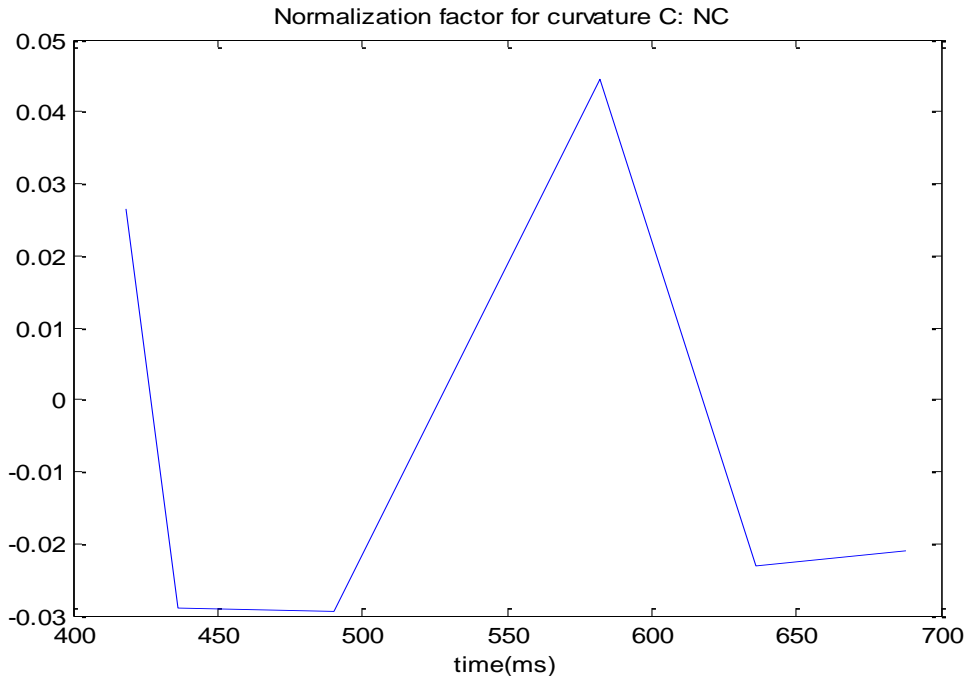


Figure 24. Normalization factor for gradient C: NC

It is clear that applying these angle-specific normalization factors to the seismic gathers (2.12) would convert them into the isotropic synthetic gather (2.13), and that this constitutes a refinement of the “conventional” procedure described above. However, we want to avoid this assumption of isotropy.

2.3.3.2 Low-cut the normalization factor NB and NC

However, we recognize that these normalization functions $N_A(t_0)$, $N_B(t_0)$, and $N_C(t_0)$, are measured over the entire logged interval, and can be analyzed as Fourier series, with spectra $N_A(f)$, $N_B(f)$, and $N_C(f)$. Because reflection amplitude (calculated from either anisotropic or isotropic expressions) varies rapidly as a function of depth or time, this contributes to the high-frequency portion of these spectra. However, the propagation effects mentioned above (except for the reflection coefficient) accumulate progressively as the wave propagates; hence they are represented by the low-frequency portion of these spectra.

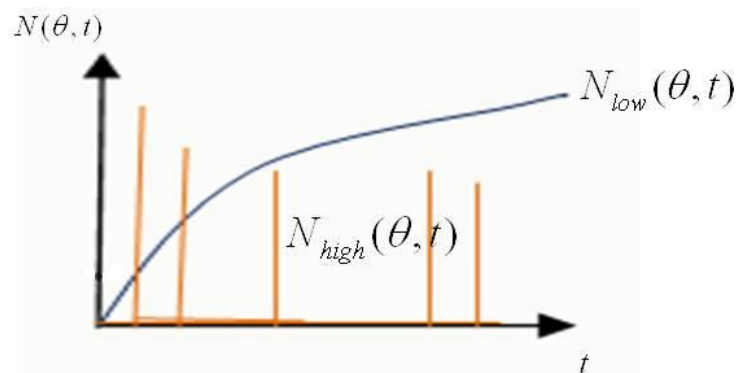


Figure 25. High and low component of normalization factor $N(\theta, t)$

Therefore we low-cut filter the normalization functions, and call these filtered functions

$$N_{A_{low}}(\theta, t_0), N_{B_{low}}(\theta, t_0), N_{C_{low}}(\theta, t_0).$$

In practice, for the Colony dataset, the logged interval is too short, and the major reflectors too sparse to make a well-behaved filter operation. So, we have implemented the following procedure, equivalent for this dataset: we find the least-squares best-fit linear function, which accounts for the low-order time-variation in each of the normalization functions above. Specifically, we compute $N_{A_{low}}(t_0)$ as the straight line which best approximates (in the least-squares sense) the function $|N_A(t_0)|$ as defined above. This straight line $N_{A_{low}}(t_0)$ is also shown in Figure 26. Similarly, we compute $N_{B_{low}}(t_0)$ and $N_{C_{low}}(t_0)$; these straight lines are shown in figures 27 and 28.

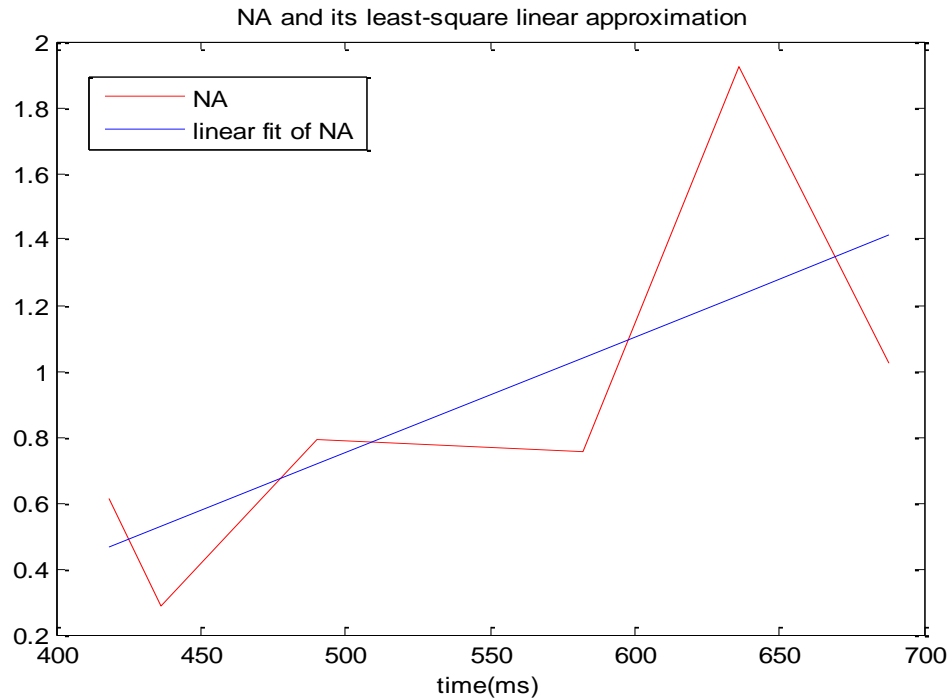


Figure 26. NA and its linear least-square fit

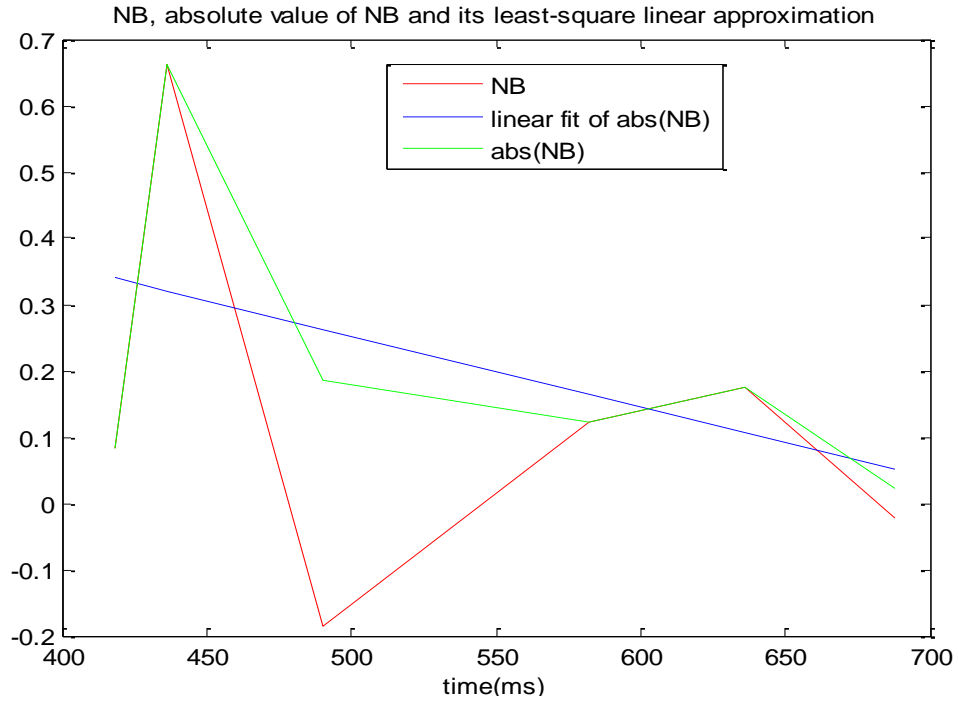


Figure 27. NB, the absolute value of NB and its linear least-square fit

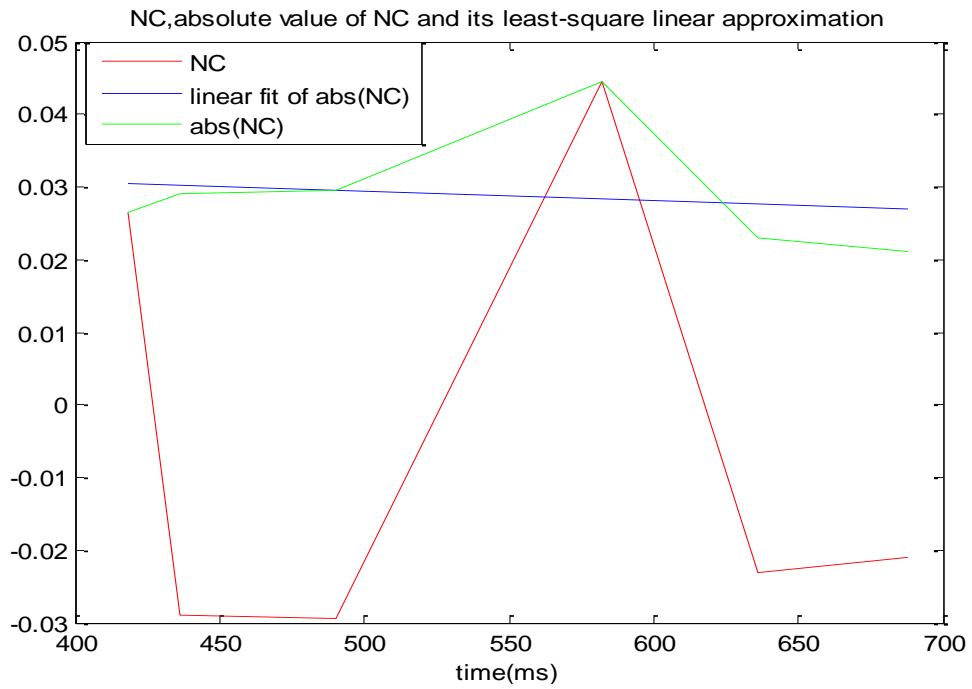


Figure 28. NC, the absolute value of NC and its linear least-square fit

This procedure approximately removes the (low-frequency) propagation effects, without damaging the (high-frequency) reflectivity effects, which contain the anisotropy.

Then we construct low-cut seismic parameters

$$\begin{aligned}
 A_{seislow}(t_0) &= N_{Alow}(t_0) \times A_{seis}^*(t_0) \\
 B_{seislow}(t_0) &= N_{Blow}(t_0) \times B_{seis}^*(t_0) \\
 C_{seislow}(t_0) &= N_{Clow}(t_0) \times C_{seis}^*(t_0)
 \end{aligned} \tag{2.19}$$

These are observable quantities, calculable from the data, as described above.

As is evident from Figure 26, the normalization factor N_A does contain some (minor) high-frequency variation. Since this is a normal-incidence parameter, this high-frequency variation cannot be explained by neglected anisotropy. In fact, within the present assumptions, there is no satisfactory explanation of this high-frequency variation in N_A . A revision of these standard assumptions is beyond the scope of this M.S. thesis, as it would constitute a deep revision in conventional thinking about the reflection process. So, for now, we ignore this variation, keeping in mind that it might affect subsequent conclusions.

1) Get residual gradient ΔB and residual curvature ΔC

Now we already have N_{Blow} and N_{Clow} . We can get the ΔB and ΔC for the final calculation about anisotropy parameters δ and ε .

$$\begin{aligned}
 \Delta B(t_0) &= B_{seislow}(t_0) - B_{syn}(t_0) \\
 \Delta C(t_0) &= C_{seislow}(t_0) - C_{syn}(t_0)
 \end{aligned} \tag{2.20}$$

The plot of the $B_{seislow}$ and B_{syn} is:

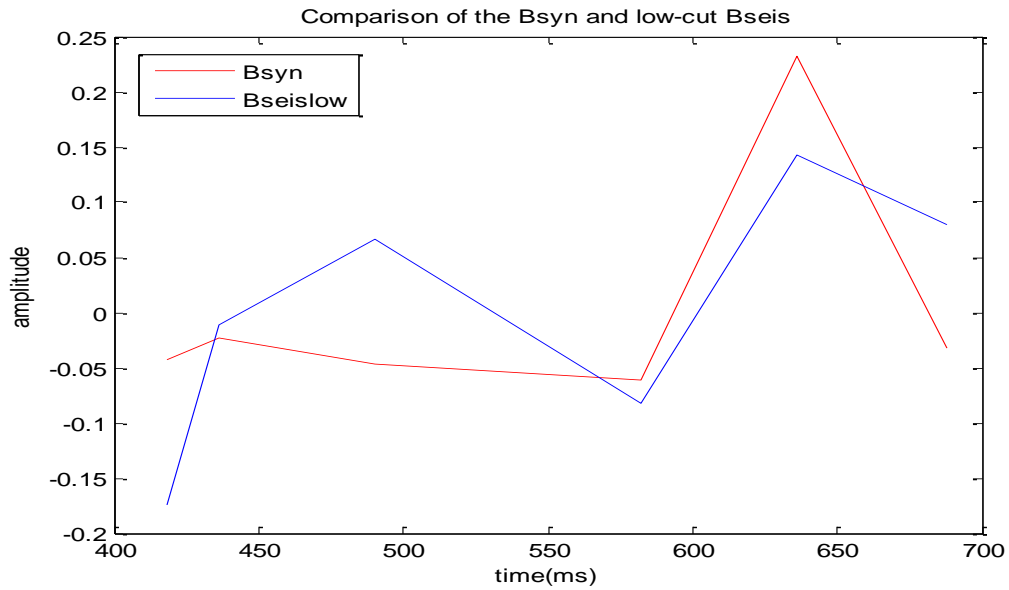


Figure 29. $B_{seislow}$ and B_{syn} comparison

The plot of the $C_{seislow}$ and C_{syn} is:

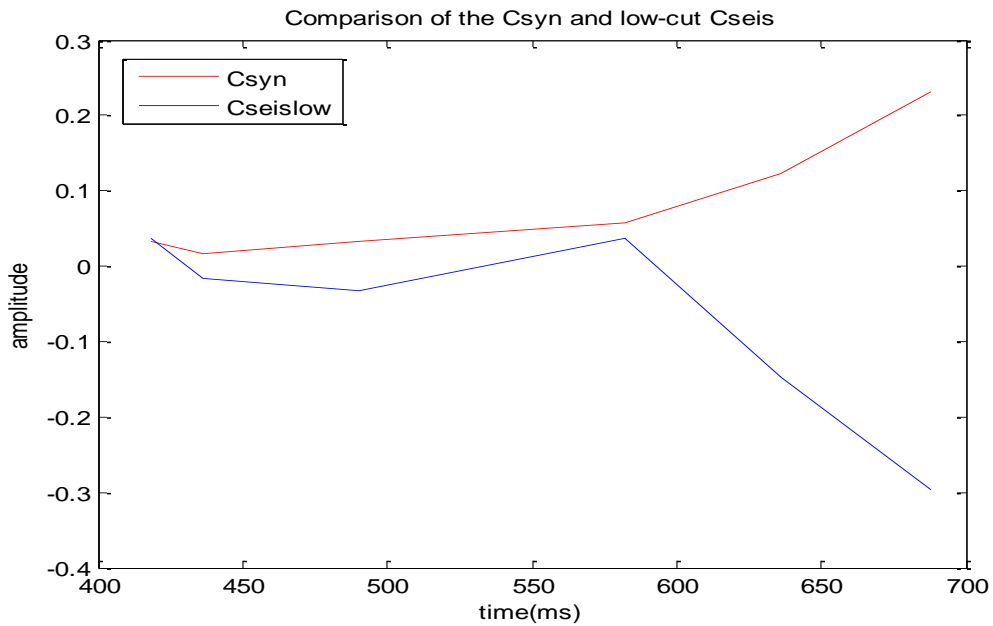


Figure 30. $C_{seislow}$ and C_{syn} comparison

The difference of $B_{seislow}$ and B_{syn} is ΔB , its plot is:

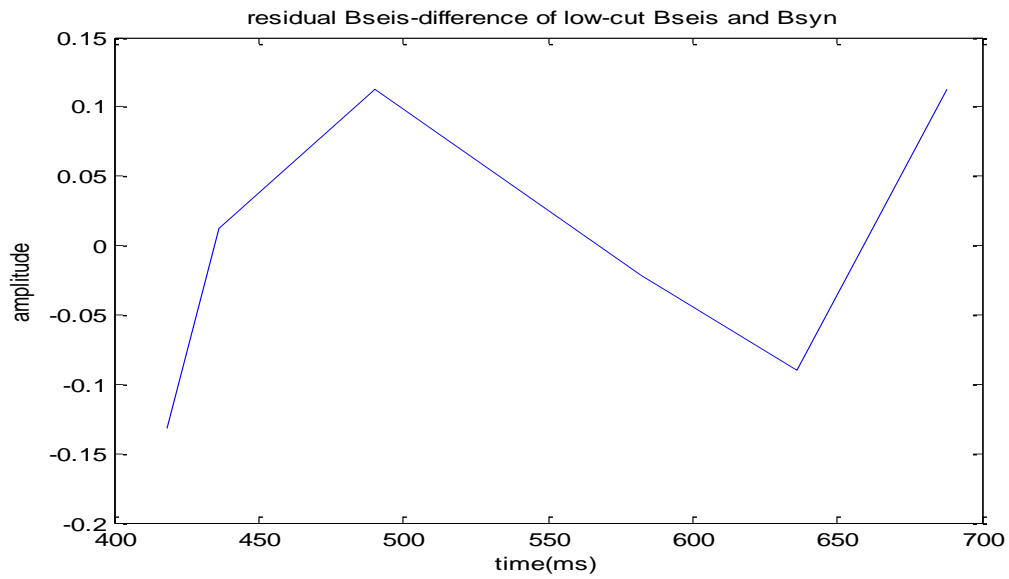


Figure 31. Plot of residual gradient $\Delta B(t)$

The difference of $C_{seislow}$ and C_{syn} is ΔC , its plot is:

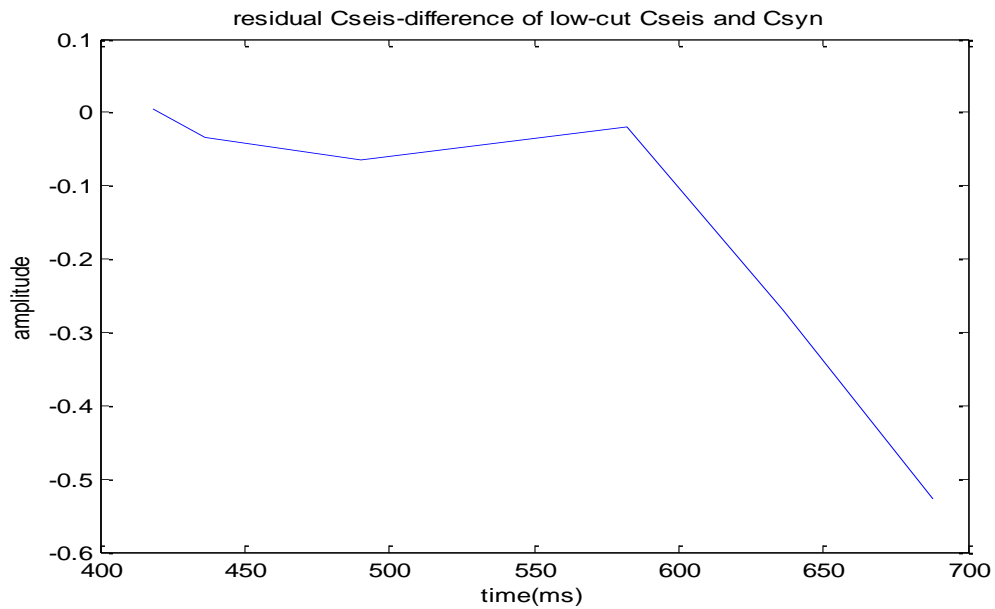


Figure 32. Plot of residual curvature $\Delta C(t)$

2.3.3.3 Solving residual anisotropy parameters from residual gradient and curvature

According to Eqn. (2.6,2.14,2.15), we get

$$\begin{aligned}
 & A_{seislow} - A_{syn} + (B_{seislow} - B_{syn}) \sin^2 \theta + (C_{seislow} - C_{syn}) \sin^2 \theta \tan^2 \theta \\
 & = 0 + \Delta B \sin^2 \theta + \Delta C \sin^2 \theta \tan^2 \theta \tag{2.21} \\
 & = \frac{1}{2} (\delta_2 - \delta_1) \sin^2 \theta * w(t) + \frac{1}{2} (\varepsilon_2 - \varepsilon_1) \sin^2 \theta \tan^2 \theta * w(t)
 \end{aligned}$$

That is, the gradient residual ΔB is half the convolution of the residual delta anisotropy $\Delta \delta$ and wavelet $w(t)$ while the curvature residual ΔC is half the convolution of the residual epsilon anisotropy $\Delta \varepsilon$ and wavelet $w(t)$. However, by picking only the peaks and troughs on the seismic data, we lose the shape of the wavelet, thus the convolution is not maintained any more.

For the optimal situation, the reflection interfaces are so sparsely distributed in depth and the wavelet is so close to a spike that the peaks and troughs of a seismic trace can be expressed as the multiplication of the reflection coefficient and the wavelet peak. Then, Eqn. (2.21) can be modified as:

$$\left\{ \begin{array}{l} \Delta B(t) = \frac{1}{2} \Delta \delta(t) \times w_0(t) \\ \Delta C(t) = \frac{1}{2} \Delta \varepsilon(t) \times w_0(t) \end{array} \right\} \tag{2.22}$$

where w_0 is the peak value of the wavelet, for zero-phase wavelet.

Here we conduct a posteriori test on whether the data we have meets the optimal situation.

Suppose it is the optimal situation, then a seismic trace can be expressed as the multiplication of the reflection coefficient and the wavelet peak. As the peak value of the zero-phase wavelet is 1, then the reflection coefficient at that depth is equal to the seismic picking value there. Thus the wavelet convolved with the seismic picking value should have the same value with the seismic picking at its depth. The result is shown in Figure 33, the seismogram colored black is the convolution result of the zero-phase wavelet and the seismic picking value(reconstructed by normalized A_{seis}^* B_{seis}^* C_{seis}^* using Aki-Richards' equation), the red curve displays the seismic picking value itself. The equation for the seismogram is Eqn.(2.14).

And a similar figure for the synthetic is also shown here (Figure 34), the seismogram colored black is the convolution result of the zero-phase wavelet and the synthetic picking value (reconstructed by normalized A_{syn} B_{syn} C_{syn} using Aki-Richards' equation), the red curve displays the synthetic picking value itself.

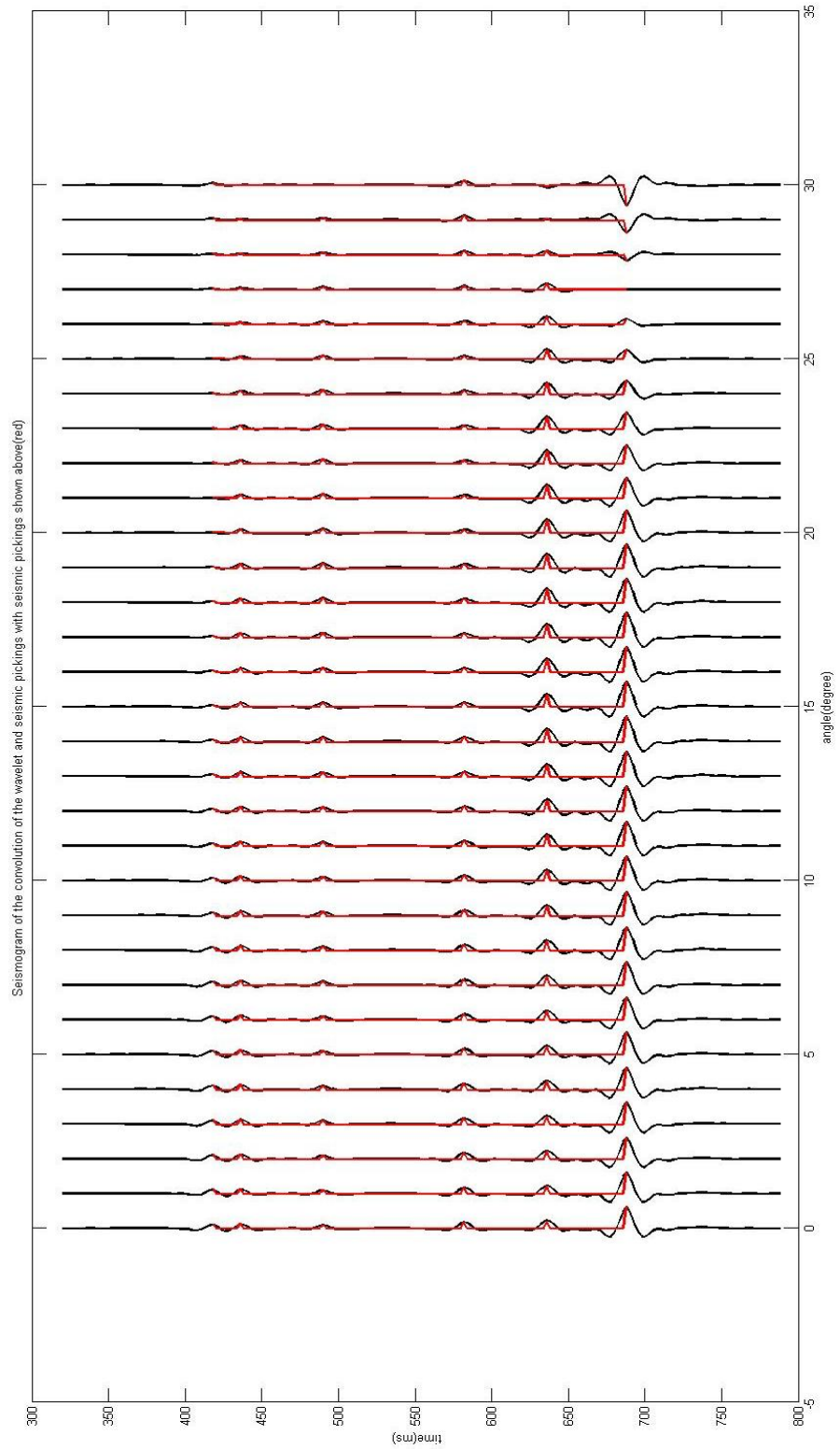


Figure 33. Seismogram of the convolution of the wavelet and seismic pickings with seismic pickings shown above

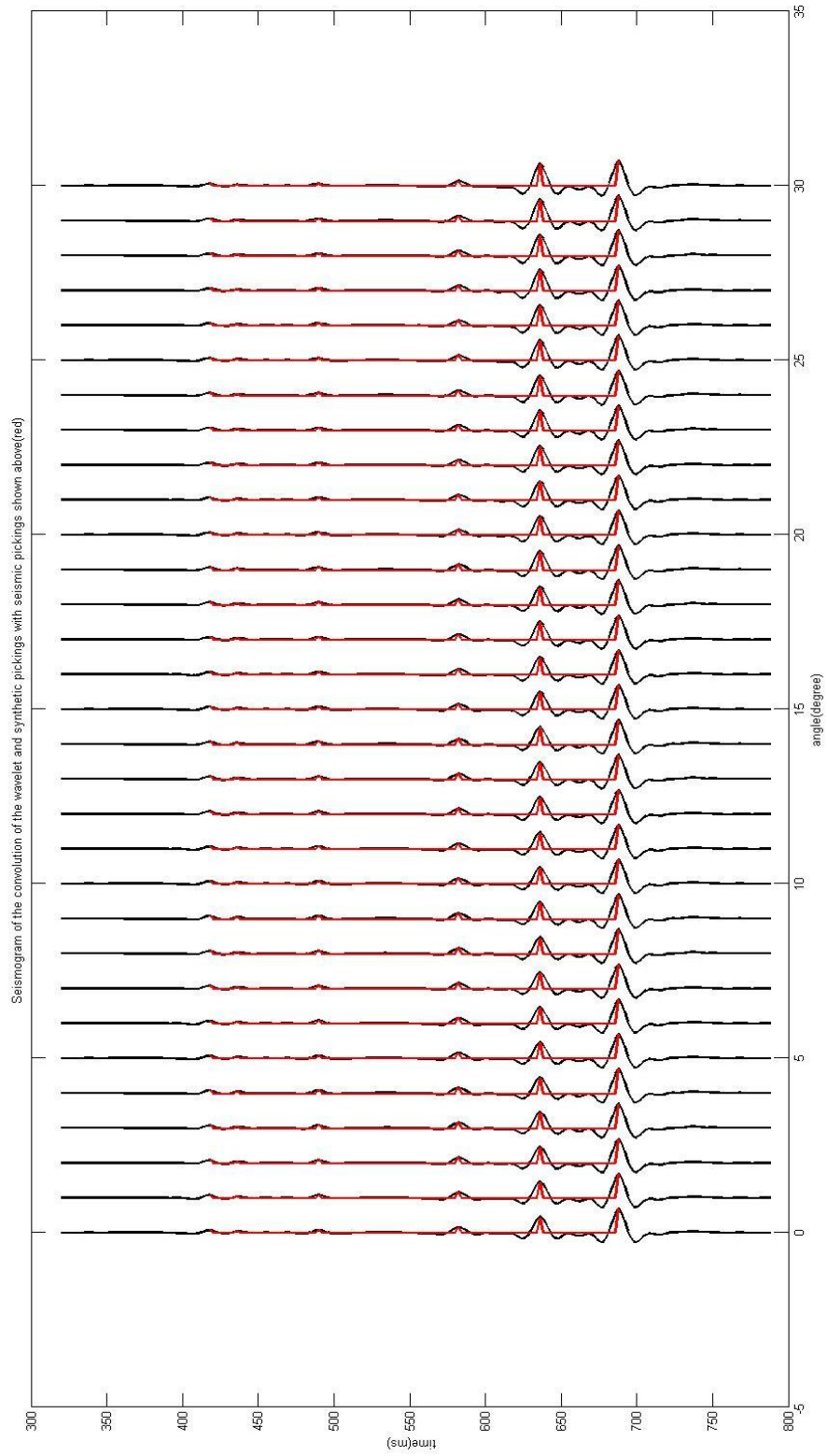


Figure 34. Seismogram of the convolution of the wavelet and synthetic pickings with seismic pickings shown above

We can find by the comparisons of the convolution and the picking itself that they are not identical, thus it is not an optimal situation.

We can try some method to make the optimal assumption more valid such as using a kind of wavelet deconvolution that can attempt to shape the known wavelet to a spike. But the biggest drawback of this method is that it will introduce more high frequencies in the data, which will influence the spectrum of the NB and NC , and further more the anisotropy parameters δ and ε .

If we accept it as the optimal situation and the relationship between the residual gradient ΔB and residual delta anisotropy $\Delta\delta$ meets Eqn. (2.22). As the peak value of the zero-phase wavelet is 1, then the residual gradient ΔB is half the value of residual delta anisotropy $\Delta\delta$. Similarly, the residual curvature ΔC is half the value of residual epsilon anisotropy $\Delta\varepsilon$.

To explore how much error will be in the $\Delta\delta$ and $\Delta\varepsilon$ parameters using this optimal assumption, we plot the $\Delta B(t)$ with the convolution of $\Delta B(t)$ and the wavelet in Figure 35, and also the $\Delta C(t)$ with the convolution of $\Delta C(t)$ and the wavelet in Figure 36.

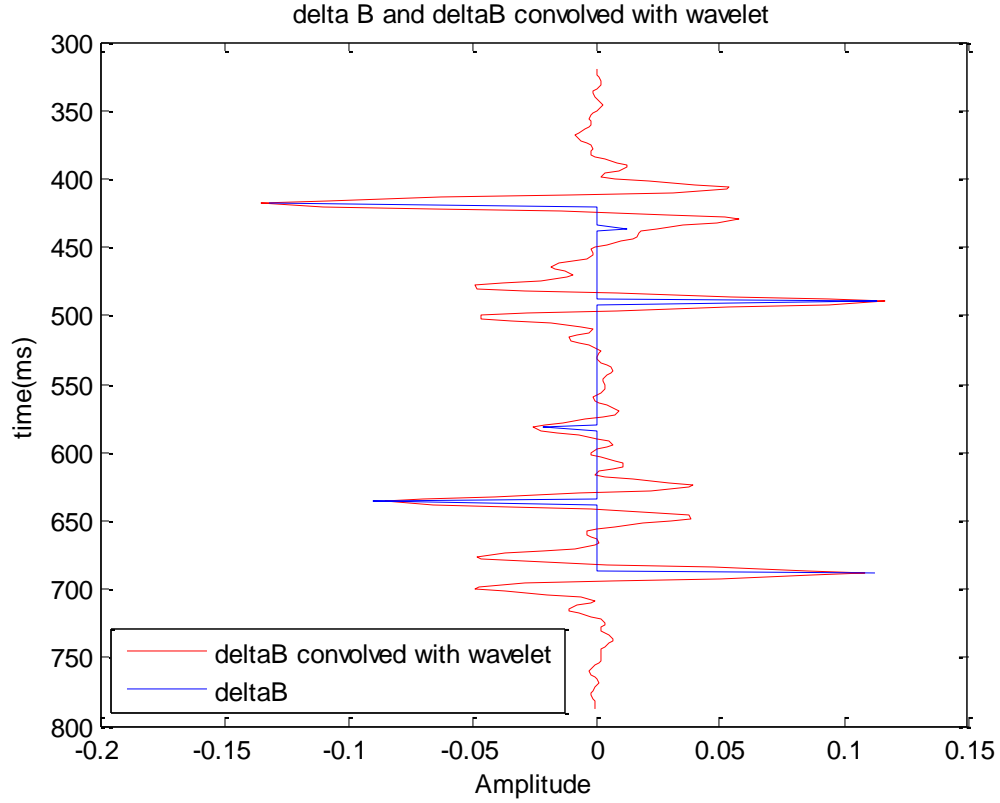


Figure 35. Comparison of one trace seismogram of the convolution of the wavelet and $\Delta B(t)$

The difference of these two curves is:

$$e = \Delta B(t) * w(t) - \Delta B(t) = \Delta B(t) * w(t) - \Delta B(t) * \Delta(t) = \Delta B(t) * (w(t) - \Delta(t)) \quad (2.23)$$

here $\Delta(t)$ is a spike in the time domain with the same amplitude of the wavelet.

The relative error of $\Delta\delta(t)$ is $\frac{\Delta B(t) * (w(t) - \Delta(t))}{\Delta B(t) * \Delta(t)}$.

From the data in Figure 35, the average value of error in $\Delta\delta(t)$ is -0.408%.

For the curvature residual $\Delta C(t)$, the comparison of $\Delta C(t)$ and the convolution of $\Delta C(t)$ and the wavelet is shown in Figure 36.

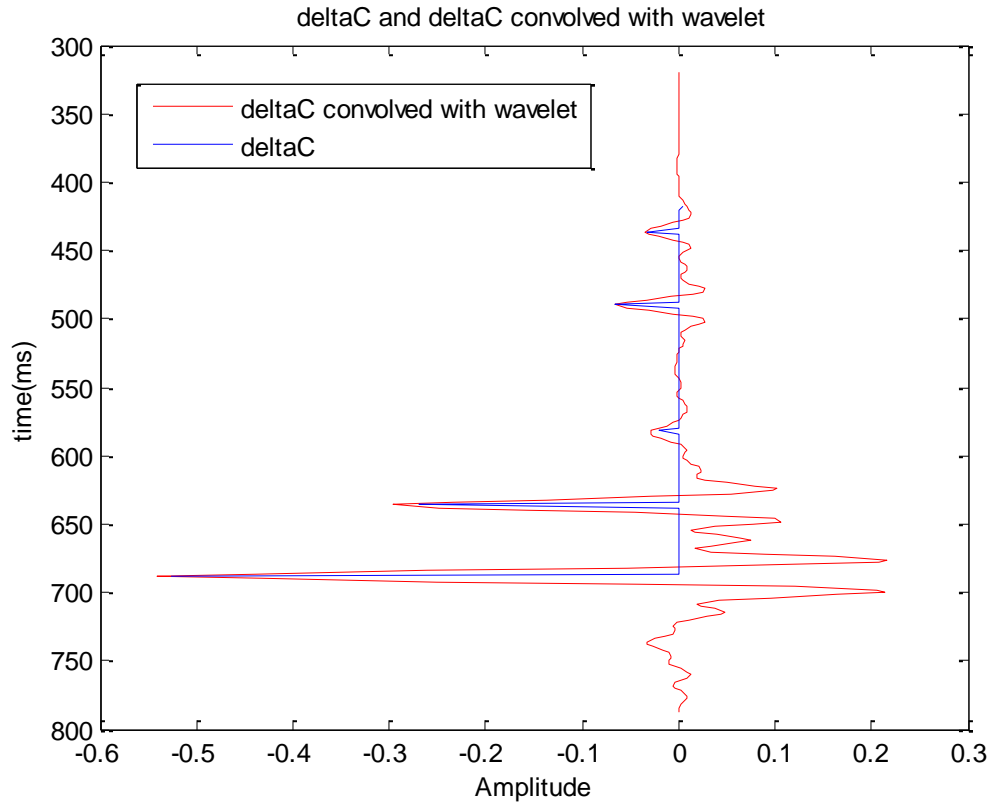


Figure 36. Comparison of one trace seismogram of the convolution of the wavelet and $\Delta C(t)$

Similarly, the error of $\Delta \varepsilon(t)$ is $\frac{\Delta C(t) * (w(t) - \Delta(t))}{\Delta C(t) * \Delta(t)}$. From the data in Figure 36, the average error in $\Delta \varepsilon(t)$ is 0.246%.

2.3.3.4 Getting anisotropy parameters for each layer

The anisotropy jump $\Delta\delta$ and $\Delta\varepsilon$ can be used to calculate the anisotropy parameters δ and ε for each layer, as long as we know the δ and ε for one arbitrary layer.

Suppose the δ parameter for layers from layer1 to layer n is $\{ \delta_1, \delta_2, \delta_3 \dots \delta_n \}$, then

$$\left\{ \begin{array}{l} \delta_2 - \delta_1 = \Delta\delta_1 \\ \delta_3 - \delta_2 = \Delta\delta_2 \\ \delta_4 - \delta_3 = \Delta\delta_3 \\ \dots\dots\dots \\ \delta_n - \delta_{n-1} = \Delta\delta_{n-1} \end{array} \right\} \quad (2.24)$$

Similarly, assume the ε parameter for layers from layer1 to layer n is $\{ \varepsilon_1, \varepsilon_2, \varepsilon_3 \dots \varepsilon_n \}$, then

$$\left\{ \begin{array}{l} \varepsilon_2 - \varepsilon_1 = \Delta\varepsilon_1 \\ \varepsilon_3 - \varepsilon_2 = \Delta\varepsilon_2 \\ \varepsilon_4 - \varepsilon_3 = \Delta\varepsilon_3 \\ \dots\dots\dots \\ \varepsilon_n - \varepsilon_{n-1} = \Delta\varepsilon_{n-1} \end{array} \right\} \quad (2.25)$$

We now have $\Delta\delta(t)$ and $\Delta\varepsilon(t)$, if we find a layer of low-shale component sand, we can assume that sand layer is isotropic and its $\delta = 0$ and its $\varepsilon = 0$.

We can locate such a sand layer based on the gamma ray curve.

The gamma ray curve for colony well is:

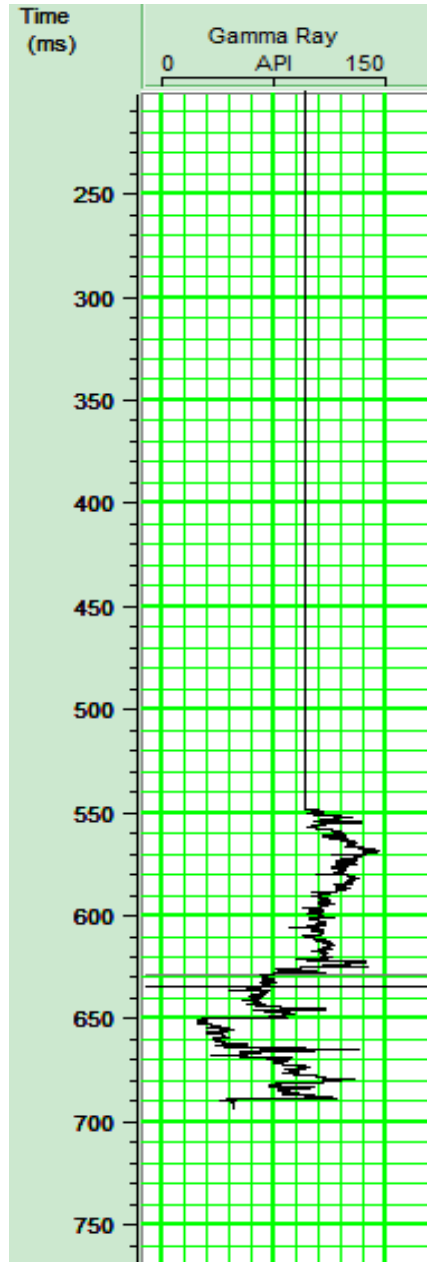


Figure 37. Gamma ray log for Colony well

From this log plot, we see that the lowest gamma ray reading is at 650ms, indicating sand layer with lowest shale component. Thus we assign δ and ε parameter at this time to be zero. As $\Delta\delta(t)$ and $\Delta\varepsilon(t)$ is sampled at 2ms interval from 418ms to 688ms, we assign $\delta_6 = 0$ and $\varepsilon_6 = 0$. Then we substitute $\delta_6 = 0$ and $\varepsilon_6 = 0$ into Eqn. (2.37) and Eqn. (2.38), we can know all the values of parameter δ and ε in the sequence. This is an intuitive description of the process known as seismic inversion, converting interface parameter-jumps to layer parameters.

Solving equations (2.24) and (2.25) we get the anisotropy parameters δ and ε in chart 1 and chart 2

Time(ms)	Parameter δ
413	0.2345
427	-0.0286
463	-0.0043
536	0.2220
609	0.1800
662	0
693	0.2258

Chart 1. Anisotropy parameters δ for layers from time 391ms to 739ms

Time (ms)	Parameter ε
413	0.7682
427	0.7782
463	0.7117
536	0.5806
609	0.5392
662	0
693	-1.0535

Chart 2. Anisotropy parameters ε for layers from time 391ms to 739ms

We can see that the δ parameter is in a reasonable range; its variation is discussed further below.

By contrast, the ε parameter doesn't make a lot of sense. A realistic ε should be > 0 (Thomsen, 1986) and within the range of 0~1. These ε parameters we have here are not consistent with these rules and they don't satisfy the weak anisotropy assumption either. We can explain it as because the C parameters we got from seismic are not reliable (c.f. Figures 15a-f). Hence, we do not discuss ε further, in this report.

The time-depth relationship is shown on Figure 38:

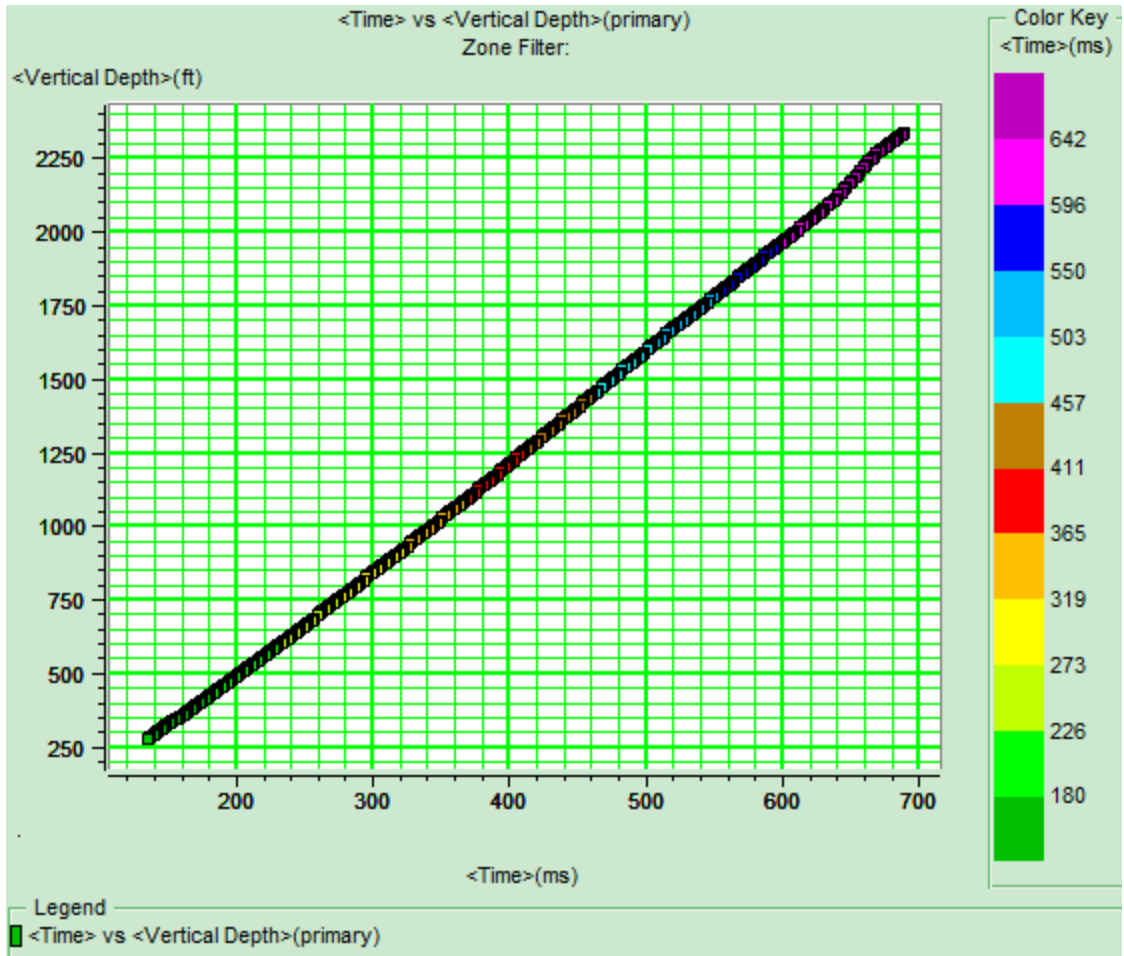


Figure 38. Time-Depth relationship

Transforming from the time domain to the depth domain, we get plots of anisotropy parameter vs. depth(Figure 39):

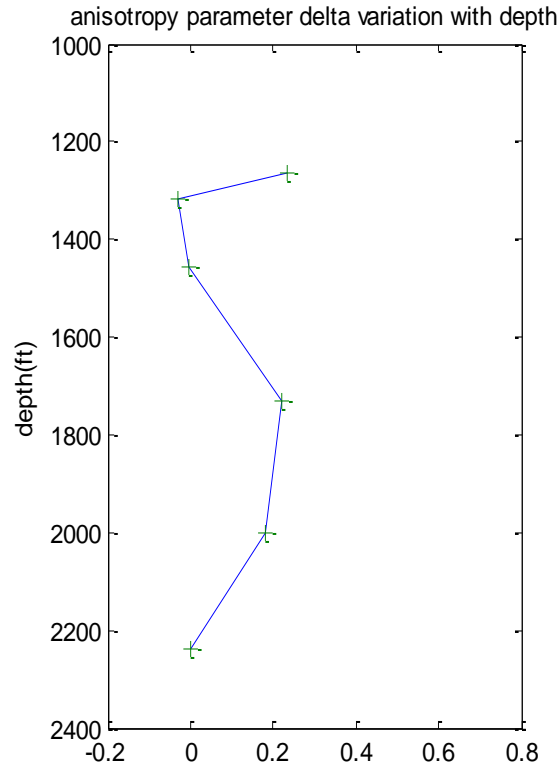


Figure 39. Anisotropy parameter δ variation with depth for colony well

2.4 Test

2.4.1 Anisotropy parameter with gamma ray log correlation

The anisotropy parameter is a combination of intrinsic anisotropy of rocks and the layer-induced anisotropy. The result may be either bigger or smaller than the intrinsic anisotropy. But we can still use the intrinsic anisotropy value estimated from rock physics information from logs to see whether the calculated anisotropy parameter makes sense.

As the gamma ray log is from 550ms to 690ms, we can compare the anisotropy parameter δ from 550ms to 690ms with the gamma ray log. Converted to depth, 550ms to 690ms is corresponding to 1780ft to 2340ft (equivalent to 542.5m to 713m).

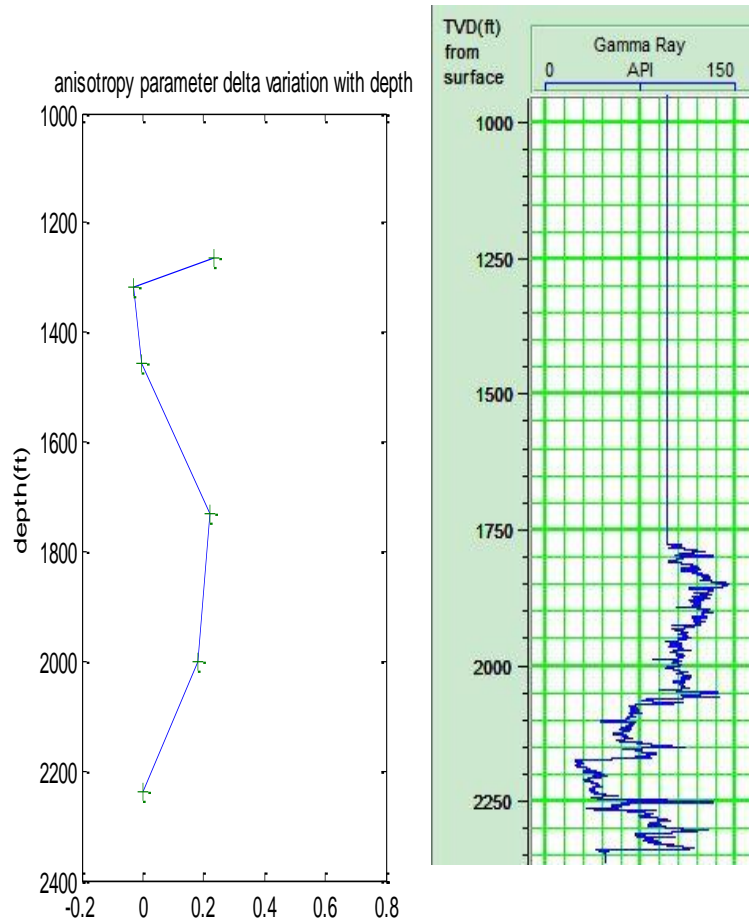


Figure 40. Anisotropy parameter δ variation with gamma ray log display

We can see that the anisotropy parameter δ is coherent with the gamma ray readings. When the gamma ray value is high, which indicates high shale component percentage is above zero, with relatively high absolute values. This further adds to the reliability of these estimated anisotropy parameters.

2.4.2 Estimating the reliability of the inferred anisotropy

Furthermore, to test the reliability of the calculated anisotropy parameter, we can use the calculated anisotropy parameters to generate an anisotropic synthetic data and compare it with the processed real seismic data, if the anisotropic synthetic ties with the real seismic data better than the isotropic synthetic, it is reasonable to believe the inferred anisotropy is reliable.

To compute the anisotropic seismic data using the anisotropy parameters δ and ε (although the ε is not reliable) we get,

the new reflection coefficient is:

$$\left\{ \begin{array}{l} A_{new}(t) = A_{syn}(t) \\ B_{new}(t) = B_{syn}(t) + \Delta\delta(t) \\ C_{new}(t) = C_{syn}(t) + \Delta\varepsilon(t) \end{array} \right\} \quad (2.26)$$

where the $A(t)$, $B(t)$, and $C(t)$ is from the log computed isotropic reflection coefficients.

Using the zero-phase wavelet shown in Figure 12, the new synthetic seismogram computed for the anisotropic reflection coefficient is:

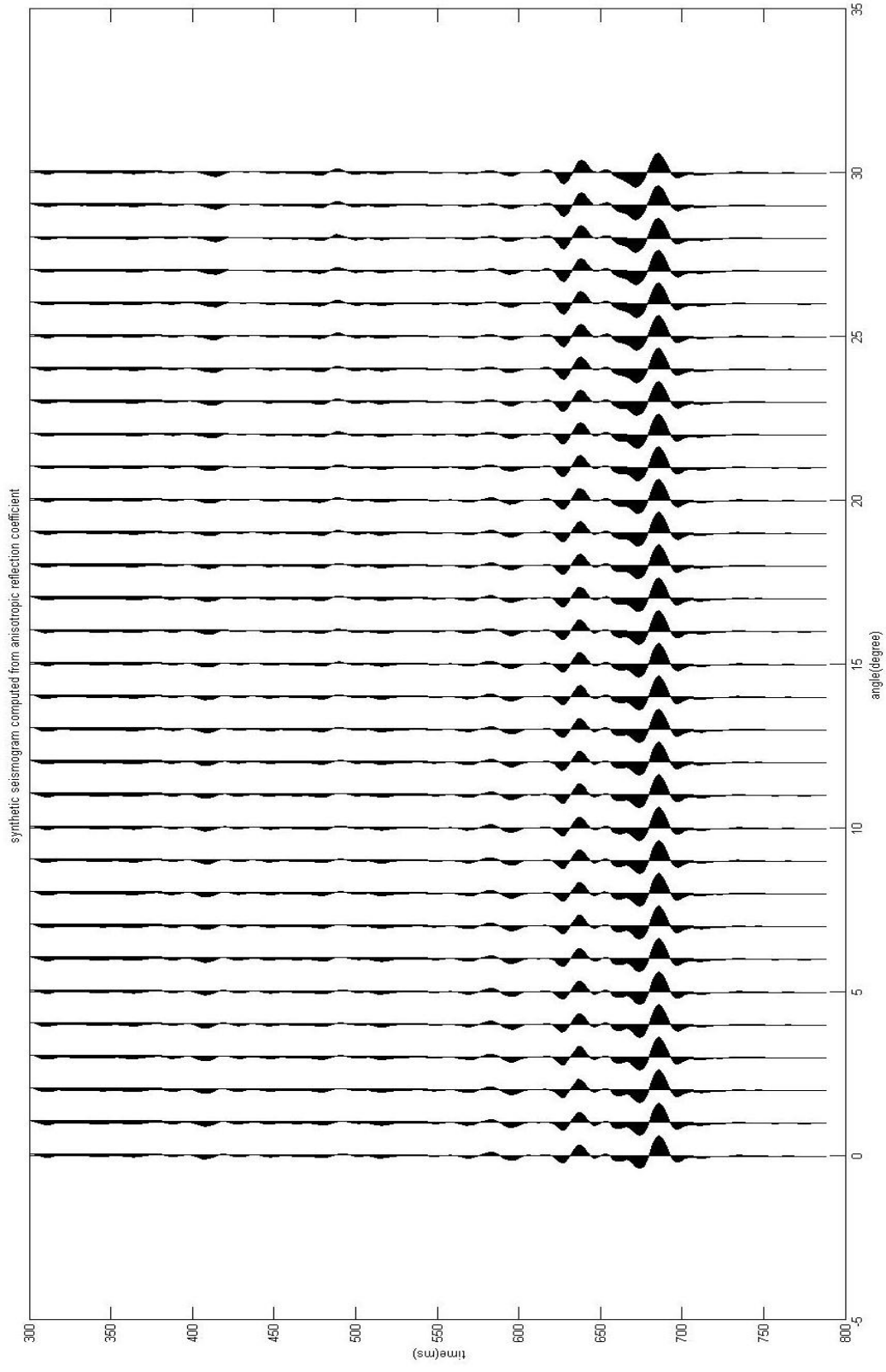


Figure 41. Synthetic seismogram computed from anisotropic reflection coefficient

The co-display of the new synthetic and the original seismic and is shown in Figure 42:

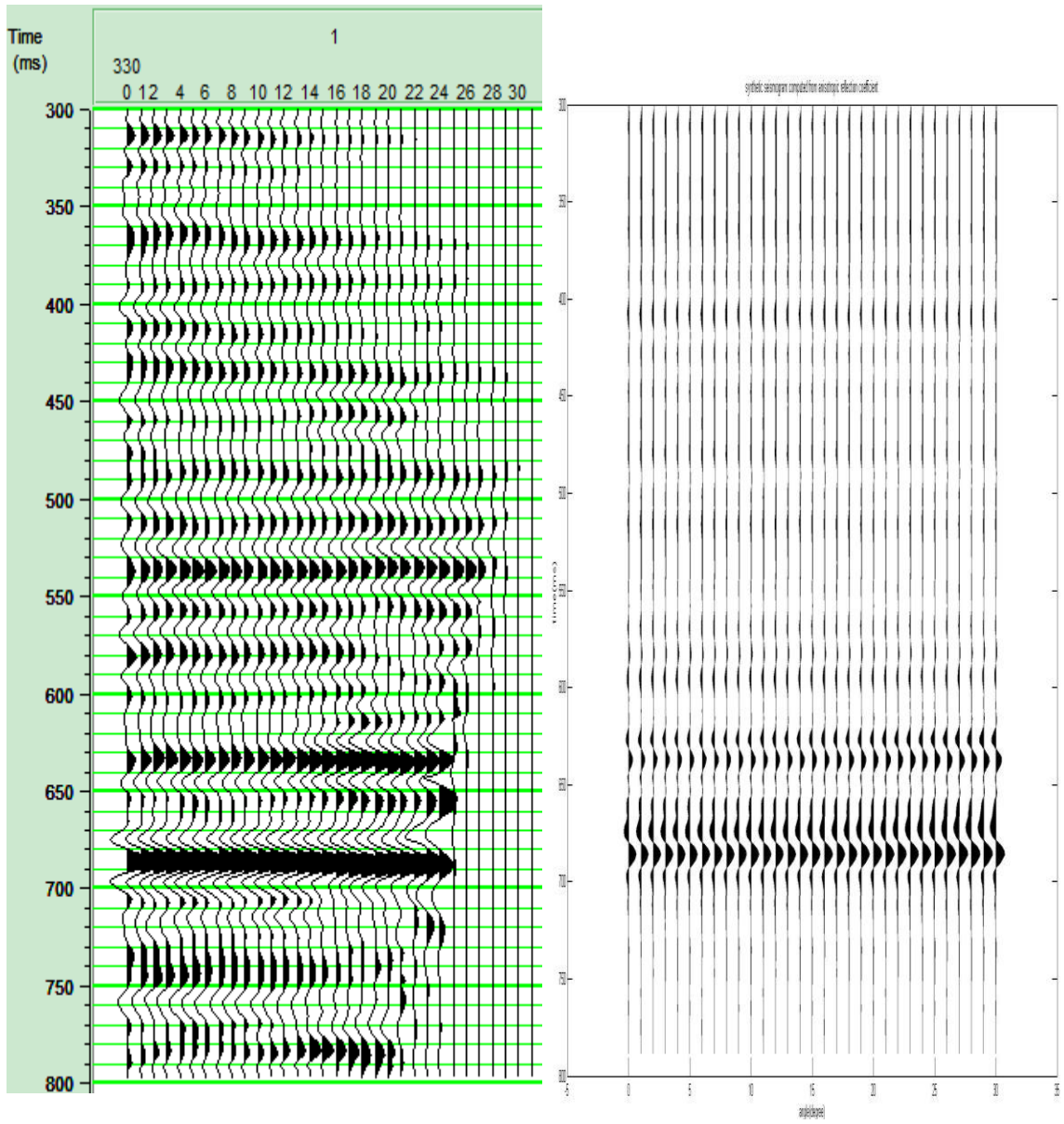


Figure 42. Comparison of the original seismic and synthetic seismogram computed from anisotropic reflection coefficient

In comparison with Figure 13, which is the co-display of the original synthetic and seismic, we can see that the new anisotropic seismogram is closer to the seismic data. Of course, this new anisotropic synthetic does not have any propagation effects in it, so we do not expect an exact match.

2.5 Conclusions and discussion

The anisotropy parameter δ we get is within the range of -0.0286~0.2345, and the anisotropy parameter ε is within the range of -1.0535~0.7782. The parameter δ is in the reasonable range of anisotropy parameters, but the value of ε parameter doesn't make sense, even though, this new method is still reliable because the problematic ε value is due to the fact that we can't get the true curvature from the Aki-Richards' approximation of the amplitude versus angle. By comparison with the gamma ray log, which is an indication of the shale component in the layers, the δ anisotropy parameters is well correlated to the gamma ray log: when the gamma ray reading is smaller, the δ has smaller absolute value, that is, the anisotropy is weaker.

In the procedure of getting the anisotropy jumps $\Delta\delta$ and $\Delta\varepsilon$ between layers, the validity of the assumption that the convolution of anisotropy jump and wavelet can be simplified as the multiplication of the anisotropy jump and the peak of the wavelet depends on two factors: the sparseness of the certain anisotropic layers and the similarity of the seismic wavelet to a spike. If the seismic resembles a spike and the certain anisotropic layers are spaced sparsely enough, then the assumption is valid and the method we use to deduce the anisotropy jumps $\Delta\delta$ and $\Delta\varepsilon$ is reliable. Furthermore, wavelet deconvolution

attempting to suppress the wavelet to a spike should be applied with concerns, because this kind of wavelet shaping can introduce more high frequencies in the data to interfere with the signal spectrum.

Besides the two major influence mentioned above, which are simplification of the convolution to a multiplication and the unreliable curvature in Aki-Richards' equation, other factors can contribute to the errors in the anisotropy parameters we get as well.

They are:

- 1) The shear wave velocity is made using mudrock line equation, not a real log measurement.
- 2) The wavelet we extracted from the seismic data in comparison of the synthetic may not be the true wavelet in the real seismic data.
- 3) We converted the offset domain to angle gather using an isotropic ray theory, which is not consistent with the anisotropy assumption.
- 4) The noise in seismic data, either low frequency or high frequency, will affect the normalization factor low-cut.
- 5) We assume the minimum value of the gamma ray we have is corresponding to an isotropic layer location with $\delta=0$ and $\varepsilon=0$, this may not be the real situation.

In a brief summary, the procedures to get the anisotropy parameters δ and ε using this method are listed as below:

- 1) Get the intercept A, gradient B and curvature C of each major horizon using Aki-Richards' equation for both the synthetic and seismic data

- 2) Divide the average of synthetic A by the average of seismic A to get the quotient as seismic normalization factor N_A .
- 3) Apply the N_A to make the seismic B and C the scale of synthetic B and C.
- 4) Divide the synthetic B and C by the scaled seismic B and C to get the quotient as normalization factor N_B and N_C .
- 5) Low cut the N_B and N_C to eliminate the propagation influence in the seismic B and C
- 6) After scaling and low-cut, the difference of the seismic B and C and synthetic B and C will be the anisotropy parameters δ and ε convoluted with the seismic wavelet
- 7) Solve for the parameters δ and ε .

REFERENCES

1. Aki, K. and Richards, P. G., 1980, Quantitative Seismology-Theory and Methods, vol.I: W.H. Freeman and Co., San Francisco.
2. Alkhalifah, T. and Tsvankin, I., 1995. Velocity analysis for transversely isotropic media: Geophysics, vol.60, p.1550–1566.
3. Castagna, J. P., Batzle, M. L., and Eastwood, R. L., 1985, Relationships between compressional-wave and shear-wave velocities in clastic silicate rocks: Geophysics, vol.50, p.571–581.
4. Gassmann, F., 1951, Elasticity of porous media: Uber die elastizitat poroser medien, Vierteljahrsschrift der Naturforschenden Gesselschaft, vol.96, p.1-23.
5. Patterson, D.J. and Tang, X. 2005, Pit Falls In Dipole Logging - Anisotropy: Cause Of Discrepancy In Borehole Acoustic Measurements: Offshore Technology Conference, 2 May-5 May 2005, Houston, Texas, Paper 17644.
6. Ruger, A.,1997. P-wave reflection coefficients for transversely isotropic models with vertical and horizontal axis of symmetry: Geophysics, vol. 62, No.3, p.713-722.
7. Sheriff, R. E., 2002, Encyclopedic Dictionary of Applied Geophysics, 4th ed., Tulsa, OK: Society of Exploration Geophysicists, p.13.
8. Shuey, R.T., 1985. A simplification of the Zoeppritz equations: Geophysics, vol.50, p.609-614.

9. Thomsen L., 1993, Weak anisotropic reflections, in Castagna J.P., Backus M., eds., Offset-dependent reflectivity: Theory and practice of AVO analysis: Investigations in Geophysics 8: Tulsa, OK, Society of Exploration Geophysicists, p. 103–111.
10. Thomsen, L., 1986, Weak elastic anisotropy: Geophysics, vol. 51, No.10, p.1954-1966.
11. Thomsen, L., 2002. Understanding Seismic Anisotropy in Exploration and Exploitation: SEG/EAGE Dist. Instrctr. Series No.5, Tulsa, OK : Society of Exploration Geophysicists, p.1-1~1-34
12. Tsvankin, I. and Thomsen, L., 1994. Nonhyperbolic reflection moveout in anisotropic media: Geophysics, vol.59, p.1290–1304.
13. Zoeppritz, K., 1919. Erdbebenwellen VIII B, On the reflection and penetration of seismic waves through unstable layers: Goettinger Nachrichten, vol.I, p.66-84.

APPENDIX A

Comparison of synthetic produced from Hampson-Russell software with what is computed from logs

This Appendix concerns only the synthetic traces, as constructed using the HR software.

We will see that their calculation raises some interesting issues.

The co-display of the Asyn, Bsyn, and Csyn picked from HR generated synthetic is (the same as in the main text) :

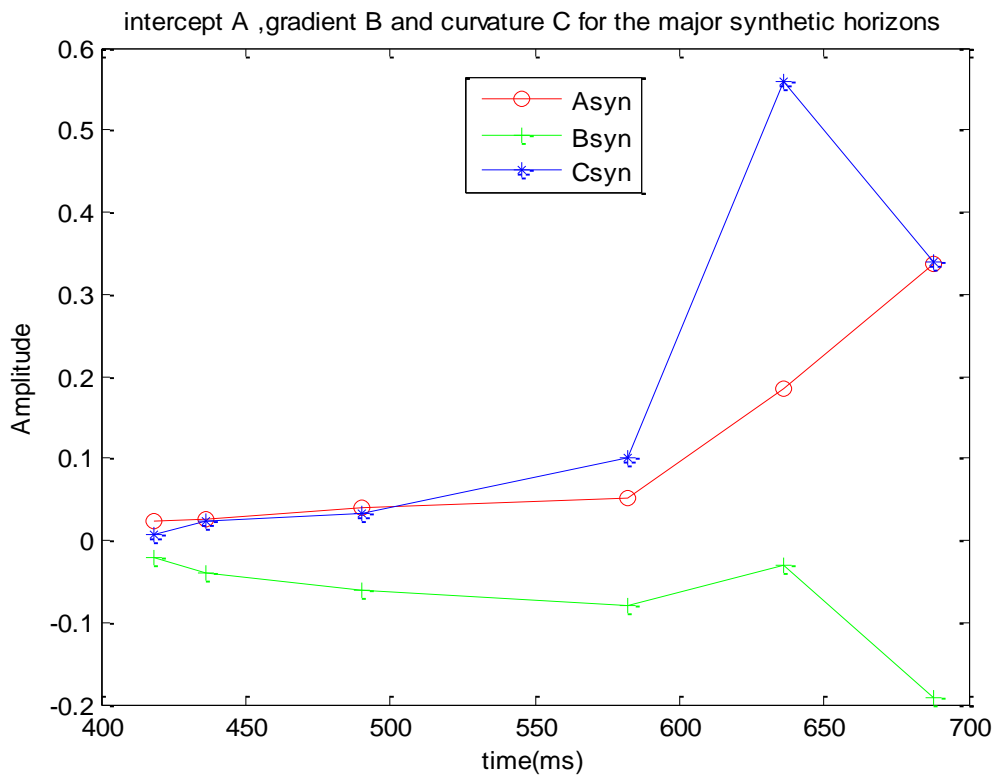


Figure A-1. Amplitude intercept A , gradient B and curvature C for the major synthetic horizons, zero phase

We may notice that the range of A parameter is from about 0.02 to 0.35, the range of B parameter is from about -0.02 to -0.2, and the range of C parameter is from about 0 to 0.6.

The range of the C parameter doesn't seem to be right, because based on equation

$$R^{iso}(\theta) = \frac{1}{2} \left[\frac{\Delta Z_0}{Z_0} \right] + \frac{1}{2} \left[\frac{\Delta Vp_0}{Vp_0} - \left(\frac{2Vs_0}{Vp_0} \right)^2 \left[\frac{\Delta G_0}{G_0} \right] \right] \sin^2 \theta + \frac{1}{2} \left[\frac{\Delta Vp_0}{Vp_0} \right] \tan^2 \theta \sin^2 \theta \quad (A.1)$$

$$= A + B \sin^2 \theta + C \tan^2 \theta \sin^2 \theta$$

We get:

$$\left\{ \begin{array}{l} A = \frac{1}{2} \left[\frac{\Delta Z_0}{Z_0} \right] = \frac{1}{2} \left[\frac{\rho_2 Vp_{02} - \rho_1 Vp_{01}}{\rho_2 Vp_{02} + \rho_1 Vp_{01}} \right] \\ B = \frac{1}{2} \left[\frac{\Delta Vp_0}{Vp_0} - \left(\frac{2Vs_0}{Vp_0} \right)^2 \left[\frac{\Delta G_0}{G_0} \right] \right] \\ C = \frac{1}{2} \left[\frac{\Delta Vp_0}{Vp_0} \right] \end{array} \right. \quad (A.2)$$

In which $Z_0 = \rho Vp_0$, $G_0 = \rho Vs_0^2$, where the notation is the same as in the main text.

Compare the formula for the parameter A and C , we find that they should be around the same value if the densities of two adjacent layers are not drastically different. However, in Figure A-1, clearly the difference between A and C is serious for deeper horizon. Evidently, their calculation is not as we have interpreted it to be.

Thus we choose another method to get the synthetic A , B , C parameters---we calculate them directly from logs. Based on Eqn. (A.1), using well logs Vp , Vs and density. These well logs begins from 135 ms to 690 ms. We get parameter A_{ref} , B_{ref} , C_{ref} as :

We get parameter A_{ref} , B_{ref} , C_{ref} as :

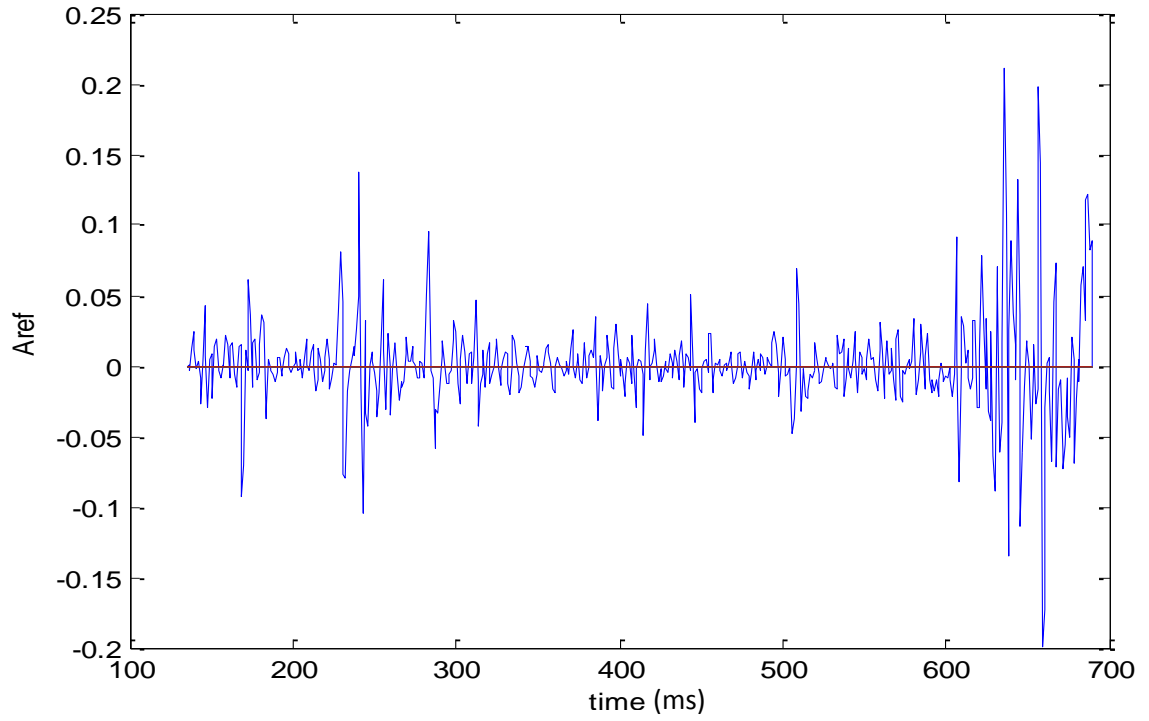


Figure A-2. A_{ref} calculated from well logs

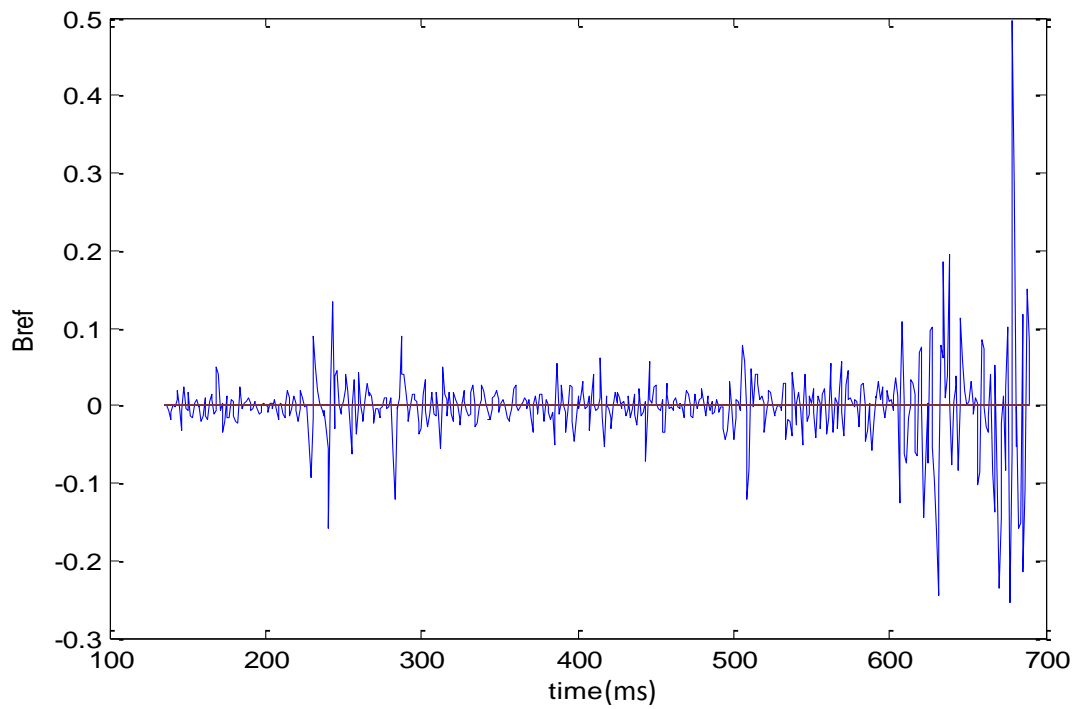


Figure A-3. B_{ref} calculated from well logs

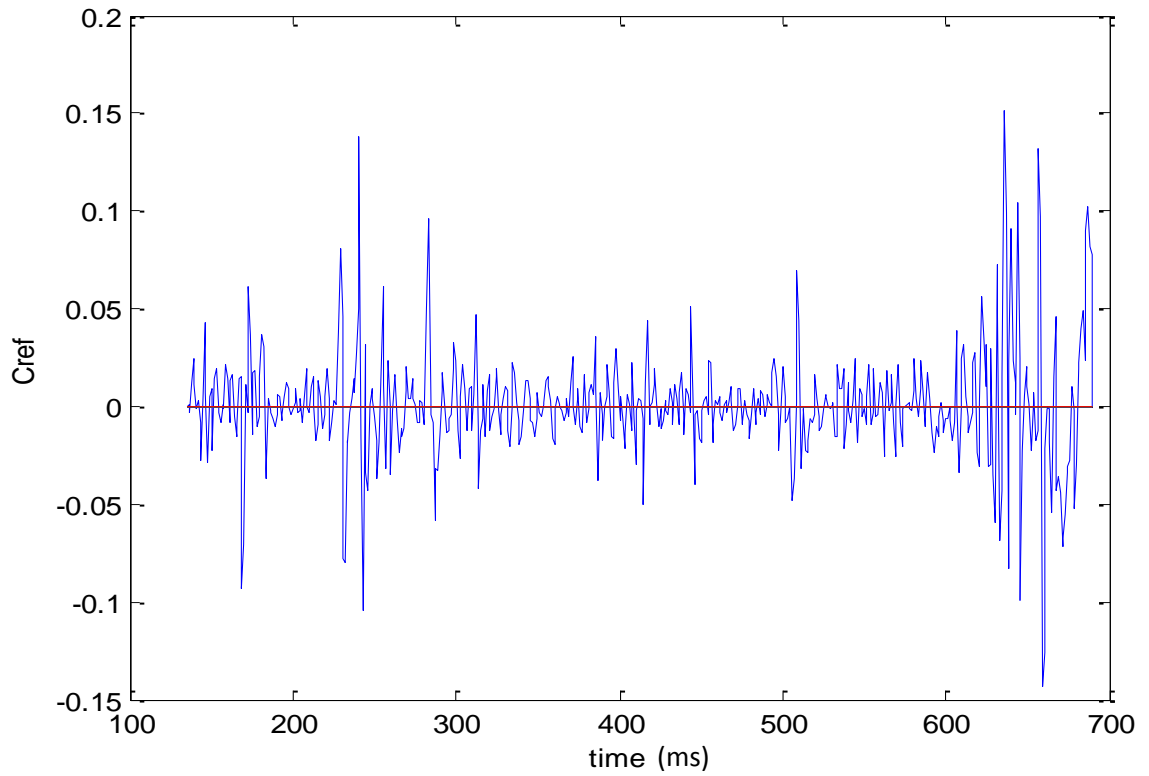


Figure A-4. C_{ref} calculated from well logs

After exporting the zero phase wavelet converted from the seismic extracted wavelet, which has been shown in Figure 7, to a readable file, we can convolve the wavelet with parameter A_{ref} , B_{ref} , C_{ref} . Then we get A_{syn} , B_{syn} , C_{syn} as :

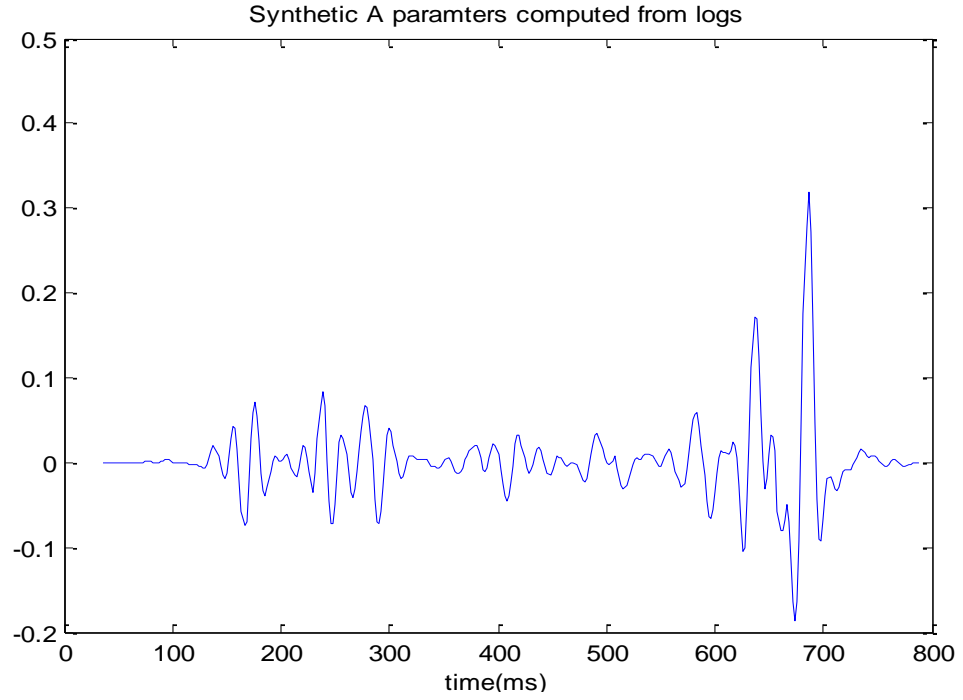


Figure A-5. A_{syn} calculated from correlation of seismic wavelet and A_{ref}

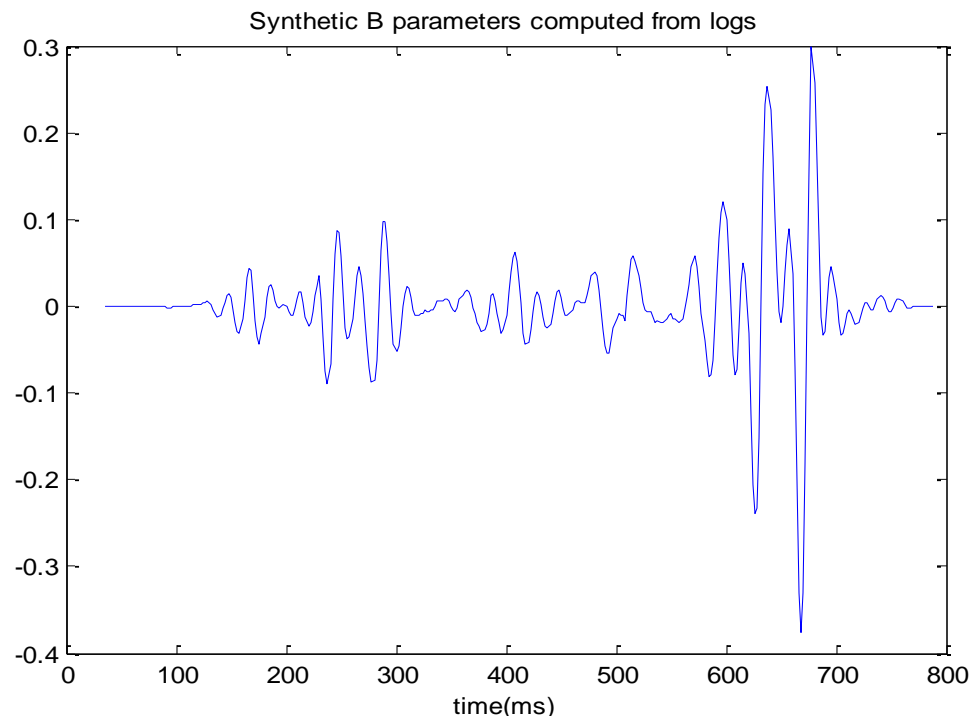


Figure A-6. B_{syn} calculated from correlation of seismic wavelet and B_{ref}

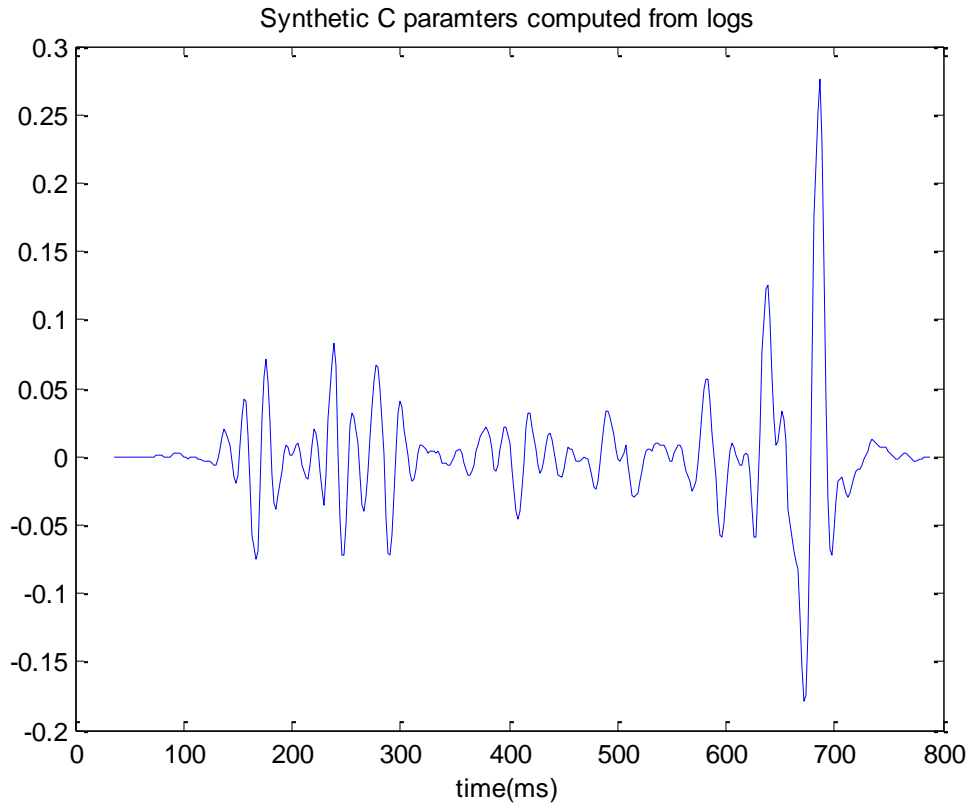


Figure A-7. C_{syn} calculated from correlation of seismic wavelet and C_{ref}

By comparison, the A_{syn} and C_{syn} are almost the same, which makes them more reliable.

And if we plot the Synthetic ABC from the synthetic picks together with the ABC calculated from correlation of seismic wavelet and logs-derived reflection coefficients for comparisons, the results are shown in figures A-8~A-10:

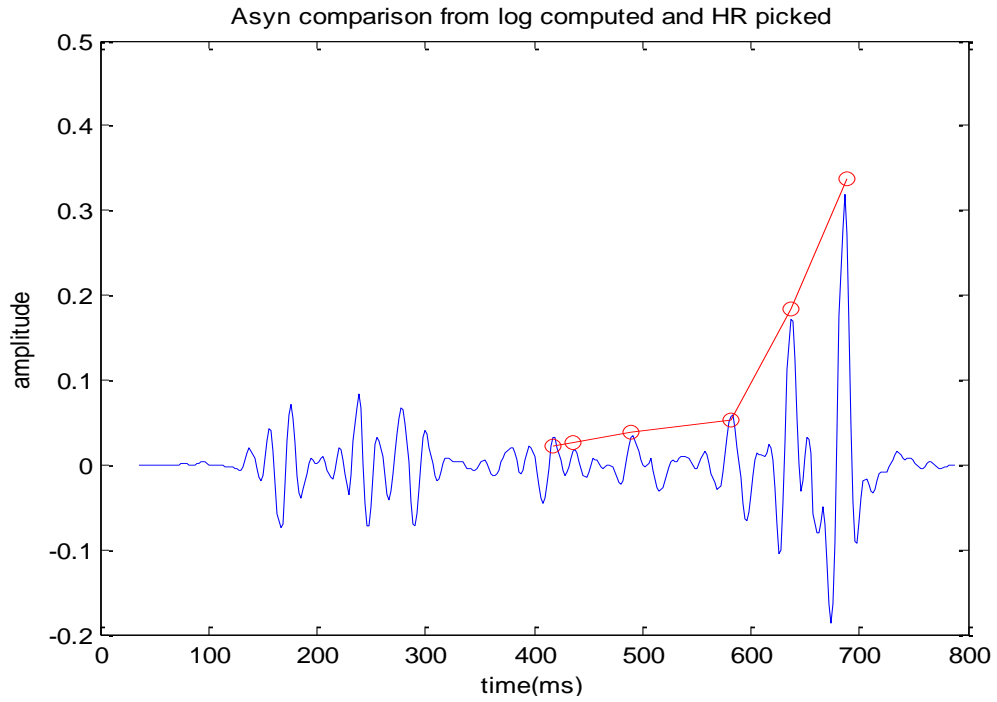


Figure A-8. A_{syn} comparison from log computation and HR software

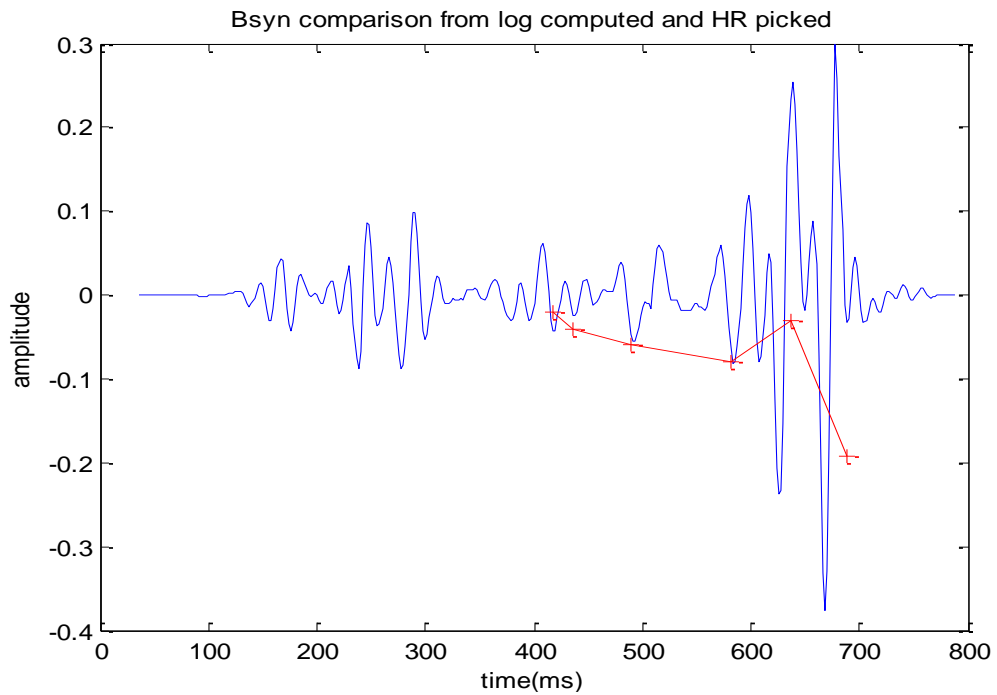


Figure A-9. B_{syn} comparison from log computation and HR software

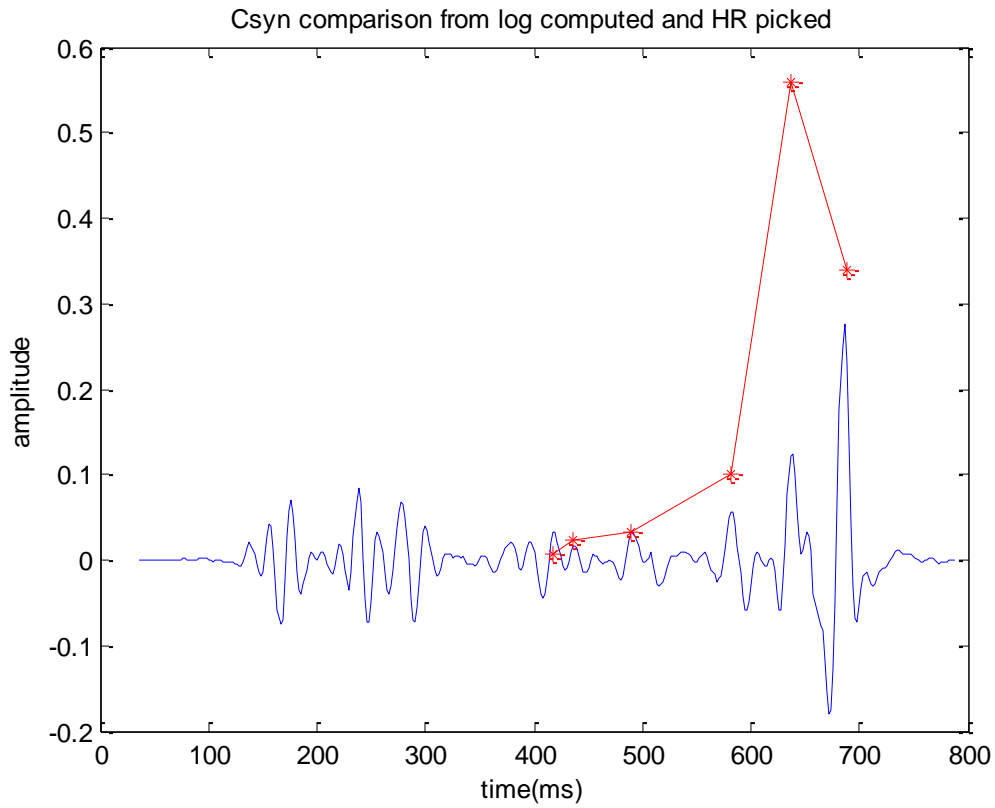


Figure A-10. C_{syn} comparison from log computation and HR software

We find that the A_{syn} parameter from both the HR software generated and log computation is almost identical, but the B_{syn} and C_{syn} parameter is different for these two methods. As we are more confident with the ones computed from the logs, in this thesis, we adopt the log computed ones instead of the HR software-generated ones.

APPENDIX B

Matlab codes for making synthetic using zero-phase wavelet and well logs to extract synthetic A,B,C

```
function [A,B,C,synlogABC]=syn0wav
% Well Name      : Colony_WELL
% Kelly Bushing Elevation : 0 m
% Surface Elevation : 0 m
% X : 0 m Y : 0 m
% First Sample at : 135.000 ms
% Last Sample at : 690.000 ms
% Sample Rate : 1.00000 ms
% Number of Samples : 556
%
% Column 1 : Domain ms
% Column 2 : Density_FRM (Density) - Units : g/cc
% Column 3 : P-wave_corr_FRM (P-wave) - Units : us/m
% Column 4 : S-wave_cast_FRM (S-wave) - Units : us/m

logs=load('logs');% read the logs
time=logs(:,1);
density=logs(:,2);
Vp=1000000./logs(:,3);% The unit for Vp and Vs is converted to m/s
Vs=1000000./logs(:,4);

A=zeros(556);% sampled 1ms from 135ms to 690ms, there are 556 points in total
for i=2:555
    A(i)=(density(i+1).*Vp(i+1)-density(i-1).*Vp(i-1))./(density(i+1).*Vp(i+1)+density(i-1).*Vp(i-1));% reflection coefficient intercept A
end
B=zeros(556);
for i=2:555
    shearmodulus2=density(i+1).*Vs(i+1).^2;
    shearmodulus1=density(i-1).*Vs(i-1).^2;
    B(i)=(Vp(i+1)-Vp(i-1))./(Vp(i+1)+Vp(i-1))-((shearmodulus2-
shearmodulus1)/(shearmodulus2+shearmodulus1)).*(2.*(Vs(i+1)+Vs(i-1)))./(Vp(i+1)+Vp(i-1)).^2;% reflection coefficient gradient B
end
C=zeros(556);
for i=2:555
    C(i)=(Vp(i+1)-Vp(i-1))./(Vp(i+1)+Vp(i-1));% reflection coefficient curvature C
end
```

```

wav=load('wave_zero_seis');% load in the zero-phase seismic extracted wavelet
[i,j]=size(wav);% i records the length of the wavelet when sampled 2ms
Maxwav=max(wav);% normalize the wavelet to make its peak is 1
wav=wav./Maxwav;

synalog=conv(A(1:2:555),wav(1:i));% because the wavelet is sampled 2ms, so we need
resample the A,B,C by 2ms.the conv is the convolution function in matlab
synblog=conv(B(1:2:555),wav(1:i));
synclog=conv(C(1:2:555),wav(1:i));

[T,ABCsyn]=loadsyn;% load in the ABC calculate from Synthetic pickings and their
time locations in T

for i=1:6 % we already know there are 6 horizons in the synthetic picks
    synlogABC(i,:)=synalog((T(i)-36)./2+1),synblog((T(i)-36)./2+1),synclog((T(i)-
36)./2+1)]% 36ms is the beginning time location of the convolved synthetic, from the
header of the 'wave_zero_seis', the wavelet begins at -99ms,135-99=36
end

```

Restrictions

Copyright, Allied Geophysical Laboratories University of Houston, Houston TX, USA Royalty free use for AGL sponsors and co-investigators for use in research, exploration, with partners, host governments, and for provision of processing/interpretation service to sponsor clients Redistribution, sale, or inclusion of this software in software products outside the sponsor worksite requires a separate commercialization agreement with the University of Houston.

Author

Rongrong Lin, University of Houston. Version April, 2013.

APPENCIX C

Matlab codes for extracting anisotropy parameters delta and epsilon from synthetic and seismic A,B,C

```
function [Bseis,Cseis]=anisoparameter

[A,B,C,ABCsyn]=syn0wav;% load in synthetic A,B,C from logs computed synthetic in
function syn0wav, as well as the reflection coefficient intercept, gradient and curvature
A,B,C
[T,ABCsei0]=loadseis;% load in seismic A,B,C and their time locations in T
NA=mean(ABCsyn(:,1))/mean(ABCsei0(:,1));% NA is the ratio of the average synthetic
amplitude and the average seismic amplitude for each horizon

for i=1:6 % we chose 6 horizons in total
ABCseis(i,:)=ABCsei0(i,:).*NA;% the new seismic is normalized by the scale factor
end

NB=ABCsyn(:,2)./ABCseis(:,2);% the normalization factor NB
NC=ABCsyn(:,3)./ABCseis(:,3);% the normalization factor NC

NBabs=abs(ABCsyn(:,2)./ABCseis(:,2)); % the absolute value of normalization factor
NB
NCabs=abs(ABCsyn(:,3)./ABCseis(:,3)); % the absolute value of normalization factor
NC

% Get the least-square linear solution for  $aT+b=NBabs$ , convert the equation to
 $Gb*mb=NBabs$ , solve for  $mb$ , then  $Gb*mb$  will be the least square linear approximation
of  $NBabs$ , which is the low cut of  $NB-NB_{low}$ 
Gb=[T,ones(6,1)];
mb=Gb\NBabs;
NBlow=Gb*mb;

% Solve for  $NC_{low}$  using the same method applied to  $NB_{low}$ 
Gc=[T,ones(6,1)];
mc=Gc\NCabs;
NClow=Gc*mc;

Ti=(T-418)./2+1;% Ti is an index of time location,418 is the beginning time.
Bseis=ABCseis(:,2).*NBlow(Ti)';% Bseis is the low-cut seismic B
dB=real(Bseis-ABCsyn(:,2));% dB is the difference between low-cut seismic B and
synthetic B
```

```

Cseis=ABCseis(:,3).*NClow(Ti);% Cseis is the low-cut seismic C
dC=real(Cseis-ABCsyn(:,3));% dC is the difference between low-cut seismic C and
synthetic C
ddelta=2*dB;% ddelta is the delta delta parameter
depsilon=2*dC;% depsilon is the delta epsilon parameter

D=zeros(7,1);% D stores the value of Delta parameter
D(6)=0;% gamma ray displays smallest value at 650 ms, as the time range for the
horizons is 413mms to 693ms, it is at the location of the 6th horizon
for i=1:5
    D(6-i)=D(7-i)-ddelta(6-i);
end
for i=6
    D(i+1)=D(i)+ddelta(i);
end
E=zeros(7,1);% E stores the value of Epsilon
E(6)=0;
for i=1:5
    E(6-i)=E(7-i)-depsilon(6-i);
end
for i=6
    E(i+1)=E(i)+depsilon(i);
end

T2=zeros(7,1); % T2 records the time location for anisotropy parameters D and E
T2(1)=T(1)-5;
T2(7)=T(6)+5;
for i=2:6
    T2(i)=0.5*(T(i-1)+T(i));% use the average of time locations of two adjacent anisotropy
jumps as the time for the anisotropy itself
end

```

Restrictions

Copyright, Allied Geophysical Laboratories University of Houston, Houston TX, USA Royalty free use for AGL sponsors and co-investigators for use in research, exploration, with partners, host governments, and for provision of processing/interpretation service to sponsor clients Redistribution, sale, or inclusion of this software in software products outside the sponsor worksite requires a separate commercialization agreement with the University of Houston.

Author

Rongrong Lin, University of Houston. Version April, 2013.

APPENDIX D

Correlation of the δ parameter with gamma ray log from other literature

From the discussion in the main text, we see that the δ parameters we get correlate well with the gamma ray log we have in Colony well. (See Figure D-1, which is the same as Figure 40 in the main text.)

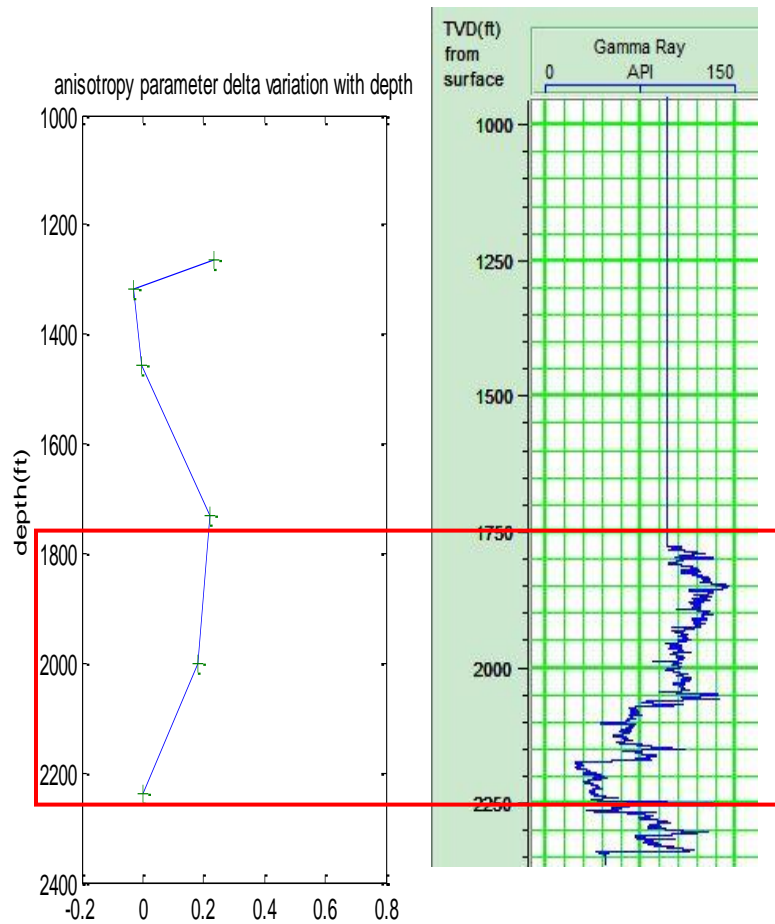


Figure D-1. Anisotropy parameter δ variation with gamma ray log display

However, the gamma ray log is only from 1750ft to 2250ft, we don't have any gamma ray log information for above 1750ft, so we look for the gamma ray log for Colony sand in other literature.

In the CREWES annual report 'Exploitation of an oil field using AVO and post-stack rock property analysis methods' by Andrew J. Royle (2001), we find a well 10-14 (See Figure D-2) drilled in the Colony sand area with a similar Colony sand layer as in our well log in the Colony sand dataset provided in the Hampson-Russell software as a default dataset.

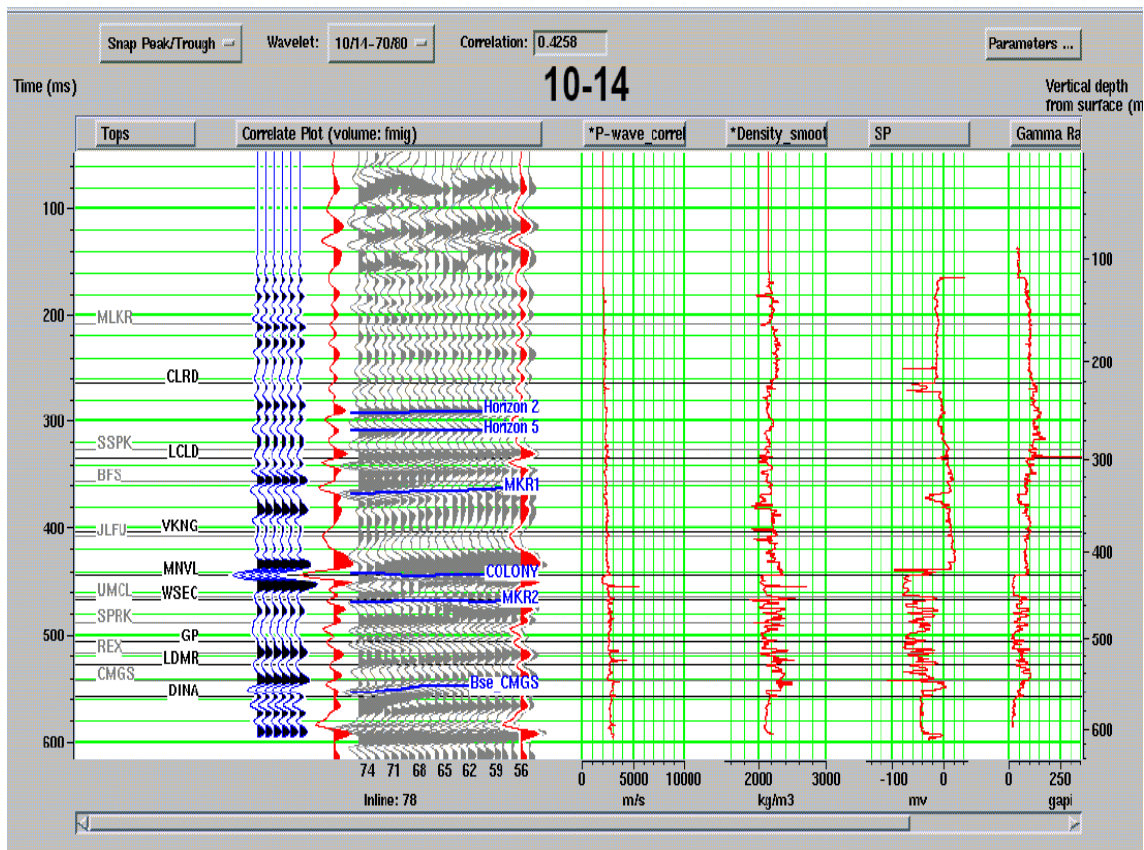


Figure D-2. Anisotropy parameter δ variation with gamma ray log display

Although this well is at a different location in the Colony field, we may use the data to extend our analysis to shallower depth, by analogy, since the stratigraphy in the area is quite flat. Figure D-3 shows a highlighted box (381m to 533m) of this gamma ray log, compared with our calculated δ function in the corresponding depth interval (1250ft-1750ft, equivalent to 381m to 533.4m). The minimum in the gamma ray reading near 440m correlates with the minimum in δ function at 1400ft(equivalent to 426.72m), giving more confidence to our method.

However, we note that the correlation is flawed, since we have not considered the possibility of lateral variation. Other logs from the area show different trends and the present analysis should be repeated in full, for each of the logs, for a satisfactory conclusion.

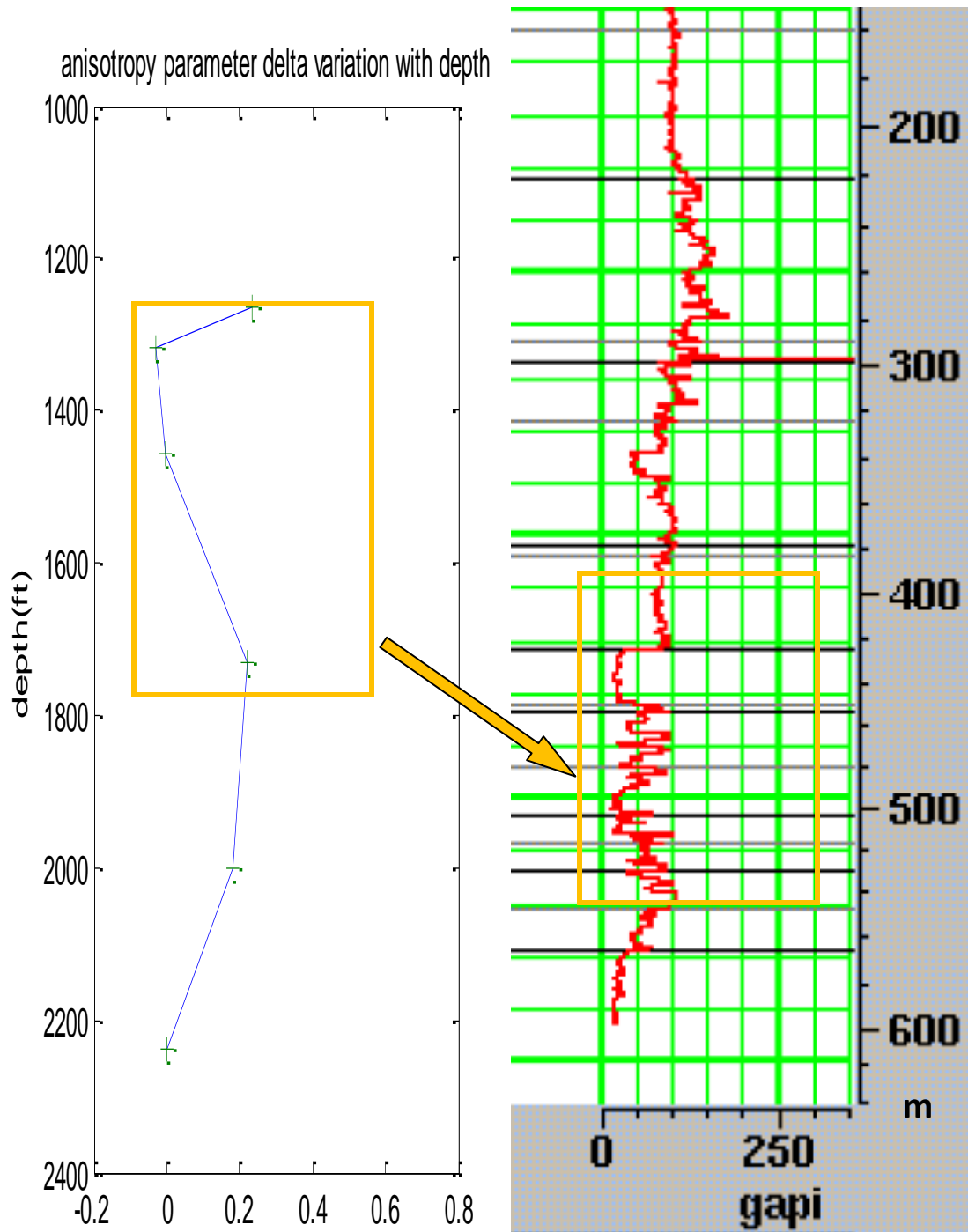


Figure D-3. Anisotropy parameter δ (from 1250ft to 1750ft, equivalent to from 381m to 533.4m) correlation with well 10-14 gamma ray log (from 381m to 533.4m)